Study on thermal properties of asphalt concrete pavement and countermeasures against its high surface temperature in tunnel

アスファルト舗装の熱特性とトンネル内舗装表面高温化の対策に関する研究

A Dissertation Submitted in Partial Fulfilment of the
Requirements for the Degree of
Doctor of Philosophy

Aibek TOKTORBAI UULU

Department of Civil Engineering

YOKOHAMA NATIONAL UNIVERSITY

August 2019

Study on thermal properties of asphalt concrete pavement and countermeasures against its high surface temperature in tunnel

A Dissertation Submitted in Partial Fulfilment of the

Requirements for the Degree of

Doctor of Philosophy

by

Aibek TOKTORBAI UULU

Yokohama National University

Thesis Supervisor: Professor Hiroshi KATSUCHI

August 2019

To my beloved family and respectable teachers

ACKNOWLEDGMENTS

I am grateful to my supervisor, **Professor Hiroshi KATSUCHI**, for his valuable and constructive suggestions during the last five years. His willingness to guide me through the dark has been very much appreciated. This work would not have been possible without his support.

I would like to express my gratitude to my advisor, **Professor Hitoshi YAMADA**. His wide knowledge and his logical way of thinking have been of great value for me.

I sincerely thank **Dr. Haeyoung KIM**, Assistant professor, for her precious guidance and continuous encouragement throughout the study.

I would also like to extend my thanks to my committee members: **Professor Kimitoshi HAYANO, Associate Professor Chikako FUJIYAMA** and **Associate Professor Hiroshi TAMURA** for their valuable time and helpful comments.

I also thank **all my friends and colleagues** in my Structural Laboratory who have shared so many special moments and for their suggestions and accompanying.

The author is highly obliged and grateful to the **Japanese Government** (文部科学省: MEXT) for their continued financial assistance and **Japanese people** for their kind hospitality during this study period in Japan.

Finally, I would like to give my special thanks to **my parents** and **my wife, my children, my brothers** and **sisters** for their constant love and encouragement throughout my life.

Above all, from my very soul, I thank **the God, The Almighty** for bestowing me with the knowledge and strength to complete my work successfully.

Aibek TOKTORBAI UULU

ABSTRACT

It is reported that the surface temperature of asphalt pavement in a road tunnel in an urban area in summer days gets hot especially when the tunnel is long and the traffic volume is heavy. Since the asphalt pavement absorbs a large amount of heat generated by vehicles and keeps it for a long time, a high-temperature environment in the tunnel also continues for a long time. This phenomenon brings uncomfortableness for users, especially for motor-bikers and maintenance workers who have to run across the road tunnel sufficiently for a long time and stay inside during inspection and repairment jobs, respectively. Yamate Tunnel, which is located in the center of Tokyo is facing this phenomenon. It is the longest road tunnel in Japan with its length of 18.2km and the second-longest road tunnel in the world. As were conducted measurements in this tunnel in the summer season, the air temperature rose to more than 40°C and the temperature of the asphalt surface was even higher than other parts of the tunnel.

On this background, this study aims to estimate the thermal parameters of the various types of asphalt concrete (AC) which includes the type used in Yamate Tunnel and investigate their effects on a high-temperature pavement surface. 6 types of AC specimens were tested in a wind-tunnel where a hot temperature air inside was generated by a forced circulation boiler system. Thermal parameters: specific heat capacity, heat conductivity, heat diffusivity, and heat transfer coefficients were analyzed using a one-dimensional partial differential heat transfer equation and a finite difference approximation method. Sequentially, the second stage of experiments was conducted to examine the effect of high wind speed and water spray. Based on the obtained data, the values of heat transfer coefficient varying with respect to wind speed were calculated. Also, the amounts of radiated heat transfer from the AC were compared between two types of AC. These values are beneficial to check and control a heat flow inside the Yamate Tunnel and mitigating the high surface temperature. Additionally, the effects of different basement boundary conditions and water spray on the surface temperature were investigated to find effective countermeasures to decrease the surface temperature of AC in the tunnel.

Besides, the heat balance and the temperature distributions inside the tunnel were visualized by making a 2D model of Yamate Tunnel through the simulations. The simulation results help to suppress the temperature increase in the tunnel in an optimal way.

Finally, analyses were performed to analyze the heat distribution percentage of asphalt pavement throughout the Yamate Tunnel by using the real measured data. As a result, the portion of the heat releasing from the asphalt radiating to the air inside the tunnel were explained.

Table of Contents

ACKNOWLEDGMENTS IV
ABSTRACT V
Table of Contents VII
List of Tables XII
List of Figures XIII
List of Nomenclatures XIV
List of Equations XV
CHAPTER I 1
1. INTRODUCTION 1
1.1 Background 1
1.2 Motivations 4
1.3 Research Objectives 6
1.4 Organization of the Dissertation 7
CHAPTER II 9
2. GENERAL BACKGROUND 9
2.1 Heat Transfer Mechanisms 9
2.1.1 Conduction 9
2.1.2 Convection 11
2.1.3 Radiation 12
2.2 Energy Balance in Asphalt Pavement 14
2.3 Thermal Parameters and Identification Techniques 16
2.3.1 Specific Heat 16
2.3.2 Thermal Conductivity 17
2.3.3 Thermal Diffusivity 19
2.3.4 Heat Transfer Coefficient 20
2.4 Literature Survey 20
2.5 Summary of Chapter 2 22
References and Suggested Readings 23

CHAPTER III 25
3. MEASUREMENT OF HEAT TRANSFER IN ASPHALT - I 25
Abstract 25
3.1 Experiment Stage #1 25
3.1.1 Introduction of experiment stage #1 25
3.2 Wind-Tunnel 26
3.2.1 Introduction 26
3.2.2 Dimensions 26
3.2.3 Tools 27
3.3 Boiler system 27
3.4 Data acquisition equipment 28
3.4.1 Data Logger 28
3.4.2 Thermocouples 29
3.5 Asphalt Specimen Types 29
3.6 Thermocouple Installations 31
3.6.1 Adhesive materials 32
3.6.2 Test for surface temperature accuracy 32
3.7 Test for Each Type of Asphalt Concrete 33
3.7.1 Test setup 33
3.7.2 Results 33
3.8 Identification of Thermal Parameters 36
3.9 Heat Transfer Equation 37
3.9.1 One Dimensional Partial Differential Heat Equation 37
3.10 Initial and Boundary Conditions 37
3.10.1 Initial Condition 37
3.10.2 Top Boundary Condition 37
3.10.3 Bottom Boundary Condition 38
3.11 Finite Difference Method 38
3.11.1 Grid Discretization 38
3.11.2 Explicit Method 39

3.11.3 Exponential interpolation 40
3.11.4 Root Mean Square Error (RMSE) approach 42
3.12 Results of Numerical Analysis 42
3.12.1 Comparison of measured and calculated results 42
3.12.2 Obtained thermal parameters of 6 types of AC 47
3.12.3 Comparison of obtained thermal parameters with prior studies 47
3.13 Conclusions and Discussions 49
3.14 Summary of Chapter 3 49
References and Suggested Readings 49
CHAPTER IV 51
4. MEASUREMENT OF HEAT TRANSFER IN ASPHALT – II 51
Abstract 51
4.1 Experiment Stage #2 51
4.1.1 Introduction of Experiment Stage #2 51
4.1.2 What are Porous Asphalt and Porous Asphalt with Water-Holding system? 53
4.1.3 Input Parameters 53
4.2 Test under High Wind Speed and Lamp-Radiation 55
4.2.1 Test setup 55
4.2.2 Results of measured temperatures affected by the high wind speed 55
4.2.3 Comparison of temperature distributions between the ordinary asphalt and water-holding porous asphalt 56
4.3 Combined Heat transfer coefficient (CHTC) 59
4.4 Derivation of Combined Heat Transfer Coefficient depending on Wind 59
4.4.1 Example of Radiated Heat Amount 60
4.4.2 Accuracy analysis 63
4.5 Derivation of Combined Heat Transfer Coefficient depending on Water-spray 64
4.5.1 Example of Radiated Heat Amount 65
4.5.2 Accuracy analysis 65

4.6 Test under Water-Spray Effect 67
4.6.1 Test input parameters 67
4.6.2 Test for temperature cooling without water-spraying 67
4.6.3 Test for temperature cooling under water spray and wind speed effect 67
4.7 Test under Tunnel-Environment Condition 70
4.7.1 Introduction of the test 70
4.7.2 Results 70
4.8 Summary of Chapter 4 72
CHAPTER V 71
5. APPROACHES TO IMPLEMENT COUNTERMEASURE AGAINST ASPHALT HIGH TEMPERATURE 71
Abstract 71
5.1 Introduction and objectives 71
5.2 5 Types of Countermeasure Approaches 72
5.2.1 Influence of Concrete Base at Thicknesses 12 cm & 30 cm 72
5.2.2 Influence of Steel Plate Base 73
5.2.3 Influence of H-beams Together with Steel Plate Base 73
5.2.4 Influence of Water-Spray 73
5.3 Results and Discussions 74
5.4 2D Simulations of Temperature Distributions in Yamate Tunnel 75
5.4.1 Introduction and objectives 75
5.4.2 Input parameters for simulation model 75
5.4.3 Meshing quality 77
5.4.4 Simulation Results 77
5.4.5 Findings on simulation 80
5.5 2D Simulations of Temperature Distributions in Yamate Tunnel considering Vehicle model 82
5.5.1 Introduction and objectives 82
5.5.2 Input parameters for simulation model 82
5.5.3 Meshing quality 83
5.5.4 Simulation Results 84

5.6 Analyses of heat distribution percentage in “Yamate” Tunnel 85
5.6.1 Introduction and model specifications 85
5.6.2 Simulation Results 86
5.7 Summary of Chapter 5 89
5.7.1 Summary of experimental results 89
5.7.2 Summary of 2D simulation results 89
5.7.3 Summary of analyses 90
CHAPTER VI 91
6. CONCLUSIONS AND RECOMMENDATIONS 91
6.1 Conclusions 91
6.2 Final Remarks 92
6.3 Prospects for future researches 93
6.3.1 Yamate Tunnel model with vehicle heat source 93
6.3.2 Water-pipe inside Yamate Tunnel 93
6.3.3 Suppression of Yamate Tunnel air temperature with Liquid Nitrogen 94
REFERENCES and SUGGESTED READINGS 95

List of Tables

Table 2.1 Emissivities of common materials at temperature 300 K 14

Table 2.2 Thermal conductivities of common materials at room temperature 18

Table 2.3 Typical values of convection heat transfer coefficient 20

Table 3.1 Asphalt specimen types and their layer thicknesses 30

Table 3.2 Numerically derived thermal parameters of 6 type of asphalt specimens 48

Table 3.3 Comparison of the obtained asphalt thermal parameters with prior studies .. 48

Table 4.1 High wind speed parameters obtained by the vehicle speed. 54

Table 4.3 Numerically obtained heat transfer coefficients with respect to wind 60

Table 4.4 Values of radiated heat amounts from asphalt surface to air with respect to wind 61

Table 4.5 Actual values of RMSE with respect to wind of AC#4 and AC#5. 63

Table 4.6 Numerically obtained CHTC with respect to water-spray amount 64

Table 4.4 Actual values of radiated heat amounts with respect to water-spray. 65

Table 4.5 Actual values of RMSE with respect to water-spray amount. 66

Table 4.6 Test input parameters 67

Table 5.1 Input parameters for simulation 76

Table 5.2 Input parameters for simulation 83

List of Figures

Figure 1.1 Illustration of a biker and a worker in a road tunnel. 1

Figure 1.2 Yamate Tunnel location between Oi Junction in Shinagawa to Takamatsu in Toshima, Tokyo. 2

Figure 1.3 High temperature in Yamate Tunnel in summer season. 3

Figure 1.4 Countermeasures against high temperature in Yamate Tunnel. 3

Figure 1.5 Illustration of ventilation system in road tunnel 4

Figure 1.6 Temperature distribution in Yamate Tunnel taken by thermal camera. 5

Figure 1.7 Measured temperature in Yamate Tunnel. June, 2017. 6

Figure 2.1 Heat conduction through a plane wall of thickness *x* and area *A*. 10

Figure 2.2 Heat transfer from a hot surface to air by convection. 11

Figure 2.3 Blackbody radiation represents the *maximum amount of radiation.* 13

Figure 2.4 Energy balance on asphalt pavement surface in open space. 15

Figure 2.5 Energy balance on asphalt pavement surface in road tunnel 16

Figure 2.6 Specific heat is the energy required to raise the temperature of a unit mass of a material by one degree. 17

Figure 2.7 A simple experimental setup to determine the thermal conductivity of a material. 19

Figure 3.1 YNU Wind-Tunnel and it's working section 26

Figure 3.2 (a) Clearing grass to access the system, (b) Boiler, (c) Water Tank, (d) Heat Exchanger that generates hot temperature inside the wind-tunnel by heated water flow loop. 28

Figure 3.3 Scheme of the experimental procedure. 28

Figure 3.4 Data Logger TDS-530 29

Figure 3.5 K-Type of Thermometer. 29

Figure 3.6 Six types of asphalt specimens for test. 31

Figure 3.7 Specimen dimensions and embedded thermometers. (a) thermometer locations at specimens: #1, 2 & #4. (b) thermometer locations at specimens: #3, 4 & #6. 31

Figure 3.8 Three kinds of adhesive materials to attach thermometer on a surface. 32

Figure 3.9 Test for three kinds of adhesive materials and their results. The correctness of the surface temperature that was measured by the clay-attached thermocouple was confirmed by an infrared temperature gun. 33

Figure 3.10 Experimentally measured results of the surface and internal temperature increments of the 6 types of asphalt concrete specimens. 36

Figure 3.11 Comparison of temperature increments between asphalt type depths at final time (3hours). 36

Figure 3.12. One-dimensional asphalt model with boundary conditions. 38

Figure 3.13. Finite difference discretization of the 1D heat equation. 39

Figure 3.14 Generated points from raw data for simulation. 15 points were created between each known value. 41

Figure 3.15 Comparison of measured and calculated temperature increments of each AC specimen locations. 45

Figure 3.16 Temperature fit at final time of 6 types of AC specimens with their accuracy values. 46

Figure 4.1 Two types of AC specimens for the test in the 2nd Stage of Wind-Tunnel Experiment. The wires are thermocouples attached to the surfaces for measurement of the surface temperature. 52

Figure 4.2 Lamp radiation system to heat AC specimens. 52

Figure 4.3 Graph of induced wind velocity by the passage of ordinary car. 54

Figure 4.4 Test set up. 55

Figure 4.5 Experimentally measured results of temperature increments of AC#4 & AC#5 58

Figure 4.6 Comparison of the surface temperature differences at final time (2h) 59

Figure 4.7 Variation of heat transfer coefficients with respect to wind 60

Figure 4.8 Variation of radiated heat amount with respect to wind. 61

Figure 4.9 Traffic volume and vehicle speed before and after the lane increase at the Itabashi/Kumanocho junction. 62

Figure 4.10 Temperature increase due to the increase of vehicles speeds in Yamate Tunnel. 62

Figure 4.11 Variation of the RMSE values with respect to wind. 63

Figure 4.12 Variation of combined heat transfer coefficients with respect to water-spray. 64

Figure 4.13 Variation of radiated heat amount with respect to water-spray..... 65

Figure 4.13 Variation of the RMSE values with respect to water-spray amount. 66

Figure 4.12 Temperature cooling under seven types of wind speed without water effect. 68

Figure 4.13 Temperature cooling under seven types of watering at the wind speed 2.4m/s. 68

Figure 4.14 Temperature cooling under seven types of watering at the wind speed 4m/s. 69

Figure 4.15 Temperature cooling under seven types of watering at the wind speed 5.3m/s. 69

Figure 4.16 (a) Water-sprayed asphalt specimen surfaces, (b) Created tunnel-environment to measure the generated humidity by water-spray. 70

Figure 4.17 Effects of “tunnel-environment” condition without the influence of wind speed. 71

Figure 4.18 Effects of the watering at the wind speed 2.4m/s under the “tunnel-environment” condition. 71

Figure 4.19 Effects of the watering at the wind speed 5.3m/s under the “tunnel-environment” condition. 72

Figure 5.1 Scheme of the test conditions with two types of concrete base thicknesses . 72

Figure 5.2 Scheme of the test condition with steel plate base 73

Figure 5.3 Scheme of the test condition with steel plate & H-beams base..... 73

Figure 5.4 Scheme of the test condition with steel plate & H-beams base..... 73

Figure 5.5 Comparison of surface temperature decrements of all “different base and water spray” test cases. 74

Figure 5.6 Comparison of surface temperature decrements of all “different base and water spray” test cases. 75

Figure 5.7 Overall traffic volume in Yamate Tunnel at summer season 76

Figure 5.8 Model of Yamate Tunnel for simulation 76

Figure 5.9 Mesh quality 77

Figure 5.10 Temperature distribution in Yamate Tunnel with ordinary asphalt type 78

Figure 5.11 Temperature distribution in Yamate Tunnel with water-holding asphalt type 79

Figure 5.12 Temperature probe of two points at wind and water-spray effects, AC #4. 80

Figure 5.13 Temperature probe of two points at wind and water-spray effects, AC #5. 81

Figure 5.14 Comparison of wind and water-spray approaches between AC #4 and AC #5 at 150cm..... 81

Figure 5.15 Comparison of wind and water-spray approaches between AC #4 and AC #5 at 30cm..... 82

Figure 5.16 Model of Yamate Tunnel with Vehicle heat source..... 83

Figure 5.17 Mesh information 83

Figure 5.18 Temperature and Air Velocity plot. Ordinary asphalt type - #4 84

Figure 5.19 Temperature and Air Velocity plot. Water-holding porous asphalt type - #5 85

Figure 5.20 Prediction model of the temperature in “Yamate Tunnel”. 85

Figure 5.20 Temperature distribution in Yamate Tunnel (Inner Track, 6/1 12:00)..... 86

Figure 5.21 Heat flux distribution in Yamate Tunnel (Inner Track, 6/1 12:00) 87

Figure 5.22 Heat distribution percentage in Yamate Tunnel (Inner Track, 6/1 12:00) .. 88

Figure 5.23 Heat flux distribution and heat distribution percentage in Yamate Tunnel (Outer Track, 6/1 12:00) 88

Figure 6.1 Model of Yamate Tunnel with water-pipe approach..... 94

Figure 6.2 Application of Liquid Nitrogen to extremely suppress the asphalt pavement temperature in order to decrease the hot air temperature inside a tunnel. 94

List of Nomenclatures

English Symbols

C	specific heat	[J/kg K]
k	thermal conductivity	[W m K]
h	heat transfer coefficient	[W m K]
L	thickness of asphalt	[m]
q	heat flux	[W/m^2]
T	temperature	[C^o]
t	time	[s]
x	space coordinate	[m]
N	total number of measurments	[-]
nt	total number of time steps	[-]

Greek Symbols

α	thermal diffusivity	[m^2/s]
ε	asphalt emissivity	[-]
α	asphalt absobtivity	[-]
ρ	asphalt density	[kg/m^3]

Subscripts

n	temeprature at specific location	(T_n)
air	temeprature of surrounding air	(T_{air})
$surf$	temperature of asphalt surface	(T_{surf})

Superscripts

i	temeprature at specific time step	(T^i)

List of Equations

(2.1) 10
(2.2) 12
(2.3) 13
(2.4) 17
(2.5) 19
(2.6) 19
(3.1) 37
(3.2) 37
(3.3) 37
(3.4) 38
(3.5) 39
(3.7) 40
(3.8a) 40
(3.8b) 40
(3.9) 40
(3.10) 40
(3.11) 41
(3.12) 41
(3.14) 42
(4.1) 59

CHAPTER I

1. INTRODUCTION

1.1 Background

The temperature of asphalt pavement surface can reach more than 60℃ due to absorbed solar radiation during summer days in Japan. The high temperature of road surface not only brings an AC to plastic deformation and rutting under traffic loads but also creates an uncomfortable environment for users and may even impact heatstroke on a human body (Yoshida et al., 2000).

In a road tunnel, the asphalt road surface is not affected by direct solar heat. However, its temperature rises due to the influence of vehicular exhaust heat especially when the tunnel is long and traffic volume is heavy (Fujimoto et al., n.d.). Since the asphalt pavement absorbs a large amount of heat generated by vehicles and keeps it for a long time and concurrently radiates it to surroundings, a high-temperature environment in the tunnel also continues for a long time. This phenomenon brings uncomfortableness for users, especially for motor-bikers and maintenance workers who have to run across the road tunnel sufficiently for a long time and stay inside during inspection and repairment jobs for a whole day, respectively.

Figure 1.1 Illustration of a biker and a worker in a road tunnel.

Yamate Tunnel, which is located in the center of Tokyo is facing this phenomenon.

It is the longest road tunnel in Japan with its length of 18.2km and the second-longest road tunnel in the world. Starting from near the Oi Junction in Shinagawa to Takamatsu in Toshima, the road tunnel is under the management of Shuto Expressway and it consists of two lanes in each direction (Figure 1.2). As the data of actual measurement shown in Figure 1.3, the temperature in the tunnel is approximately 15ºC higher than the outside temperature. Moreover, the average tunnel temperature is around 38ºC, and the highest temperature rises up to 42ºC. Interestingly, the asphalt surface temperature even dominates the temperature of the tunnel air up to 2ºC. This crucial situation is resulting in the user's claims, and thus, the owner is still in search of the optimum solution by conducting various types of countermeasures against hot temperature. The conducted countermeasures were installing a mist spray facility (Figure 1.4) so the high air temperature might cool down. Another one was increasing the ventilation volume. Spraying a mist can cool down the temperature, however, it increases the humidity level and generates a condensation (humid) on a vehicle side mirrors. Increasing the ventilation volume is effective by decreasing the air temperature 2~3ºC. But, it causes a large cost. Therefore, another way of a solution to decrease the high temperature inside the tunnel is essential which would be easily applicable and less cost.

Source: https://ringosya.jp/syutokou-yamatetonneru-kasai-0406-24751

Figure 1.2 Yamate Tunnel location between Oi Junction in Shinagawa to Takamatsu in Toshima, Tokyo.

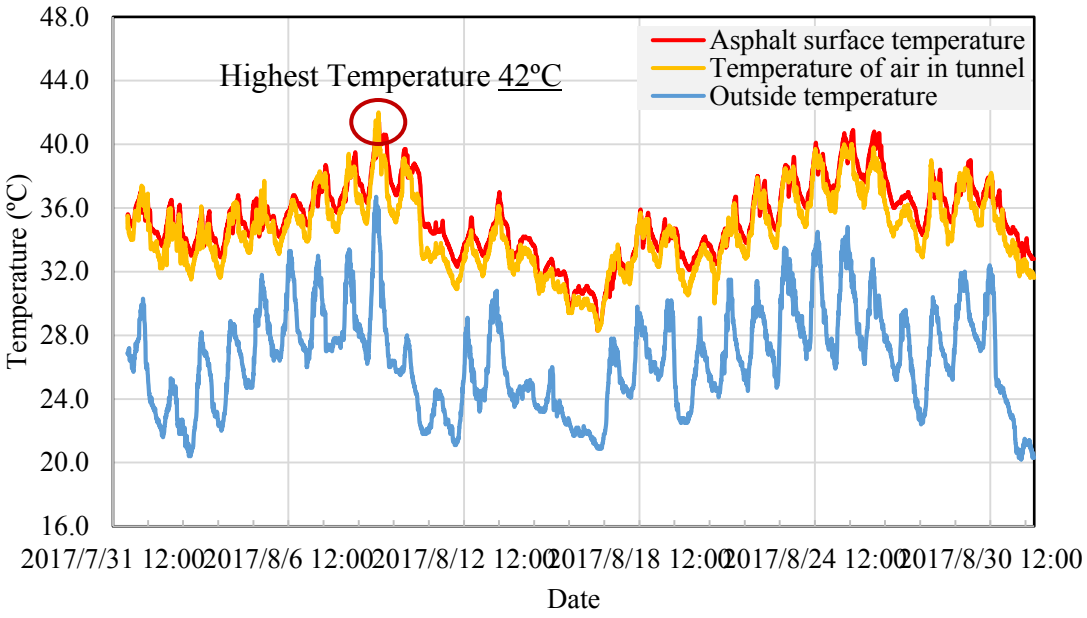

Figure 1.3 High temperature in Yamate Tunnel in summer season.

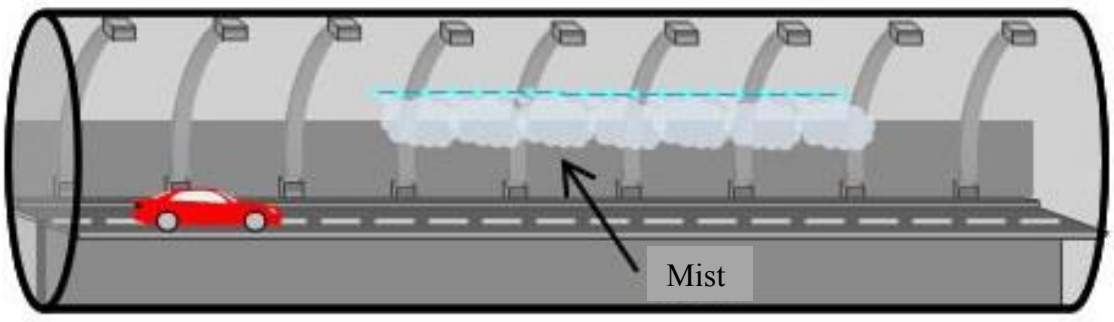

(a) Illustration of Mist-Spray facility

(b) Real case of mist spraying and generated humid on a car side mirror.

Figure 1.4 Countermeasures against high temperature in Yamate Tunnel.

Figure 1.5 Illustration of ventilation system in road tunnel

1.2 Motivations

When our team measured the temperature distribution by a thermal camera inside the Yamate Tunnel in the summer season, the air temperature rose to more than 40°C and the temperature of the asphalt surface was even higher than other parts of the tunnel as shown in Figure 1.6. The one-month data of the actual measured temperature by Shuto Expressway (Figure 1.7) also confirms the asphalt temperature dominance at any time of a day. From this, it is clear that the high temperature of asphalt pavement largely contributes to becoming high temperature inside the tunnel. Therefore, it was important to analyze the thermal characteristics of asphalt pavement and obtain their accurate thermal parameters. As reviewing the previous researches on this topic, many works can be found on identifying thermal characteristics and parameters by considering the solar radiation as a heat source. However, no works can be found that consider tunnel conditions. Because, the asphalt pavement in a tunnel does not affect by solar radiation, and it experiences thermal attack mostly by vehicle, i.e., vehicle passage, tire friction or engine radiant heat. Thus, it was interesting as well to study on this new topic to contribute to mitigating the hot temperature in the Yamate Tunnel.

(a) Normal case

(b) Taken by Thermal Camera

Figure 1.6 Temperature distribution in Yamate Tunnel taken by thermal camera.

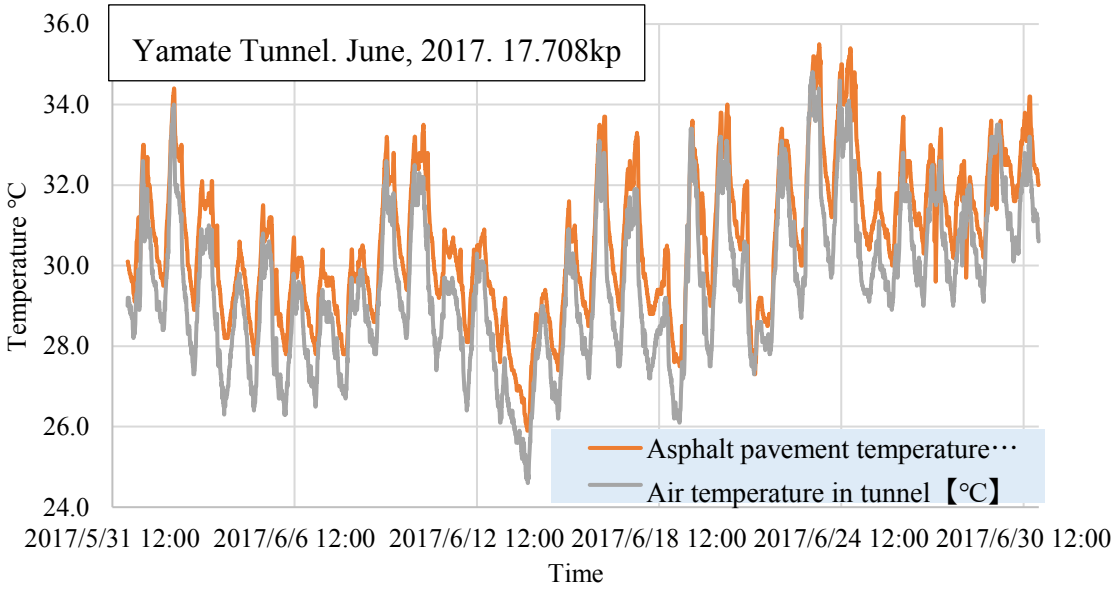

Figure 1.7 Measured temperature in Yamate Tunnel. June, 2017.

1.3 Research Objectives

Our study aimed to estimate the thermal parameters of the various types of asphalt concrete (AC) and investigate their effects on a high-temperature pavement surface. Furthermore, high wind speed and water spray effects are considered to be clarified as will be detailed in Chapter 3. Finally, several approaches to mitigate the hot surface temperature of asphalt pavement and effective AC type have to be proposed. The list of goals and objectives are summarized below:

Goal #1. Wind Tunnel Experiment Stage #1.

✧ In the Experiment Stage #1, six types of AC specimens will be tested in a wind-tunnel where a hot temperature air inside is generated by a forced circulation boiler system. The obtained results of temperature profile will help to calculate the thermal parameters of each type of AC numerically. The thermal parameters are: *thermal conductivity*, *thermal diffusivity, specific heat capacity,* and *heat transfer coefficient.* Accurate values of these parameters are essential for managing heat flows and mitigating a high surface temperature.

Goal #2. Wind Tunnel Experiment Stage #2.

✧ In the second experiment stage, ordinary (dense-graded) asphalt specimen and water-holding porous asphalt specimen will be examined under the effect of high wind speed and water spray to compare the effectiveness of these two types. Additionally, based on the obtained experimental data, the values of heat transfer coefficient varying with respect to wind speed will be calculated. Also, the amounts of radiated heat transfer from the AC will be compared. These values are beneficial to check and control a heat flow inside the Yamate Tunnel.

Goal #3. Countermeasures against high temperature.

✧ The effects of different basement boundary conditions and water spray on the surface temperature will be investigated to find effective countermeasures to decrease the surface temperature of AC in the tunnel. Finally, the heat balance and the temperature distributions inside the tunnel will be visualized by making a 3D model of Yamate Tunnel through the simulations. The simulation results help to control the ventilation volume optimally.

1.4 Organization of the Dissertation

The main body of this dissertation has six chapters. The organizations are as follows:

Chapter 1: Give general information regarding the Yamate Tunnel. Besides, the issues that the tunnel is facing. Also, talk about the countermeasures that have been conducted to improve the situation. Then, the necessity of this research will be addressed. Finally, this chapter clearly defines the research motivations, aim and objectives.

Chapter 2: A general background of the current state of research on the heat identification of thermal parameters of asphalt concrete will be presented. It also includes the basics of heat transfer mechanisms as like conduction, convection, and radiation. Besides, the identification technique of the asphalt concrete thermal parameters (specific heat, heat conductivity, heat diffusivity, and heat transfer coefficient) will be explained.

Chapter 3: This chapter contains the main goal of this study and has the biggest volume among other chapters. In this chapter, the test of six types of AC specimens where will be tested in wind-tunnel where a hot temperate air inside is

generated by a forced circulation boiler system. Based on the obtained experimental data, numerical simulations will be performed to derive thermal parameters of each asphalt type. Additionally, the results of the obtained thermal parameters will be compared with prior studies.

Chapter 4: Two types of AC specimens: ordinary type AC (dense-graded) and water-holding porous AC will be tested in the wind-tunnel under the wind and water spray effect to analyze the efficiency of water-holding porous asphalt at the high air temperature. The specimens will be heated by the direct radiative heat lamps. Based on the obtained experimental data, the values of heat transfer coefficients (h) will be numerically calculated. These values are essential and useful in controlling the temperature rise in a road tunnel Finally, the test under "Tunnel-Environment condition" will be performed to check the temperature changes as well as the humidity fluctuation at the air adjacent to the asphalt specimen surfaces.

Chapter 5: In this chapter, the effects of different basement boundary conditions and water spray on the surface temperature were investigated to find effective countermeasures to decrease the surface temperature of AC in the tunnel. Additionally, 2D model of heat transfer simulations of Yamate Tunnel considering asphalt type effects including the wind and water-spray approaches were performed to investigate the effects of water-holding porous asphalt to decrease the hot air temperature in the Tunnel. Then, it was extended to the model with vehicle heat sources. Finally, analyses were performed to analyze the heat distribution percentage in Yamate Tunnel.

Chapter 6: Major conclusions obtained from the previous chapters are summarized and several prospects for future researches have been proposed.

CHAPTER II

2. GENERAL BACKGROUND

2.1 Heat Transfer Mechanisms

The heat is defined as the form of energy that can be transferred from one body to another as a result of temperature difference. The science that acts to determine the rates of such energy transfers is the heat transfer. The main regulation in heat transfer is that the heat always flows from the higher-temperature medium to the lower-temperature one, and heat transfer stops when the two mediums reach the same temperature. The modes of heat transfer are categorized into three different modes: conduction, convection, and radiation. All these modes of heat transfer need the existence of a temperature difference, and all modes move from the high-temperature medium to a lower-temperature medium. A brief description of each mode is given below.

2.1.1 Conduction

Conduction is the process of transferring energy from the more energetic particles of a substance to the less energetic ones as a result of interactions between the particles due to the difference of temperature between adjoining regions. Conduction can take place in solids, liquids, or gases and the conductivity rate varies between materials due to the nature of the existence of atom and molecules. It is found to be highest in metallic solids, followed by non-metallic solids and it is lower in all kinds of liquids and lowest in all gaseous materials. There are a few factors which affect the outcome of conduction and the rate at which this conduction takes place. These are as follows:

1) The conducting material

2) Cross-section of the conducting material

3) Length of the conducting material

4) Temperature difference between the different zones of the material

When we consider steady heat conduction through a large plane wall of thickness $\Delta x = L$ and area A as shown in Figure 2.1, the temperature difference across the wall is $\Delta T = T_{hot} - T_{cold}$. Experiments showed that the rate of heat transfer $\dot{Q}$ through the wall is doubled when the temperature difference ΔT across the wall or the area A normal to the direction of heat transfer is doubled. But it is halved when the wall thickness L is doubled. Thus, it is concluded that the rate of heat conduction through a plane layer is proportional to the temperature difference across the layer and the heat transfer area, but is inversely proportional to the thickness of the layer. This is called Fourier's law of heat conduction after J. Fourier, who reported it first in his heat transfer text in 1822. The equation is:

$$\dot{Q}_{cond} = -kA\frac{dT}{dx} \quad (W) \tag{2.1}$$

where the k is the thermal conductivity of the material (constant of proportionality), which is *a measure of the material ability to conduct heat.*

Here dT/dx is the temperature gradient, which is the slope of the temperature curve on a T-x diagram which indicates the change of temperature with respect to x-direction at location x. The relation above specifies that the rate of heat conduction in a direction is proportional to the temperature gradient in that direction. Heat is conducted in the direction of decreasing temperature, and the temperature gradient becomes negative when temperature decreases with increasing x. The negative sign in Equation 2.1 assures that heat transfer in the positive x-direction is a positive quantity.

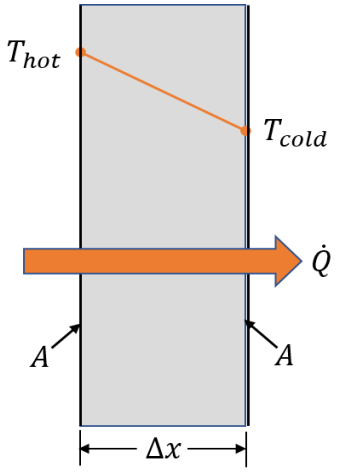

Figure 2.1 Heat conduction through a plane wall of thickness *x* and area *A*.

2.1.2 Convection

Convection is the mode of energy transfer between a solid surface and the adjoining gas or liquid that is in motion, and it involves the combined effects of conduction and fluid motion. The faster the fluid motion, the greater the convection heat transfer. In the absence of any bulk fluid motion (bulk fluid motion is simply motion in a fluid which contains mass or fluid particles), heat transfer between a solid surface and the adjacent fluid is by pure conduction. The presence of bulk motion of the fluid increases the heat transfer between the solid surface and the fluid, but it also complicates the determination of heat transfer rates.

As shown in Figure 2.2, cooling of a hot solid material by blowing cool air over its top surface is illustrated. Energy is first transferred to the air layer adjacent to the solid by conduction. This energy is then carried away from the surface by convection, that is, by the combined effects of conduction within the air that is due to the random motion of air molecules and the bulk or macroscopic motion of the air that removes the heated air near the surface and replaces it by the cooler air.

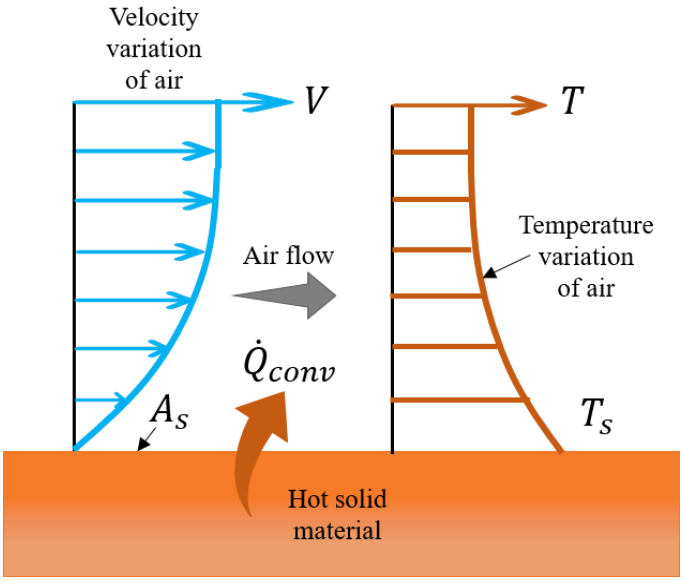

Figure 2.2 Heat transfer from a hot surface to air by convection.

If the fluid is forced to flow over the surface by an external cause such as a fan, pump, or the wind, then it is called *forced convection*. In contrast, convection is called *natural (or free) convection* if the fluid motion is caused by buoyancy forces that are induced by density differences due to the variation of temperature in the fluid. For

example, natural convection occurs when there is no fan at the heat transfer from the surface of the hot solid to air as shown in Figure 2.1. In this case, since any motion in the air will be due to the rise of the warmer (and thus lighter) air near the surface and the fall of the cooler (and thus heavier) air to fill its place. Heat transfer between the solid and the surrounding air will be by conduction if the temperature difference between the air and the block is not large enough to overcome the resistance of air to move.

Despite the complexity of convection, the rate of convection heat transfer is observed to be proportional to the temperature difference and is handily expressed by **Newton's law of cooling** as

$$\dot{Q}_{conv} = hA_s(T_s - T_\infty) \quad (W) \tag{2.2}$$

where h is the *convection heat transfer coefficient* in W/m^2 °C or Btu/h ft^2 °F. A_s is the surface area through which convection heat transfer occurs, T_s is the surface temperature and T_∞ is the temperature of the fluid sufficiently far from the surface. Should be noted that at the surface, the fluid temperature equals the surface temperature of the solid.

2.1.3 Radiation

Radiation is the energy emission by as electromagnetic waves or as moving subatomic particles that results of the changes in the electronic configurations of the atoms or molecules. In contradistinction to conduction and convection, the transfer of energy by radiation does not require the presence of an intermedium. In point of fact, energy transfer by radiation is fastest (at the speed of light), and it experiences no damping in a vacuum. This is how the sun energy reaches the earth.

In heat transfer studies we are interested in thermal radiation, which is the form of radiation emitted by bodies because of their carrying a temperature. It differs from other forms of electromagnetic radiation such as x-rays, radio waves, gamma rays, television waves, and microwaves, that are not related to temperature. All bodies at a temperature above absolute zero emit thermal radiation.

The rate at which a body radiates (or absorbs) thermal radiation depends on the nature of the surface. Materials that are good emitters are also good absorbers (Kirchhoff's radiation law). A surface is an excellent emitter as well as an excellent

absorber if its surface is blackened. If the same surface is silvered, it becomes less emitter and less absorber as well. A blackbody is one that absorbs all the radiant energy that is incident. Such a perfect absorber is also obviously a perfect emitter. The maximum rate of radiation that can be emitted from a surface at an absolute temperature Ts (in K) is given by the **Stefan–Boltzmann law.** That is

$$\dot{Q}_{emit} = \varepsilon \sigma A_s T_s^4 \quad (W) \tag{2.3}$$

where $\sigma = 5.67x10^{-8}$ (W/m2 · K^4) is the **Stefan–Boltzmann constant.** Blackbody radiation represents the maximum amount of radiation that can be emitted from a surface at a specified temperature (Figure 2.3). ε is the **emissivity** of the surface and it ranges between 0 ~ 1. The emissivities of common materials are given in Table 2.1.

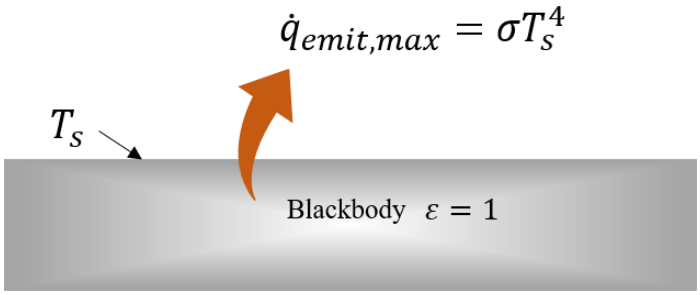

Figure 2.3 Blackbody radiation represents the *maximum amount of radiation.*

Another important radiation property of a material is its **absorptivity** α, which is the part of the incident radiation energy that is absorbed by the surface. Similar to emissivity, its value is in the range between 0 ~ 1.

The difference between the rates of radiation emitted and the radiation absorbed by the surface is the net radiation heat transfer. If the rate of absorbed radiation is greater than the rate of the emitted radiation, the surface gains energy by radiation. Otherwise, the surface loses energy by radiation. In general, the establishment of the net rate of heat transfer by radiation between two surfaces is a complicated theme. Because, it depends on the properties of the surfaces, their orientation relative to each other, and the interaction of the medium between the surfaces with radiation.

Table 2.1 Emissivities of common materials at temperature 300 K

Materials	Emissivity
Asphalt pavement	0.85–0.93
Concrete	0.92~0.95
Wood	0.82–0.92
Red brick	0.93–0.96
Aluminum foil	0.07
Anodized aluminum	0.82
Polished copper	0.03
Polished gold	0.03
Polished silver	0.02
Polished stainless steel	0.17
Black paint	0.98
White paint	0.90
White paper	0.92–0.97
Human skin	0.95
Soil	0.93–0.96

2.2 Energy Balance in Asphalt Pavement

Generally, the temperature profile in asphalt pavements in the outside roads is affected directly by the environmental conditions such as incident solar energy, wind, and precipitations. The primary modes of the heat transfer are incident solar radiation (short wave), thermal radiation (long-wave) between the pavement surface and sky, convection due to heat transfer between the pavement surface and the fluid (air or water) that is in contact with the surface, and conduction inside the pavement as shown in Figure 2.4

However, in the tunnel the environment and heat sources are different. There is no solar heat. Instead, there is a heat generates by a vehicle passage, vehicle exhaust heat, tire friction, and engine radiant heat. Another difference is the base layer of asphalt

pavement is typically made by concrete in tunnels, unlike outside road pavements that base layers are generally composed by aggregates.

The surface energy balance on the pavement consists of the sum of all heat gains through the surface equal to the heat conducted in the pavement. The direction of the heat flux due to convection and thermal radiation is dependent on the temperature difference between the pavement surface and the bulk air temperatures. In case, where the bulk air temperature is lower than the pavement surface temperature, a cooling of the surface occurs while the surface might simultaneously be heated through incident solar radiation or vehicle exhaust heat. Thus, depending on the magnitudes of individual heat rates, heating or cooling of the pavement takes place.

A bottom surface of pavement can be assumed as adiabatic if its thickness is sufficiently thick and thus, no heat transfer between the pavement and sub-grade layers occurs. Similarly, side surfaces of the pavement (pavement edges) are considered to be adiabatic for sufficiently large horizontal road expansions. Because, temperature changes in the vertical direction will be much greater than horizontal changes, and thus any heat transfer through pavement edge surfaces can be neglected.

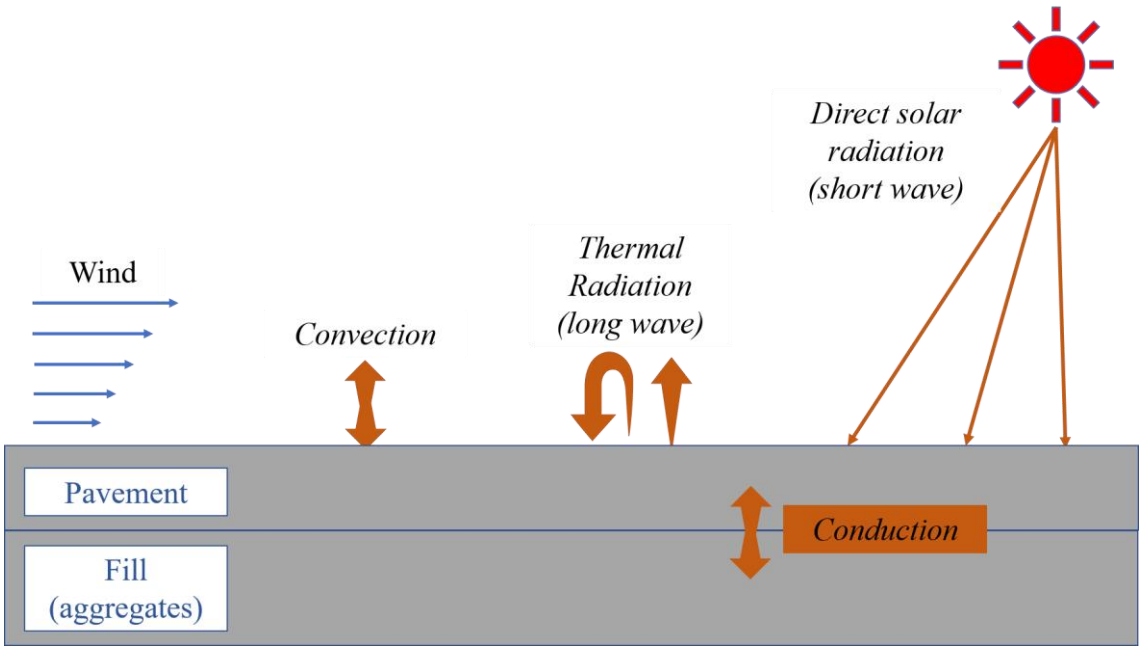

Figure 2.4 Energy balance on asphalt pavement surface in open space.

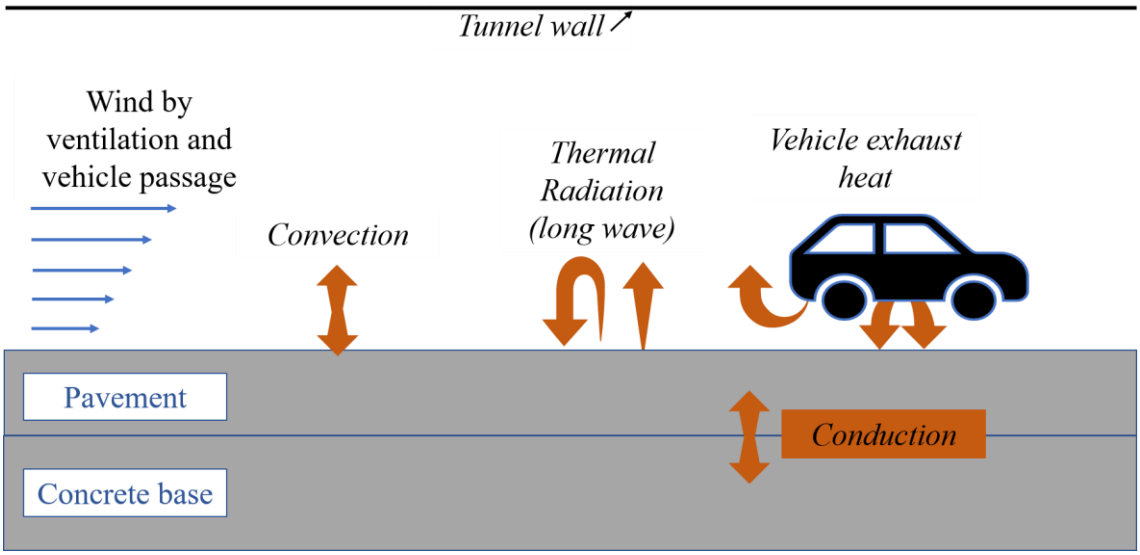

Figure 2.5 Energy balance on asphalt pavement surface in road tunnel

2.3 Thermal Parameters and Identification Techniques

Last several decades, many researchers have studied the identification of thermal parameters such as specific heat capacity, thermal conductivity, and heat transfer coefficient of asphalt pavements as well as other materials. These parameters can be determined by actual measurements or laboratory experiments using various types of sensors and equipment as well as through mathematical calculations.

2.3.1 Specific Heat

The different materials store heat differently depending on their nature, and the specific heat property (C_p) measures a material's ability to store thermal energy. In other word, *Specific Heat* is defined as the energy required to raise the temperature of a unit mass of a material by one degree (Figure 2.6). For example, $C_p = 4.18 kJ/kg \cdot °C$ for water and $C_p = 0.45 kJ/kg \cdot °C$ for iron at room temperature, which indicates that water can store almost 10 times the energy per unit mass than iron.

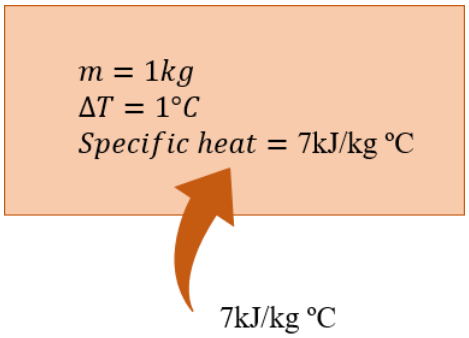

Figure 2.6 Specific heat is the energy required to raise the temperature of a unit mass of a material by one degree.

A material called an **incompressible material** whose specific volume (or density) does not change with temperature or pressure. Major solid's and liquid's specific volumes essentially remain constant during a process, and thus they can be approximated as incompressible material without sacrificing much in accuracy. The specific heats of incompressible materials depend on temperature only. Hence, the change in the internal energy ΔU of solids and liquids can be stated as

$$\Delta U = mC_{ave}\Delta T \quad (J) \tag{2.4}$$

where C_{ave} is the average specific heat evaluated at the average temperature. As the equation 2.4 shows, the average specific heats can be determined very easily by measuring just the internal energy change of a system (if it remains in a single phase: liquid, solid, or gas during the process).

2.3.2 Thermal Conductivity

Similar to specific heat, the *thermal conductivity* k is a measure of a material's ability to conduct heat through it. For example, $k = 0.608W/m\cdot°C$ for water and $k = 80.2W/m\cdot°C$ for iron at room temperature, which indicates that iron conducts heat more than 100 times than water.

Equation 2.1 for the rate of conduction heat transfer under steady-state conditions can also be applied as the describing equation for thermal conductivity. Hence, the thermal conductivity of a material can be defined as the rate of heat transfer through a unit thickness of the material per unit area per unit temperature difference. A high value

for thermal conductivity indicates that the material is a good heat conductor, while a low value indicates that the material is a poor heat conductor or insulator. The thermal conductivities of some common materials at room temperature are presented in Table 2.2.

Figure 2.7 explains a simple experimental setup to determine the thermal conductivity of a material. A material with known thickness and area is heated from one side by a heater of specific heat capacity. If the other surfaces of the sample material are well insulated, and all the generated heat by the heater is transferred through the material, then its thermal conductivity can be determined by measuring the two surface temperatures of the material when steady-state heat transfer is reached.

Table 2.2 Thermal conductivities of common materials at room temperature

Material	Thermal Conductivity $k, W/m\cdot°C$
Diamond	2300
Silver	429
Copper	401
Gold	317
Aluminum	237
Iron	80.2
Concrete	1.6
Glass	0.78
Brick	0.72
Water	0.613
Human skin	0.37
Wood	0.17
Soft rubber	0.13
Glass fiber	0.043
Air	0.026

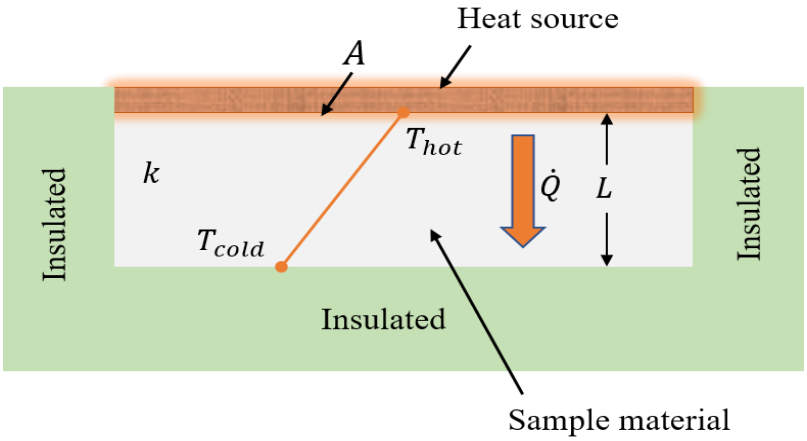

$$k = \frac{L}{A(T_{hot} - T_{cold})}\dot{Q} \qquad (2.5)$$

Figure 2.7 A simple experimental setup to determine the thermal conductivity of a material.

2.3.3 Thermal Diffusivity

The term ρC_p which is frequently appeared in heat transfer analysis is called the *heat capacity* of a material. Both the specific heat (m^2/s) and the heat capacity ρC_p represent the material heat storage capability. But C_p expresses it *per unit mass,* on the other hand, ρC_p expresses it *per unit volume,* as can be noticed from their units J/kg · °C and J/m^3 · °C, respectively. Another thermal property that arises in the transient heat conduction analysis is the *thermal diffusivity*, which represents how fast heat diffuses through a material and is defined as

$$\alpha = \frac{Heat\ conducted}{Heat\ stored} = \frac{k}{\rho C_p} \qquad (m^2/s) \qquad (2.6)$$

We know that the thermal conductivity k represents how well a material conducts heat, and the heat capacity ρC_p represents how much heat a material can store per unit volume. Accordingly, the thermal diffusivity of a material can be taken as the ratio of the heat conducted through a material to the heat stored per unit volume. A material with its high thermal conductivity or low heat capacity will have a large thermal diffusivity. The larger

the thermal diffusivity, the faster the propagation of heat into the medium. A small value of thermal diffusivity means that heat is mostly absorbed by the material and a small amount of heat will be conducted onward. Also, interestingly the thermal diffusivities of beef and water are the same. This is not surprising, because meat, as well as fresh fruits and vegetables are mostly water, and hence they own the thermal properties of water.

2.3.4 Heat Transfer Coefficient

Convection *heat transfer coefficient* h can be defined as the rate of heat transfer between a solid surface and an adjacent fluid per unit surface area per unit temperature difference. The convection heat transfer coefficient is not a property of the fluid. It is an experimentally determined parameter whose value depends on various aspects such as the surface geometry, the bulk fluid velocity, the properties of the fluid, and the nature of fluid motion. Typical values of h are given in Table 2.3.

Table 2.3 Typical values of convection heat transfer coefficient

Type of convection	Heat transfer coefficient $h, W/m^2 \cdot °C$
Free convection of gases	2-25
Free convection of liquids	10-1000
Forced convection of gases	25-250
Forced convection of liquids	50-20000
Boiling and condensation	250-100000

2.4 Literature Survey

A literature review was conducted to analyze the previous works done in the field of thermal parameter identifications of asphalt pavements as a function of thermal environmental conditions. The literature survey was focused basically on Japanese researcher works since this study was done in Japan focusing on seeking a solution to solve the issue occurring in Japan.

Thermal parameters of Asphalt Concrete were derived by many types of research

through various methodologies. Almost all of them were performed considering the open space road pavements where the dominant heat source comes from solar energy. No researches can be found on deriving of asphalt pavement properties considering a road in the tunnel, where no direct effect of solar energy.

Himeno et al. (1986) measured the temperature distributions in asphalt pavement with depth considering clear and cloudy weather for a year. They concluded that the difference of pavement structure does not affect surface temperature significantly, and pavement temperature is related not only to changes in air temperature but also to other climate parameters as solar radiation, wind velocity, and precipitation.

Kosaku et al. (2005) determined specific heat and thermal conductivities of four types of AC through experimental work mainly focusing on the water-holding pavement. The types of ACs are dense-graded AC, Low-noise type AC and two kinds of water-holding AC (A: containing calcium chloride, B: blast furnace slag type). Also, they measured the moisture desorption performances. They also concluded that the water-holding AC has a higher thermal conductivity when it is in wet condition.

Aoki, Yoshinaka, & Fujinami (2005) also obtained thermal parameters of four types of AC by field measurements considering weather forecast the measured asphalt pavement temperature profile through the back-calculation methods using the Gauss-Newton algorithm. They concluded the results as below:

a) Thermal diffusivity can be determined by giving the temperatures of the upper and lower surfaces of an asphalt specimen and performing inverse analysis so that the measured temperature and the simulated temperature match at the corresponding internal nodes.
b) The specific heat and the convective heat transfer coefficient can be estimated by using the weather forecast that is measured at the pavement surface. They confirmed that by using this result, the thermal diffusivity was also calculated, which was almost the same as the result of (a).
c) The validity of the estimated values was confirmed since the measured temperature, and the analyzed temperature were relatively well matched.
d) When the inverse analysis is carried out with the 3-layer model, the degree of matching of the temperature inside the dense-graded pavement was poor, however with the 4-layer model in which the roadbed was divided into two

at the sensor position, the degree of matching of the internal temperature was greatly improved.

Kawana et al. (2012) presented the predicting method of thermal parameters (heat capacity and heat transfer coefficient) using the measured data by two thermometers located on the upper and lower surfaces of pavement and one heat flux sensor located between them. They also performed back-calculation analyses to identify the thermal parameters and by using these values they estimated the surface temperature and compared it with the measured temperature.

Goto et al. (2009) examined the characteristics of four thermal properties such as heat capacity, specific heat, thermal conductivity, and thermal diffusivity not for the asphalt pavement, but sediments found in the eastern flank of the Juan de Fuca Ridge. The results showed that the thermal properties of clay sediments depend strongly on the distribution of porosity. The vertical distribution of the thermal properties of sand and mixed lithology is less variable; rather it was a constant porosity distribution of these lithologies with depth.

In this study, we estimated the thermal parameters of the six types of asphalt concrete (AC) and investigated their effects on a high-temperature pavement surface. All AC specimens types were tested in a wind-tunnel where a hot temperature air inside was generated by a forced circulation boiler system. In a road-tunnel, since the asphalt pavement experiences larger thermal attack mostly by vehicle, i.e., vehicle passage, tire friction or engine radiant heat, the present study focused on the asphalt itself, i.e., its thermal ability: thermal conductivity, thermal diffusivity, specific heat capacity, and heat transfer coefficient. Accurate values of these parameters are essential for managing heat flows and mitigating a high surface temperature.

2.5 Summary of Chapter 2

As we are engineers, we are often interested in the rate of heat transfer, which is the topic of the science of heat transfer. This chapter reviewed the fundamental concepts of thermodynamics that form the framework for heat transfer. First, the three basic mechanisms of heat transfer, which are conduction, convection, and radiation was generally introduced. Second, the energy balance in asphalt pavements was explained considering the boundary conditions and heat source differences in open space and inside

the tunnel, respectively. Next, as this study mostly focuses as well, the theory of thermal parameters such as specific heat, thermal conductivity, thermal diffusivity, and heat transfer coefficient was discussed including their identification methodologies. Finally, we close this chapter with a discussion of the literature survey that how the researchers previously determined the thermal parameters of asphalt concrete and consequently the significance of this study was presented.

References and Suggested Readings

Aoki, D., Yoshinaka, T., & Fujinami, K. (2005/12). A study of thermal parameter estimation for pavement. *J-STAGE, 10*, 225-231 (in Japanese).

Fujimoto, A., Saida, A., Fukuhara, T., & Futagami, T. Heat transfer analysis on road surface temperature near a traffic light. ResearchGate, Pub. No 268351732, n.d.

Goto, S., & Matsubayashi, O. (2009). Relations between the thermal properties and porosity of sediments in the eastern flank of the Juan de Fuca Ridge. Earth Planets Space. *61,* 863–870.

Himeno, K., Watanabe, T., & Suguro, F. (1986). Estimation of the temperature distribution in the asphalt pavement. *J-STAGE, 4,* No 366, 123-132 (in Japanese).

Kawana, F., Kawamura, N., & Matsui, K. (2012). Evaluation of pavement thermal properties using heat flux sensor. *J-STAGE, Vol. 68,* No 3, I_5- I_12 (in Japanese).

Kosaku, K., & Hiroshima, M. (2005). *Measurement of Specific Heat, Thermal Conductivity, and Diffusible Humidity for Water-absorptive Pavement*, (Report No. ISSN 0387-2416, 233-238). The Institute of Civil Engineering of the Tokyo Metropolitan Government (in Japanese).

Shutoko driver's website (2015). Countermeasures against high temperature in Yamate Tunnel. Retrieved from ttps://www.mathworks.com/help/matlab/ref/interp1.html

Siti, H., Syarifah, I., Salmia, B., & et al. (2017). Heat Lump in Different Pavement Layer Using Ethylene Glycol as A Solar Heat Collector. *MATEC Web of Conferences 87, 01015.*

Yoshida, N., Nishimura T., & Hino, Y. (2000). Experimental Study on Association of Surface Characteristics of Road Pavement with Surface Temperature. *J-STAGE, 29,* No 7, 66-74 (in Japanese).

Yunus A. Cengel, (Second Edition). Heat Transfer. A practical approach.

CHAPTER III

3. MEASUREMENT OF HEAT TRANSFER IN ASPHALT - I

Abstract

Wind-tunnel experiment (WTE) will be used as the main tool to conduct an investigation on the mechanisms of heat transfer in asphalt pavements. In this chapter, the detail of wind tunnel facilities as *boiler system*, *heat exchanger*, *lamp radiation* as well as the *test parameters* will be illustrated. Also, data-logger and thermometer type for the measuring of temperate will be illustrated. Besides, one-dimensional partial differential heat transfer equations and a finite difference approximation method to obtain thermal parameters of six asphalt types will be introduced. In the last section of this chapter, the results of the numerical analysis will be discussed and compared with the previous research results.

3.1 Experiment Stage #1

3.1.1 Introduction of experiment stage #1

In the 1st stage of the wind-tunnel experiment, the boiler system will be used as a heat generator to obtain temperature profiles of the six types of asphalt specimens. Every specimen will be isolated from all sides except the top surface to ensure that the heat comes only from the to side. No wind effects will be influenced. The hot temperature generated by the boiler system will keep constant value as much as possible. Measured temperatures will be applied to the numerical analysis as input parameters and boundary conditions.

3.2 Wind-Tunnel

3.2.1 Introduction

An open circuit wind-tunnel with a unique test facility of Yokohama National University (YNU), Japan was used to measure the thermal characteristics for various types of AC specimens. Figure 3.1 shows the general view (a) and the working section (b) of the wind-tunnel.

3.2.2 Dimensions

The size of the working section is 1.3m wide and 1.3m high. The wind tunnel can generate a uniform flow at high flow velocity of up to 20 m/s.

(a) General view of YNU Wind-Tunnel

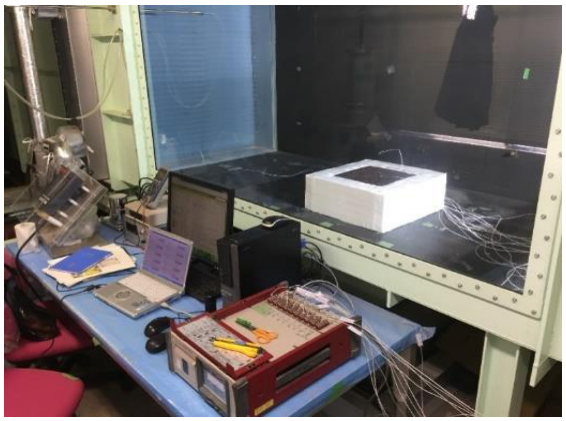

(b) Working Section

Figure 3.1 YNU Wind-Tunnel and it's working section

3.2.3 Tools

The wind-tunnel also has other tools that work together. They are: forced circulation (a) boiler system, lamp-radiation system, particle ejection system and rain-drop simulation system. Among these tools, the boiler system and the lamp-radiation system will be used in this study. The details will be explained in the next sections.

3.3 Boiler system

Preparation for the experiment started with the cutting grass by a sickle to access the system. The pictures of the forced circulation boiler system are shown in Figure 3.2. A detailed scheme of the experimental procedure is depicted in Figure 3.3. The system comprises a heated water flow loop and fixed asphalt specimen for test. A pump power causes the water to circulate in the pipe that passes through the boiler and the heat exchanger. Then, the air inside the wind-tunnel is heated. The temperature of the heated air can be adjusted by the temperature controller.

(a)

(b)

(c)

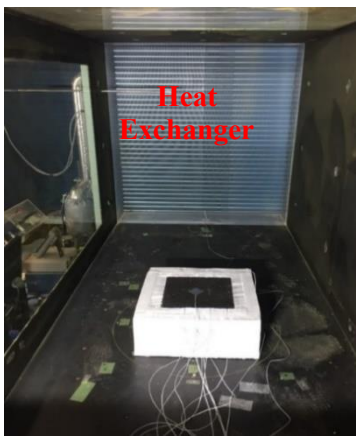

(d)

Figure 3.2 (a) Clearing grass to access the system, (b) Boiler, (c) Water Tank, (d) Heat Exchanger that generates hot temperature inside the wind-tunnel by heated water flow loop.

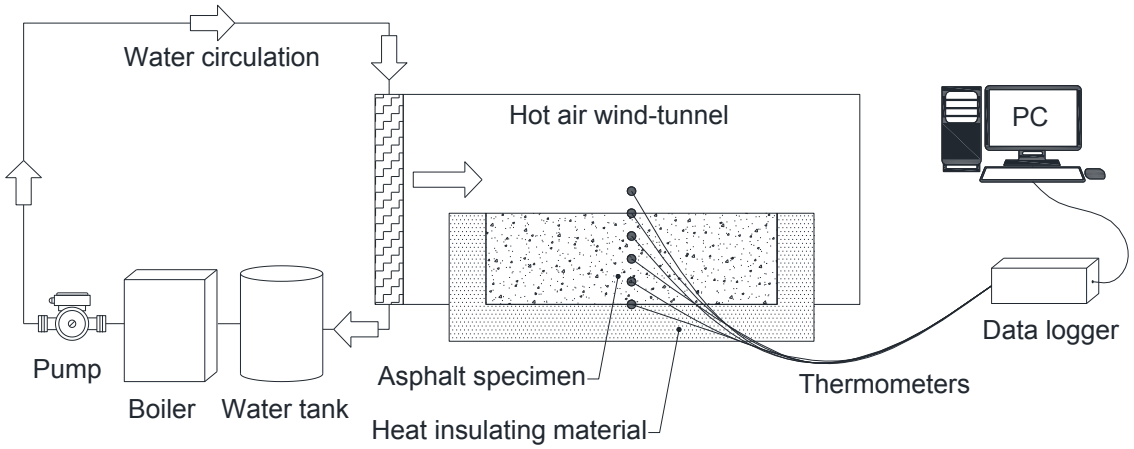

Figure 3.3 Scheme of the experimental procedure.

3.4 Data acquisition equipment

3.4.1 Data Logger

Data Logger TDS-530 was used for automatic measurement of the temperature (Figure 3.4). The thermometers that installed in specimens were contacted to this equipment. The Data Logger has operable display and touch panel. Moreover, it is also controlled by its software that can be installed in a PC. The measured data directly records in the PC in Microsoft Excel file, thus largely eases a job. The interface is equipped with Ethernet LAN, USB 2.0, RS-232C, and 30Channels, and it is possible to expand the channels up to 1000ch by external switch box. In this study, the temperature was measured every 10 seconds.

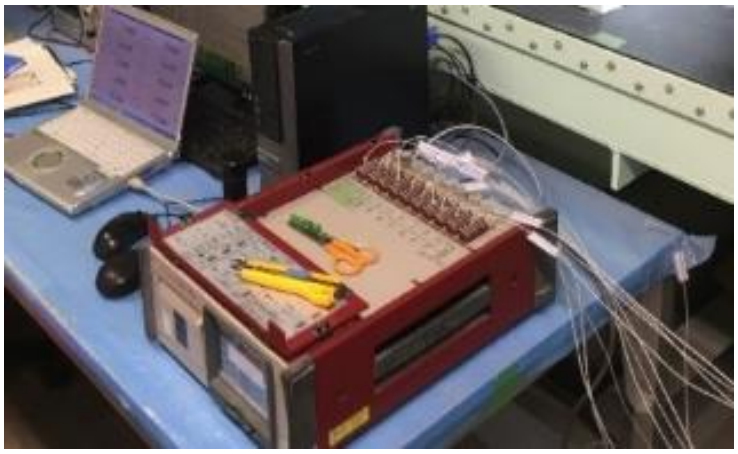

Figure 3.4 Data Logger TDS-530

3.4.2 Thermocouples

K-Type of thermometers were embedded inside at 3 locations and on top and bottom surfaces as well to measure the temperature increments. Installing a thermometer in a surface is a bit challengy, since the outside temperature may affect it. Our method of installing on a surface will be explained in section 2.6. The thermometer capacity is between -75°C to +480°C.

Figure 3.5 K-Type of Thermometer.

3.5 Asphalt Specimen Types

Six types of AC specimens were tested. Pictures of each asphalt type are illustrated in Figure 4. All specimens have same dimensions: 0.3m length x 0.3m wide x 0.08m thick. Four specimens consist of two layers: base and surface made by a different type of materials. The materials differ from each other basically in three types: dense-graded AC, coarse-graded AC, and water-holding porous AC. Specifics are summarized in Table 1.

Table 3.1 Asphalt specimen types and their layer thicknesses

#	Asphalt specimen types	Thickness of each layer (cm)	Density (kg/m^3)
1	Coarse-graded (Pen. Index: 40/60)	8	2407
2	Dense-graded (Polymer-modified - Type II)	8	2371
3	Surface: Coarse-graded (40/60) Base: Reproduced coarse-graded.	3 5	2407 2358
4	Surface: Dense-graded (Polymer-mod. - Type II) Base: Dense-graded (40/60)	3 5	2371 2384
5	Surface: Water-holding porous (Small size aggr. TH) Base: Dense-graded (Polymer-mod. - Type III-W)	4 4	2360 2251
6	Surface: Dense-graded + heat insulation unit Base: Dense-graded (40/60)	3 5	2512 2384

#1

#2

#3

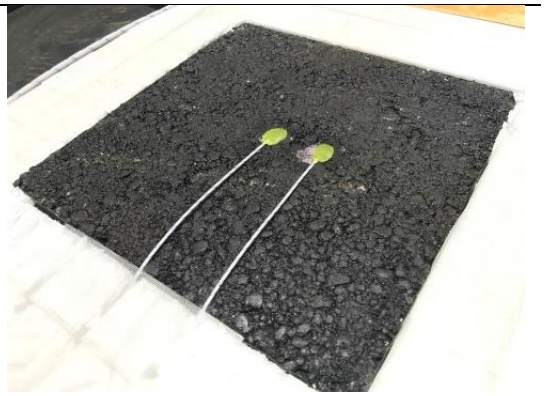

#4

#5 #6

Figure 3.6 Six types of asphalt specimens for test.

3.6 Thermocouple Installations

Type K thermometers were embedded in the vertical direction in 5 locations. Figure 3.7 shows the specimen dimensions and locations of embedded thermometers.

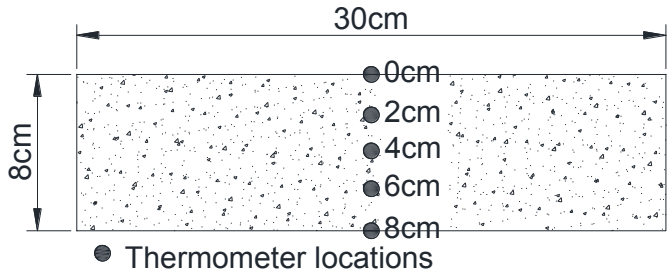

(a)

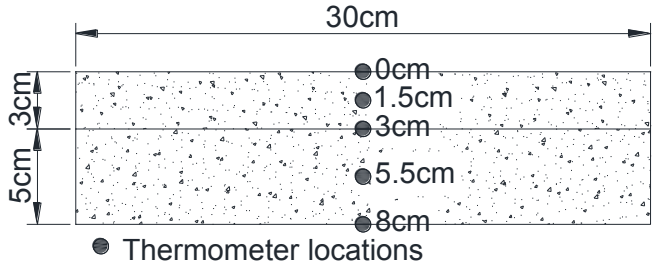

(b)

Figure 3.7 Specimen dimensions and embedded thermometers. (a) thermometer locations at specimens: #1, 2 & #4. (b) thermometer locations at specimens: #3, 4 & #6.

3.6.1 Adhesive materials

As briefly mentioned before, installing a thermometer in a surface is a bit challengy, since the outside temperature may affect it. Therefore, we have tested three kinds of adhesive materials: a) *glue,* b) *aluminum-tape* and c) *clay* to attach the thermometers on the AC specimens to identify the best one that can be less influenced by the outside temperature.

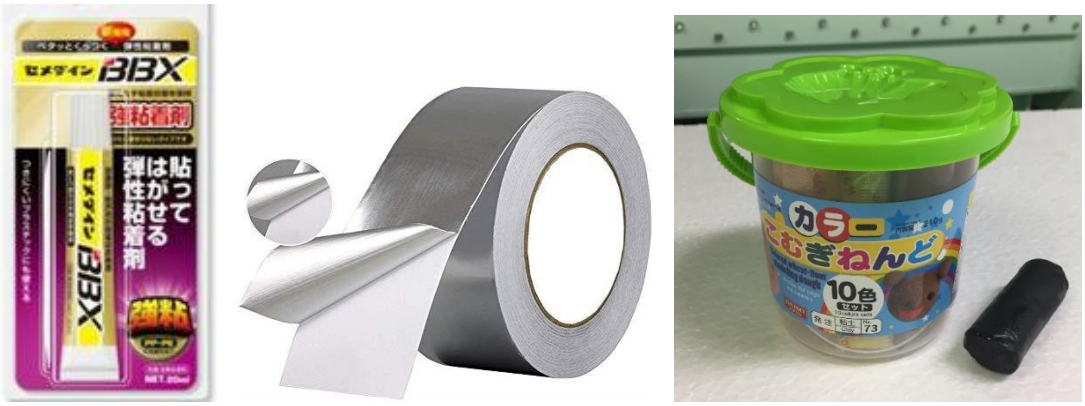

Figure 3.8 Three kinds of adhesive materials to attach thermometer on a surface.

3.6.2 Test for surface temperature accuracy

The thermometers on the upper and lower surfaces were examined for the accuracy of the surface temperature measurement. Because thermometers may get influenced by air temperature if they are not covered with proper adhesive material. As the test result is shown in Figure 3.9, the clay and aluminum tape give more accurate results while the glue shows affected temperature by the air temperate. Thus, the adhesive material of clay was chosen to be used for the subsequent experiments because of its durability and simplicity to use.

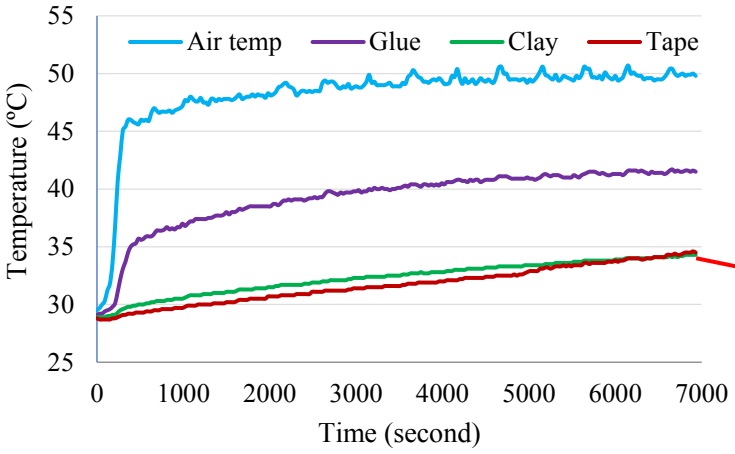

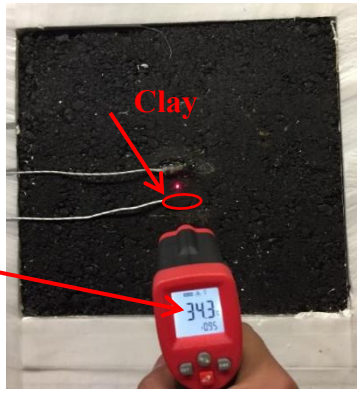

Infrared temperature gun measuring asphalt

Figure 3.9 Test for three kinds of adhesive materials and their results. The correctness of the surface temperature that was measured by the clay-attached thermocouple was confirmed by an infrared temperature gun.

3.7 Test for Each Type of Asphalt Concrete

3.7.1 Test setup

Bottom surface and side surfaces were covered with 10cm thick heat insulated material to ensure that the heat would be transferred one-dimensionally only from the upper surface. The air temperature inside the wind-tunnel was controlled to be around 53°C (±2°C) due to the control system. Insignificant wind (wind speed less than 0.1m/s) from the heat exchanger side was applied to cause the air circulation in the wind-tunnel. The air temperature was measured at the 10cm high from the specimen surface to implement on numerical calculations. The temperature was recorded at every 10 seconds for totally 12000seconds (about 3.3 hours).

3.7.2 Results

Figure 7 shows the experimental results of the transient temperature profile of the six types of asphalt specimens. The initial air temperatures were the same as specimen's initial temperatures and once the heating started, the air temperatures quickly increased. The surface and internal temperatures increased keeping the same rate with the increase of the time till the final time 10800seconds (3hours). The comparison of temperature increments of each depth between each asphalt type at final time is plotted in Figure 8.

Here, one layered specimens AC #1, #2 revealed 1~2℃ higher top surface temperature increments than the specimens with two layers AC #3, #4, even the content of the materials were the same. It can be explained the small air gap between the two layers affected the heat to be transferred poorer due to the low conductivity of the air (Engineering ToolBox, 2003). AC #5 and #6 showed similar surface temperature increments but 1℃ lower than the one layered specimens. The temperature increments at the internal and bottom locations remained close and did not differ significantly among the specimen types.

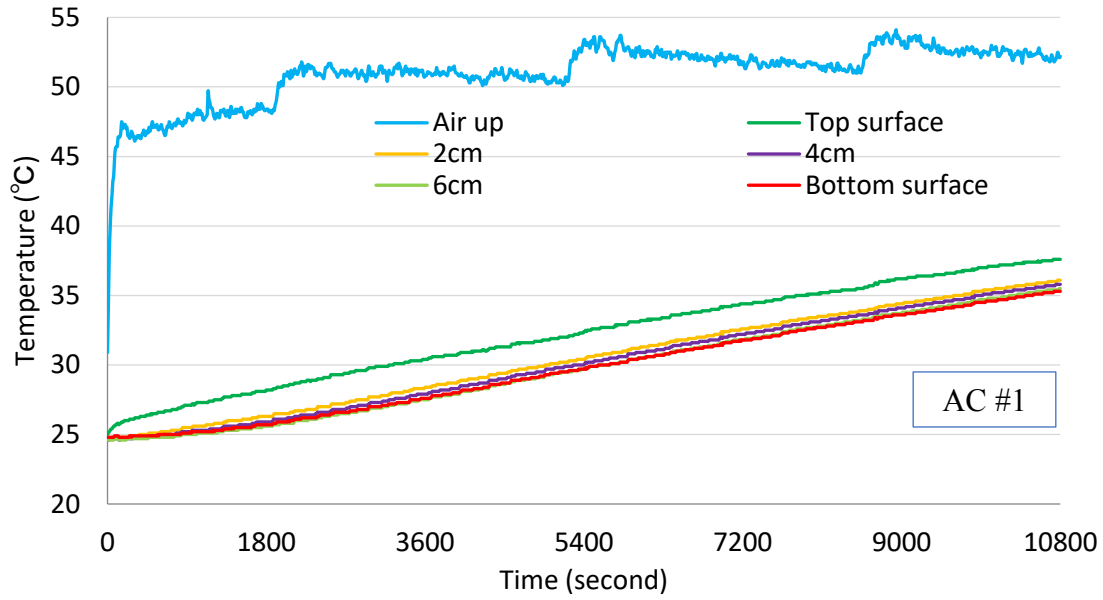

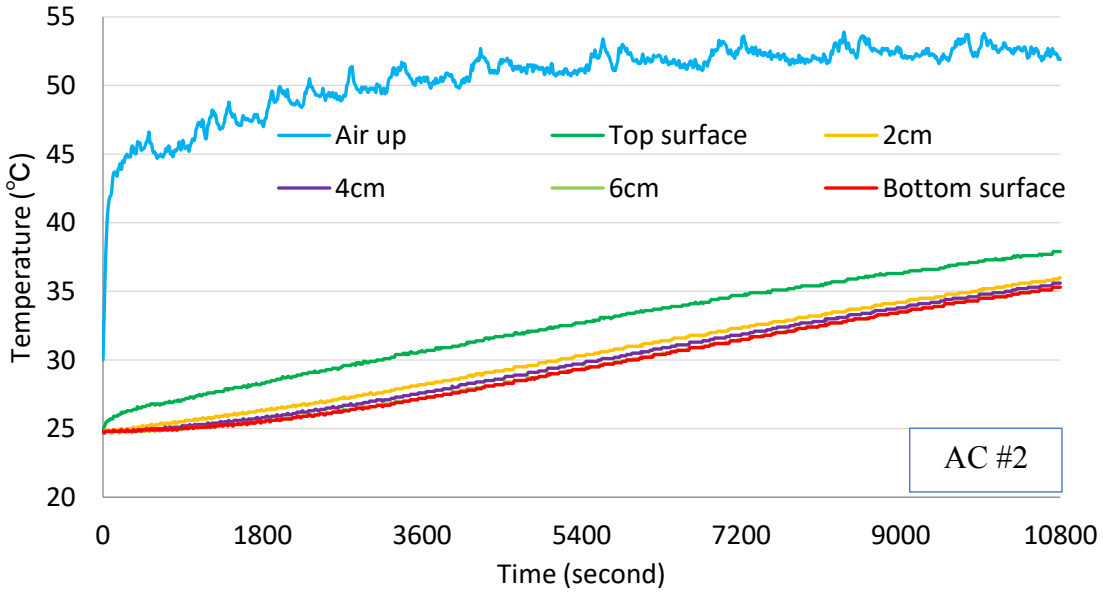

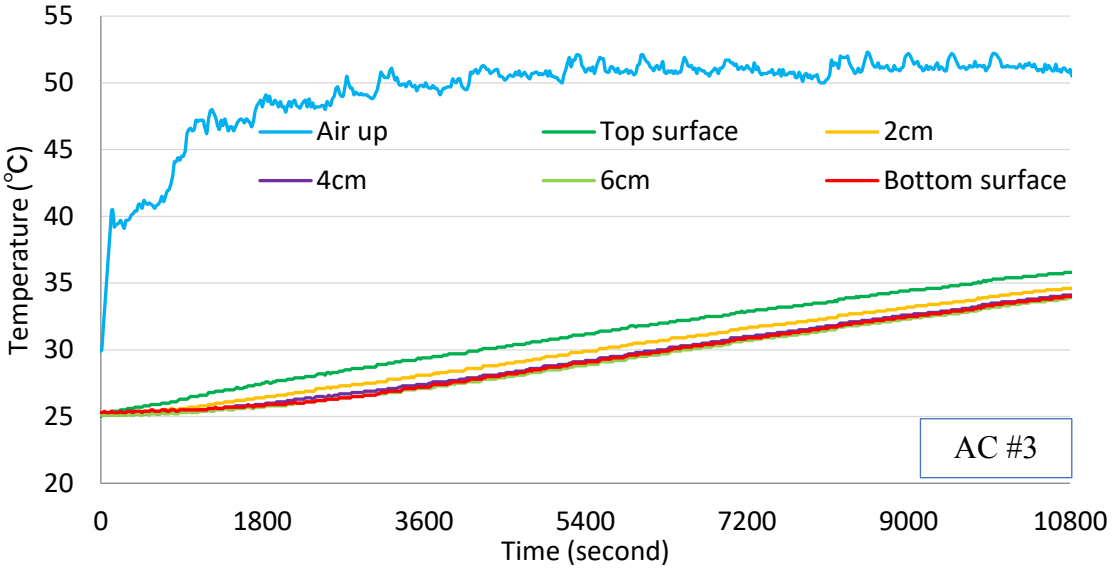
55
50
45
40
35
30
25
20
Temperature (°C)
Air up
Top surface
2cm
4cm
6cm
Bottom surface
AC #3
0
1800
3600
5400
7200
9000
10800
Time (second)

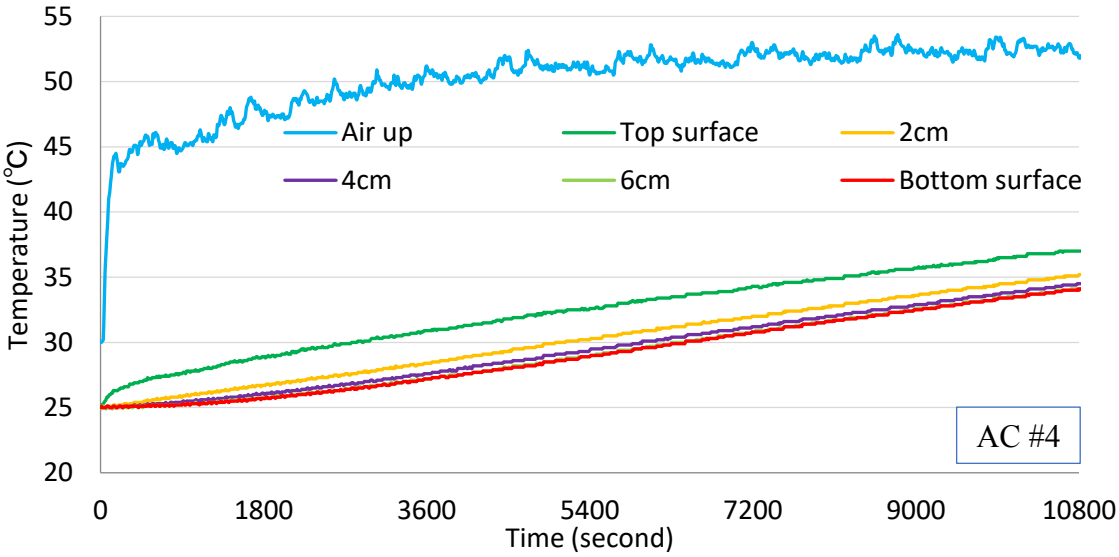
55
50
45
40
35
30
25
20
Temperature (°C)
Air up
Top surface
2cm
4cm
6cm
Bottom surface
AC #4
0
1800
3600
5400
7200
9000
10800
Time (second)

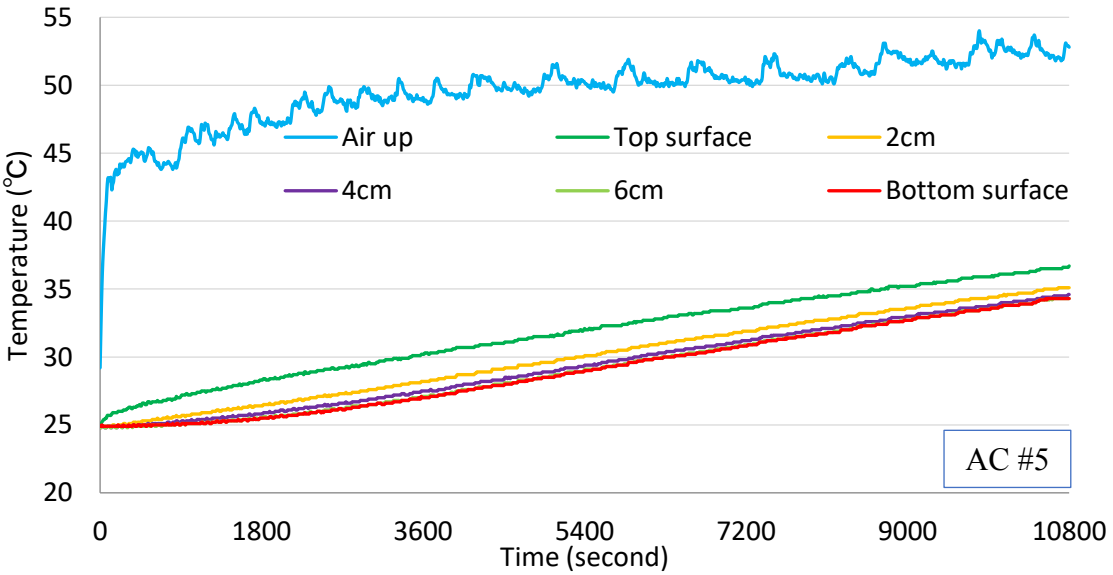
55
50
45
40
35
30
25
20
Temperature (°C)
Air up
Top surface
2cm
4cm
6cm
Bottom surface
AC #5
0
1800
3600
5400
7200
9000
10800
Time (second)

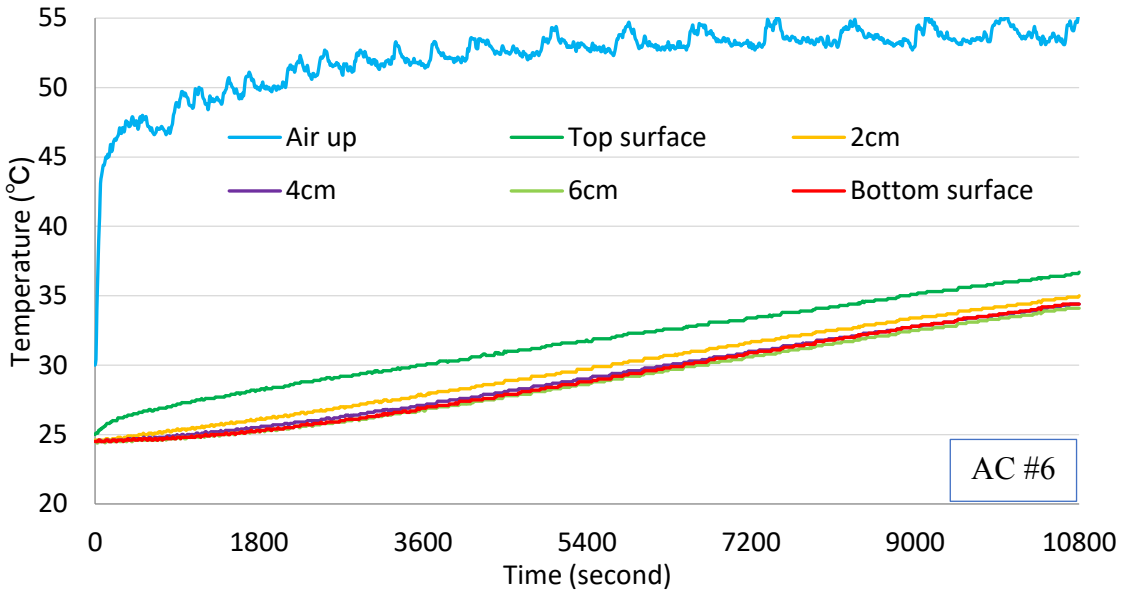

Figure 3.10 Experimentally measured results of the surface and internal temperature increments of the 6 types of asphalt concrete specimens.

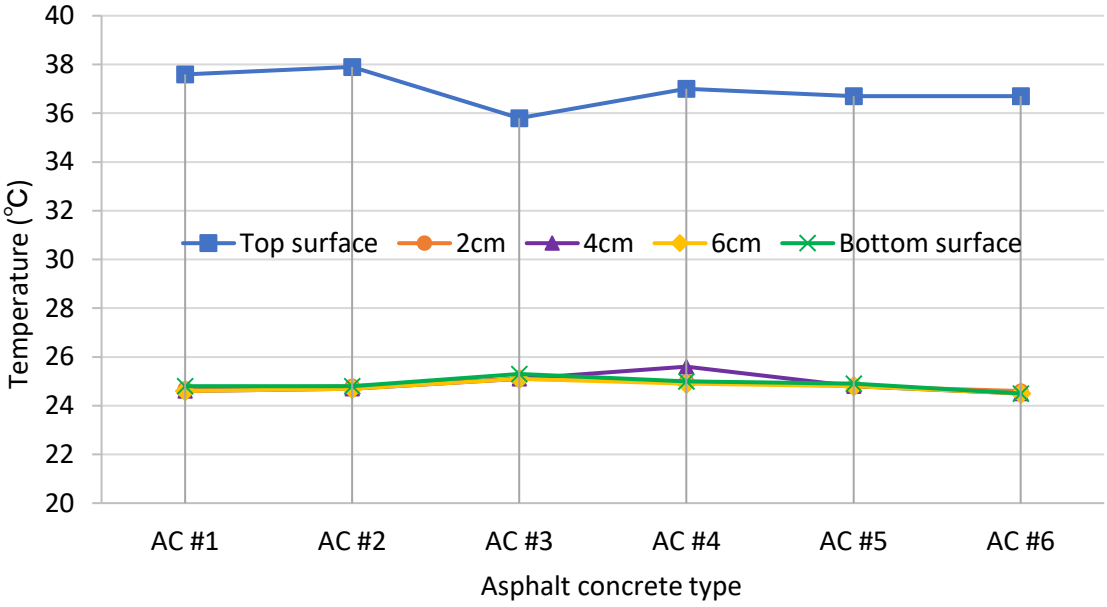

Figure 3.11 Comparison of temperature increments between asphalt type depths at final time (3hours).

3.8 Identification of Thermal Parameters

A mathematical model was developed to identify the thermal parameters of each type of AC specimens using the experimental data based on one-dimensional partial

differential heat transfer equation (PDE) and finite difference approximation method.

3.9 Heat Transfer Equation

3.9.1 One Dimensional Partial Differential Heat Equation

For the study under consideration, the heat transfer can be considered one-dimensional since the side faces are insulated. The specimens are assumed to be homogeneous and anisotropic structure in the sense of macro-scale level. The one-dimensional partial differential heat transfer equation is

$$\frac{\partial T}{\partial t}(x,t) = \alpha \frac{\partial^2 T}{\partial x^2}(x,t) \quad \alpha = \frac{k}{\rho C} \tag{3.1}$$

where T refers to temperature, t is time, x is the location in the vertical direction, α is the thermal diffusivity, k is thermal conductivity, ρ is density and C is heat capacity.

Figure 3.12 shows the asphalt specimen model with boundary conditions. The top surface is subjected to heat flux, and the bottom surface is insulated.

3.10 Initial and Boundary Conditions

3.10.1 Initial Condition

The initial condition for all x when $t = 0$,

$$T(x,0) = T_1 \quad 0 < x < L \tag{3.2}$$

3.10.2 Top Boundary Condition

The top surface boundary condition is “convection surface condition”:

$$-k \left. \frac{\partial T}{\partial x} \right|_{x=0} = h\left[T_{air} - T(0,t)\right] \quad t > 0 \tag{3.3}$$

where h represents a heat transfer coefficient and T_{air} is the temperature of the surrounding air.

3.10.3 Bottom Boundary Condition

At the bottom it is an "insulated surface condition" where the temperature gradient is zero:

$$-k\left.\frac{\partial T}{\partial x}\right|_{x=L}=0 \tag{3.4}$$

It is assumed that the specific heat, material density, and heat transfer coefficient do not change over the time interval being estimated.

$$k\frac{\partial T(x,t)}{\partial x}=q(t)$$

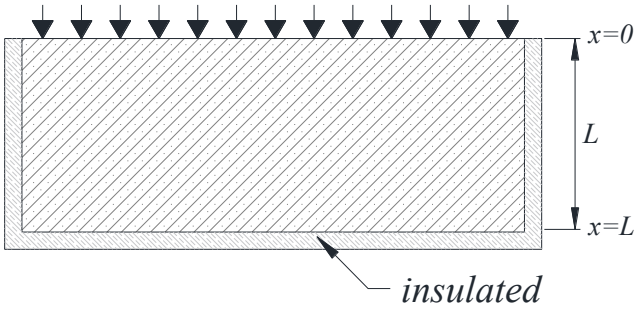

$$\frac{\partial T(x,t)}{\partial x}=0$$

Figure 3.12. One-dimensional asphalt model with boundary conditions.

3.11 Finite Difference Method

The finite difference method (FDM) is one of the common discretization methods for obtaining a numerical solution by solving continuous PDE. For complex nonlinear heat transfer problems, the FDM works well (Necati Özişik,1994).

3.11.1 Grid Discretization

To solve the Eq. (3.1) numerically, first, we divided the domain into respective finite grids as shown in Figure 3.13 where i refers to the temperature at the current time step, whereas $i+1$ represents the new (future) temperature. The subscript n refers to the

location. Here, i varies from 0 to nt (total number of time steps) and n varies from 0 to N (total number of grid points). White circles are the grid points where the derivatives of the partial differential equation are approximated. The black circles demonstrate the Euler's calculation method of the unknown temperature. Details of the procedures will be explained in the next section.

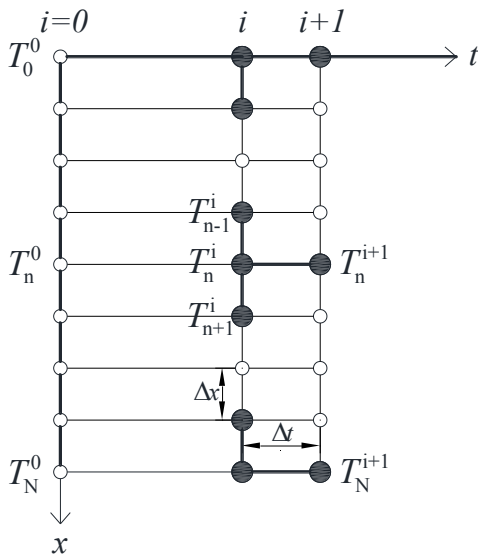

Figure 3.13. Finite difference discretization of the 1D heat equation.

3.11.2 Explicit Method

We approximate the time derivative by using forward difference scheme as

$$\frac{\partial T}{\partial t} = \frac{T_n^{i+1} - T_n^i}{\Delta t} \tag{3.5}$$

The spatial term is derived by central differencing scheme as

$$\frac{\partial^2 T}{\partial x^2} = \frac{T_{n+1}^i - 2T_n^i + T_{n-1}^i}{\Delta x^2} \tag{3.6}$$

Substituting Eqs. 3.5 and 3.6 into Eq.3.1, we obtain

$$\frac{T_n^{i+1}-T_n^i}{\Delta t}=\alpha\frac{T_{n+1}^i-2T_n^i+T_{n-1}^i}{\Delta x^2} \tag{3.7}$$

With *Euler Method,* the equation can be solved easily for the unknown temperatures at the time step $i+1$ from the known temperature values at the time step i without solving any additional equations.

Next, we rearrange the discretized equation (3.7) as

$$T_n^{i+1}=\frac{\alpha\Delta t}{\Delta x^2}\left(T_{n+1}^i-2T_n^i+T_{n-1}^i\right)+T_n^i \tag{3.8a}$$

$$T_n^{i+1}=Fo\left(T_{n+1}^i+T_{n-1}^i\right)+\left(1-2Fo\right)T_n^i \quad Fo=\frac{\alpha\Delta t}{\Delta x^2} \tag{3.8b}$$

The term Fo is called Fourier Modulus. In order to keep the numerical solution stable, the Fourier Modulus value must be

$$Fo\le\frac{1}{2} \tag{3.9}$$

It means that for the smaller grid thickness Δx, smaller time step Δt needs to be applied.

3.11.3 Exponential interpolation

Since the temperature is available only from the five locations at the experimental data, the values that lie between known data locations were estimated by the exponential interpolation method (MathWorks, R2006a) (see Fig. 3.14). By this way, totally 64 grid numbers (Δx=13mm) were created. The Δt was chosen finely 0.5 second for stability and the total time step is 7200.x

To calculate the heat transfer at the top surface occurring by convection, we simply use the following equation:

$$k\frac{T_{n-1}^i-T_n^i}{\Delta x}+h(T_{air}^i-T_n^i)=pc\frac{\Delta x}{2}\frac{T_n^{i+1}-T_n^i}{\Delta t} \tag{3.10}$$

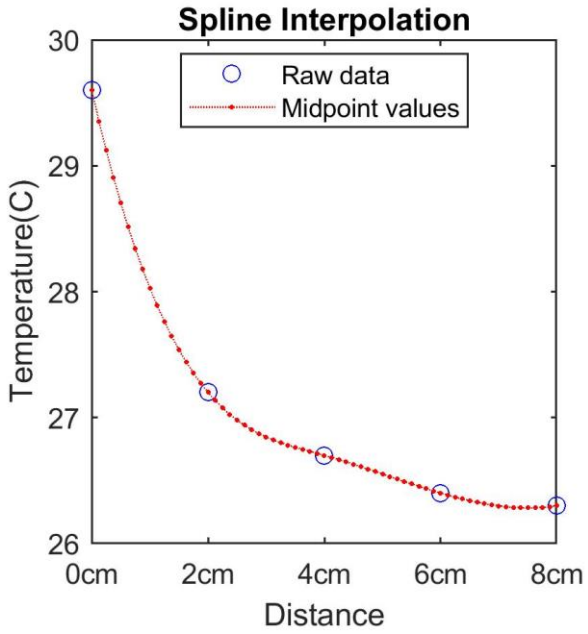

Figure 3.14 Generated points from raw data for simulation. 15 points were created between each known value.

Rearranging the above equation, we get:

$$T_0^{i+1} = 2Fo\left(T_1^i + BiT_{air}\right) + \left(1 - 2Fo - 2BiFo\right)T_0^i \qquad Bi = \frac{h\Delta x}{k} \tag{3.11}$$

where Bi is Biot Number, which is the ratio of the conductive heat resistance within the specimen to the conductive heat transfer resistance at the surface. For stability purposes, we must keep the following condition:

$$Fo\left(1 + Bi\right) \le \frac{1}{2} \tag{3.12}$$

The equation for the bottom boundary condition is as follows:

$$T_M^{i+1} = 2FoT_{M-1}^i + \left(1 - 2Fo\right)T_M^i \tag{3.13}$$

3.11.4 Root Mean Square Error (RMSE) approach

Root mean square error (RMSE) approach was applied to measure the differences between values obtained from the experiment and simulation.

$$RMSE = \sqrt{\frac{\sum_{n=1}^{n=N}\left(E_n - C_n\right)^2}{N}} \tag{3.14}$$

where E_n is the experimentally measured value, C_n is the predicted one, and N is the number of measurements.

3.12 Results of Numerical Analysis

3.12.1 Comparison of measured and calculated results

Based on the above mathematical model, we plotted the temperature increments of each location of an every AC specimen together with the measured data (see Figure 15). The graphs perform well, showing similar temperature increment rates between calculated and measured analysis. Figure 12 illustrates the temperature at the final time step of every AC specimens of both measured and calculated analysis. The results confirm that both analyses have a good fit with satisfied RMSE values. Based on the literature studies, a good predictive model RMSE value should be less than 0.5 (Veerasamy, 2011).

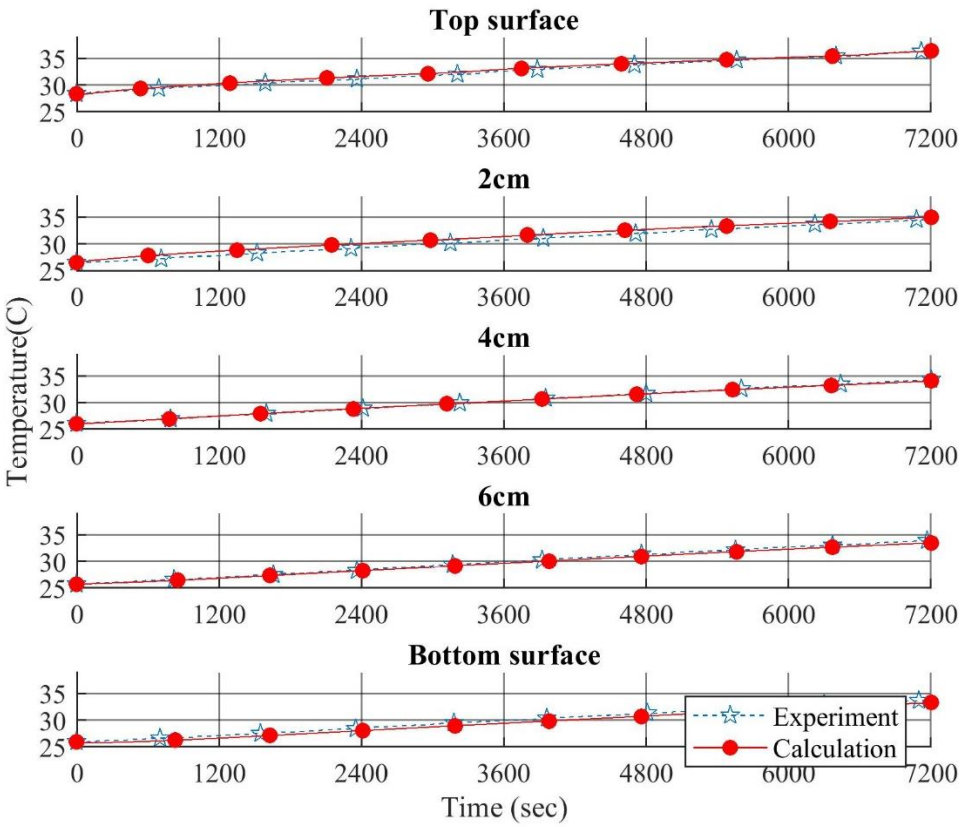

AC #1 - Coarse-graded (Pen. Index: 40/60) (1 layer).

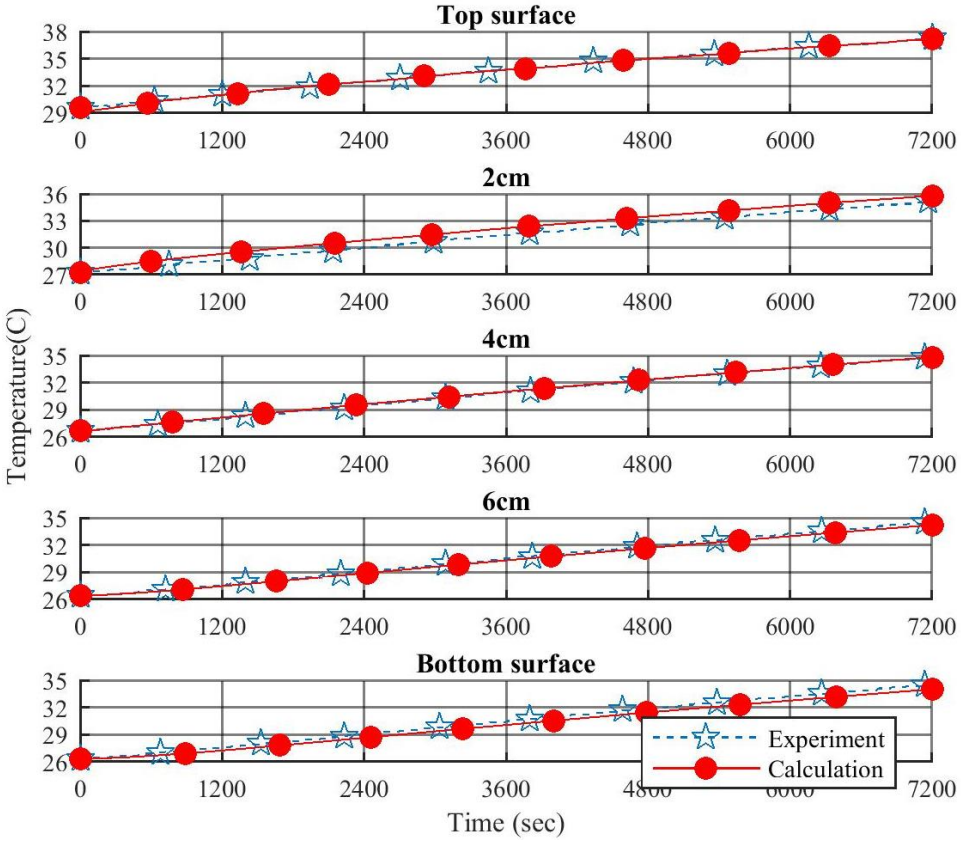

AC #2 - Dense-graded (Polymer-modified - Type II) (1 layer).

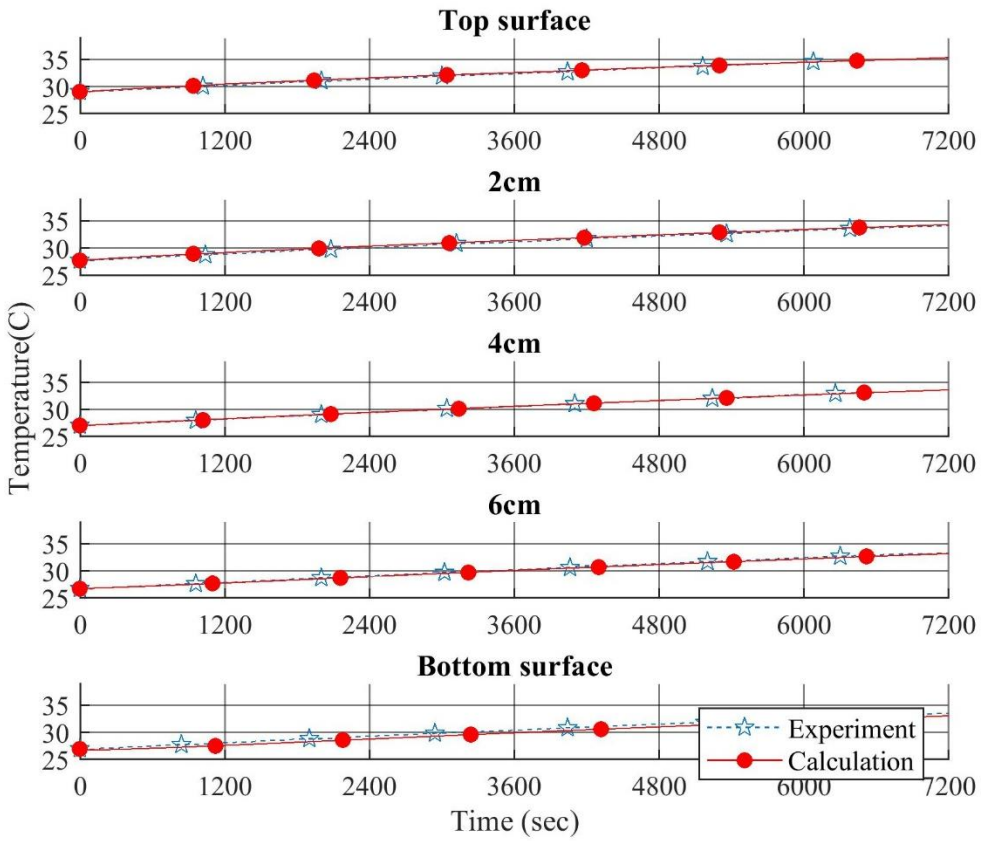

AC #3 - Coarse-graded (40/60) & Reproduced coarse-graded (2 layer).

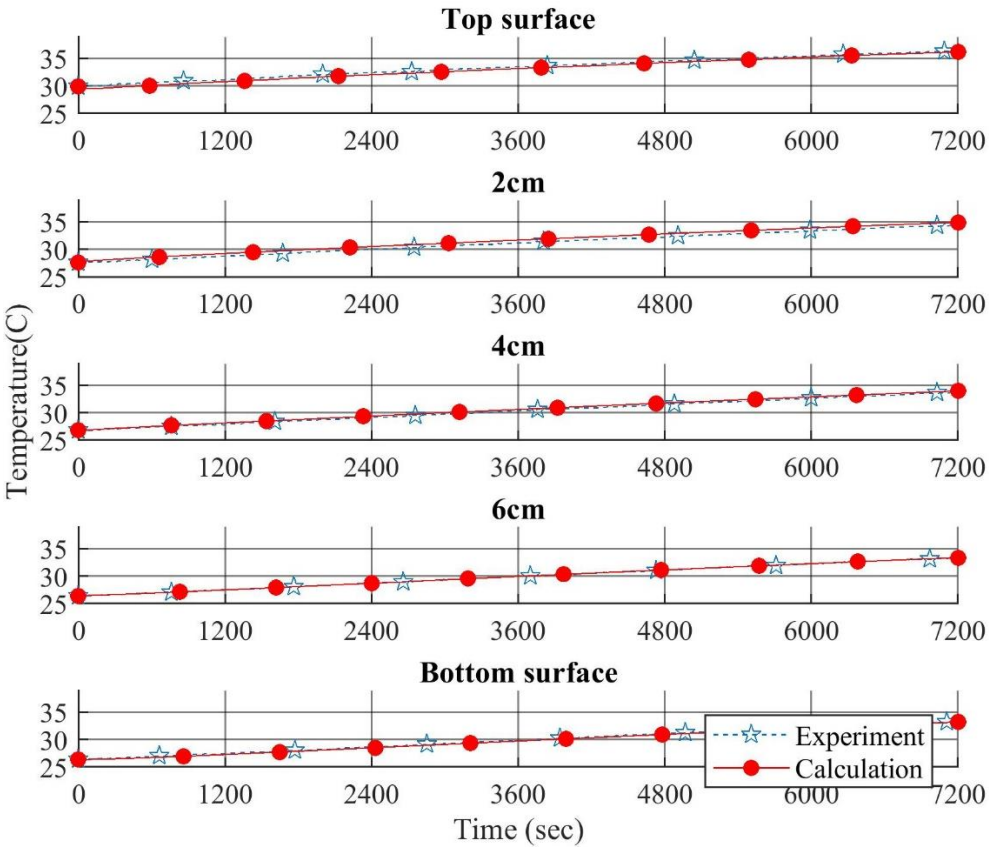

AC #4 - Dense-graded (Polymer-mod. - Type II) & Dense-graded (40/60) (2 layer).

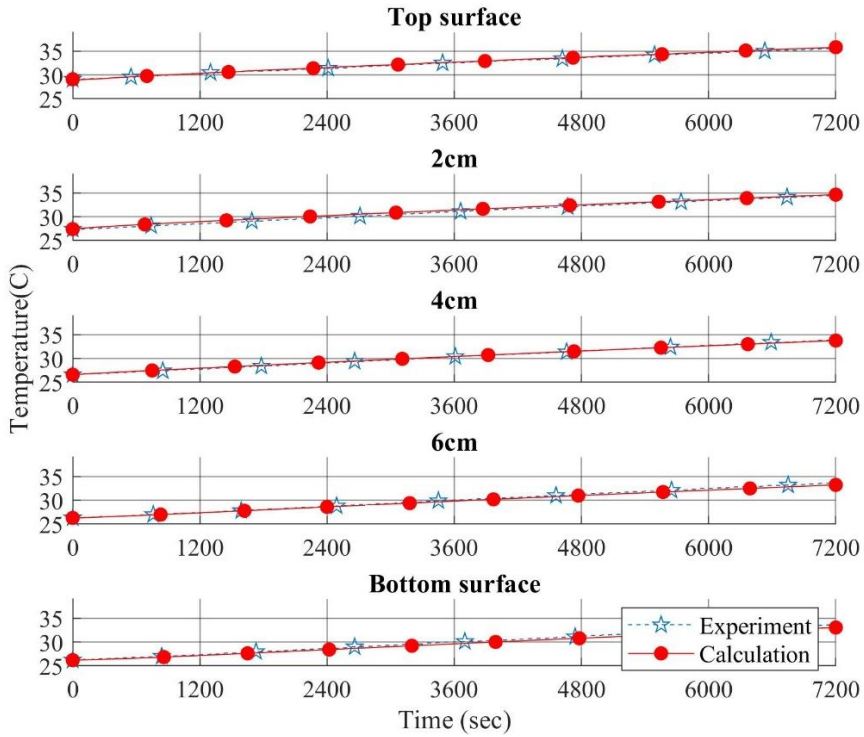

AC #5 - Water-holding porous (Small size aggr. TH) & Dense-graded (Polymer-mod. - Type III-W) (40/60) (2 layers).

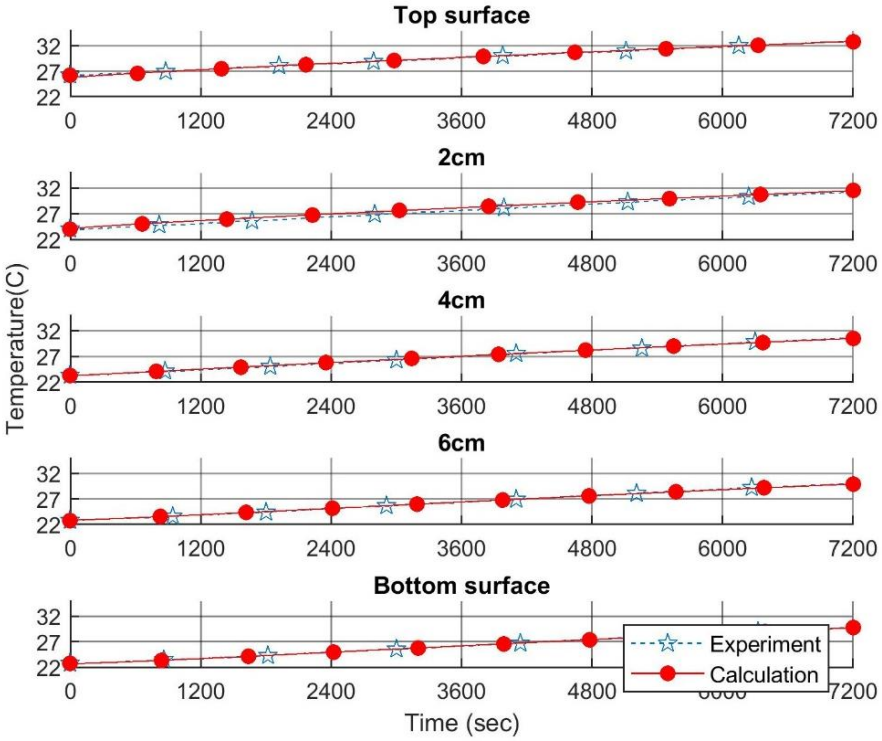

AC #6 - Dense-graded + heat insulation unit & Dense-graded (40/60) (2 layer).

Figure 3.15 Comparison of measured and calculated temperature increments of each AC specimen locations.

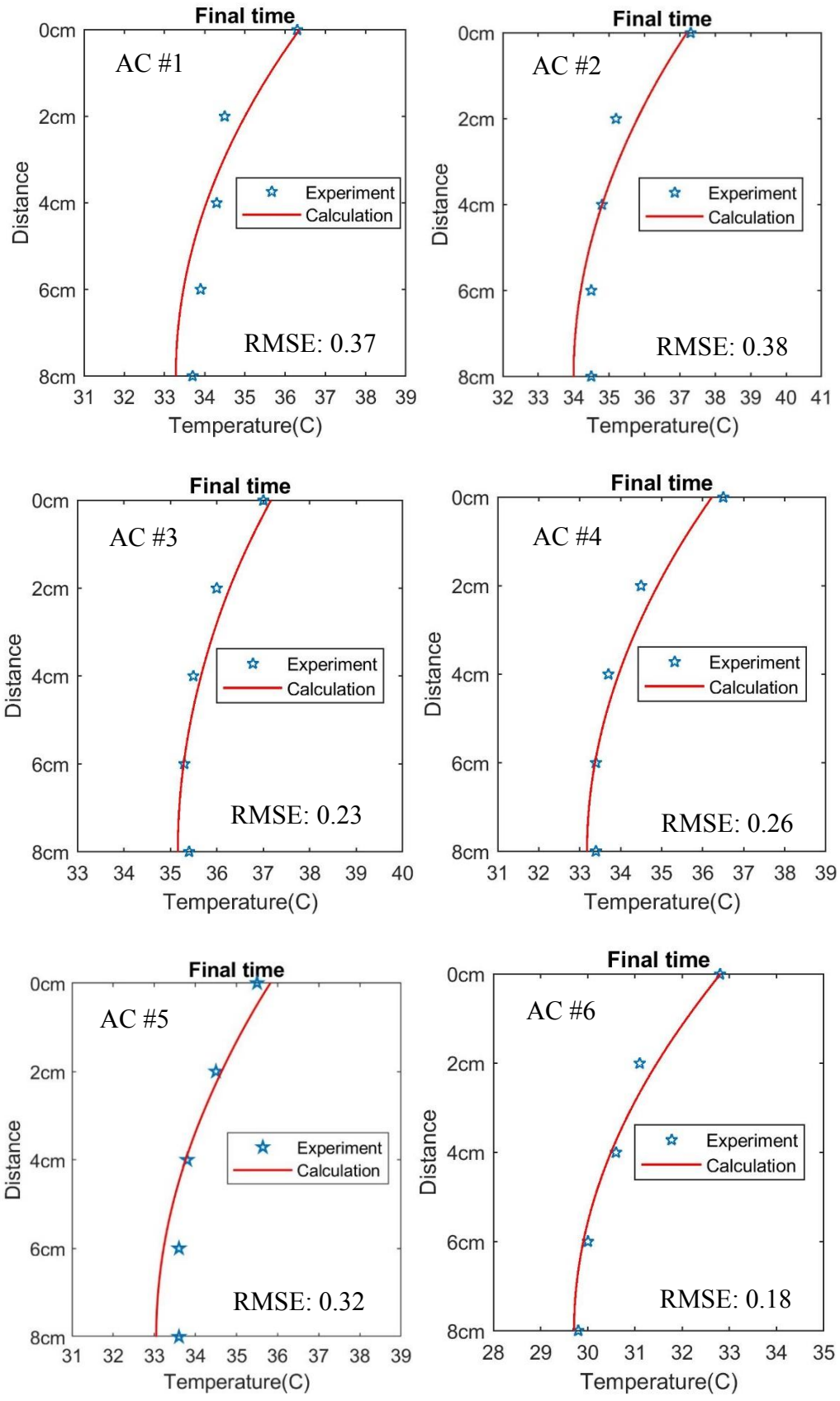

Figure 3.16 Temperature fit at final time of 6 types of AC specimens with their accuracy values.

3.12.2 Obtained thermal parameters of 6 types of AC

Numerically determined thermal parameters of 6 types of AC specimens are shown in Table 3.2. The coarse materials revealed higher specific heat capacities than dense and water-holding porous materials. This indicates that more energy is required to increase the inside temperature of the coarse-graded asphalt pavement. It is worth to note that the water-holding porous asphalt revealed significantly low specific heat: 520 (J/kg K), which was exactly same with the experimentally determined value by JFE Steel Cor., (2006) (see Table 3.3). Regarding thermal conductivity properties, again the water-holding porous asphalt revealed the lowest value which is desirable as less heat is conducted from the asphalt surface to subsequent base layer. However, even it has a lower heat conductivity, it revealed the highest thermal diffusivity due to its low specific heat capacity. Thus, the balance between heat conductivity and specific heat capacity is desirable to control a heat transfer rate through the material. As for the heat transfer coefficient, since it is directly proportional to the amount of heat transfer between the surface and surrounding air, a lower heat transfer coefficient is preferable. Here, the water-holding porous asphalt gives a desirable result in comparison with other types of asphalt specimens.

3.12.3 Comparison of obtained thermal parameters with prior studies

The thermal parameters of the basic type of asphalt specimens derived by this methodology are compared with the prior studies listed in Table 3.3. As the values on the prior studies differ from each other, the values obtained from this study differed as well. Despite that, they have still close agreements. Especially, the porous asphalt thermal properties showed identical values with the values reported by JFE Steel Cor., (2006). However, the specific heat of porous asphalt and the thermal conductivity of coarse-graded and dense-graded asphalt specimens significantly differ from the reported values by Kosaku (2005). As referring to the findings by Goto & Matsubayashi (2009), thermal parameters depend on the material porosity. Accordingly, we assume the porosities of asphalt specimens might be different in the study of Kosaku.

Overall, our results are broadly in line with the result of prior studies and these findings provide a potential mechanism for heat transfer control on the several types of AC specimens.

Table 3.2 Numerically derived thermal parameters of 6 type of asphalt specimens

#	Asphalt specimen materials	Specific heat C (J/kg K)	Thermal conductivity k (W/m K)	Thermal diffusivity x 10-7 α (m2/s)	Heat transfer coefficient h (W/m2 K)
1	Coarse-graded (Pen. Index: 40/60)	880	2.2	10.39	10.0
2	Dense-graded (Pol.-mod. Type II)	850	2.0	9.92	10.0
3	Coarse-graded (Pen. Index: 40/60)	880	2.1	9.91	8.0
	Reproduced coarse-graded	870	2.3	11.21	–
4	Dense-graded (Pol.-mod. Type II)	860	2.0	9.81	9.0
	Dense-graded (Pen. Index: 40/60)	860	1.9	9.27	–
5	Water-hold. porous (Small aggr. TH)	520	1.5	12.22	6.0
	Dense-graded (P-m. Type III-W)	810	1.85	10.15	–
6	Dense-graded + heat insulation unit	870	1.9	8.69	8.0
	Dense-graded (Pen. Index: 40/60)	850	1.9	9.38	–

Table 3.3 Comparison of the obtained asphalt thermal parameters with prior studies

Asphalt specimen material	Prior studies	Specific heat (J/kg K)	Thermal conduct. (W/m K)	Thermal diffusivity x 10^{-7} (m^2/s)	Heat transfer coefficient (W/m^2 K)	Density (kg/m3)
Coarse-graded	This study	880	2.2	10.39	10	2407
	Kosaku et al., 2005	830	1.29	7.33	-	2121
Dense-graded	This study	850	2	9.92	10	2371
	Kosaku et al., 2005	850	1.6	7.88	-	2388
	JFE Steel Cor., 2006	900	2	10.30	-	2157
Water-hold. porous	This study	520	1.5	12.22	6	2360
	Kosaku et al., 2005	810	1.44	7.29	-	1914
	JFE Steel Cor., 2006	520	1.46	11.90	-	2360

Note: - not available

3.13 Conclusions and Discussions

Based on the experimental and numerical analysis the following conclusions can be drawn from this chapter:

(1) One layered coarse-graded and dense-graded asphalt specimens revealed 1~2℃ higher top surface temperature increments than the specimens with two layers (#3, #4) when the content of the materials was the same. The water-holding porous asphalt and the dense-graded asphalt with heat insulation unit had a similar surface temperature trend showing 1℃ lower than the one layered specimens.
(2) The internal and bottom temperature increments at the different type of asphalt specimens: coarse-graded, dense-graded, water-holding porous and dense-graded with heat insulation unit asphalt did not differ from each other significantly.
(3) Among the different asphalt specimen types, the water-holding asphalt gave a good thermal performance i.e. lower heat conductivity and lower heat transfer coefficient. It conducts less heat transfer from the asphalt surface to the subsequent base layer and prevents a big amount of heat transfer between the surface and surrounding air.

3.14 Summary of Chapter 3

This chapter contains the main goal of this study and thus the volume is the biggest among other chapters. In this chapter, six types of AC specimens were tested in a wind-tunnel where a hot temperate air inside was generated by a forced circulation boiler system. Based on the obtained experimental data, numerical simulations were performed to derive thermal parameters of each asphalt type. Additionally, the results of the obtained thermal parameters were compared with prior studies.

References and Suggested Readings

Toktorbai uulu, A., Katsuchi, H., Yamada, H., & Kim, H. (2019). Study on thermal parameters of asphalt concrete for countermeasures against high surface temperature of pavement in tunnel. Journal of Road Materials and Pavement Design (in progress).

Engineering ToolBox, (2003). Thermal Conductivity of common Materials and Gases. Retrieved from https://www.engineeringtoolbox.com/thermal-conductivity-d_429.html

Necati Özişik, M. (1994). Finite Difference Methods in Heat Transfer. Boca Raton, Florida: CRC Press, inc.

Yunus A. Cengel, (Second Edition). Heat Transfer. A practical approach.

Veerasamy, R., Rajak, H., Jain, A., Sivadasan1. S., Varghese, C., & Agrawal, R. (2011/9). Validation of QSAR Models - Strategies and Importance. International Journal of Drug Design and Discovery, 2, 511-519.

Goto, S., & Matsubayashi, O. (2009). Relations between the thermal properties and porosity of sediments in the eastern flank of the Juan de Fuca Ridge. Earth Planets Space. 61, 863–870.

Kawana, F., Kawamura, N., & Matsui, K. (2012). Evaluation of pavement thermal properties using heat flux sensor. J-STAGE, Vol. 68, No 3, I_5- I_12 (in Japanese).

Kosaku, K., & Hiroshima, M. (2005). Measurement of Specific Heat, Thermal Conductivity, and Diffusible Humidity for Water-absorptive Pavement, (Report No. ISSN 0387-2416, 233-238). The Institute of Civil Engineering of the Tokyo Metropolitan Government (in Japanese).

JFE Steel Corporation. (2006). Experimental data of performance test of water-holding block.

K-Type thermometer specs. Retrieved from https://jp.rs-online.com/web/p/thermocouple-extension-wire/0151209/

Data-Logger TDS-530-30H. Retrieved from https://www.techno.co.jp/pc_rental/cmp/search/detail_2203TQ0045.html

CHAPTER IV

4. MEASUREMENT OF HEAT TRANSFER IN ASPHALT – II

Abstract

In the 2nd stage of the wind-tunnel experiment (WTE), we will measure the asphalt specimens temperature distributions under high wind speed effect and lamp-radiation effect. For that, the built-in facility of wind tunnel so-called, *lamp radiation* system will be used as a radiative heat source. The high wind speed up to 16.3m/s will be applied. Besides, two types of asphalt concrete (AC): ordinary type AC (dense-graded) and water-holding porous AC will be tested under water spray effect to analyze the efficiency of water-holding porous asphalt at the high air temperature. Finally, the calculations of the heat transfer coefficient (h) under high wind speed and water-spray effect will be presented. The values of h are absolutely essential and useful in controlling the temperature rise in a road tunnel.

4.1 Experiment Stage #2

4.1.1 Introduction of Experiment Stage #2

In the 2nd stage of the wind-tunnel experiment, two types of AC (Figure 4.1):

- ✧ Dense-graded asphalt (#4)
- ✧ Porous asphalt with water-holding system (#5)

were tested under high wind speed and water spray effect to analyze the effectiveness of the water-holding porous asphalt against a high air temperature. The dense graded asphalt which can be considered as a conventional asphalt was chosen as well to compare the

results. Figure 4.2 illustrates the experimental set-ups. The asphalt specimens were heated by direct radiative lamps. Simultaneously, they were exposed to various wind speed.

#4 - ordinary type AC (dense-graded)

#5 - water-holding porous AC

Figure 4.1 Two types of AC specimens for the test in the 2nd Stage of Wind-Tunnel Experiment. The wires are thermocouples attached to the surfaces for measurement of the surface temperature.

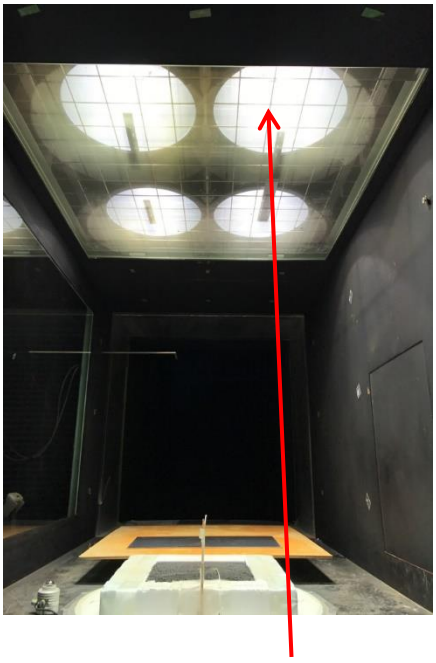

Radiative Lamps

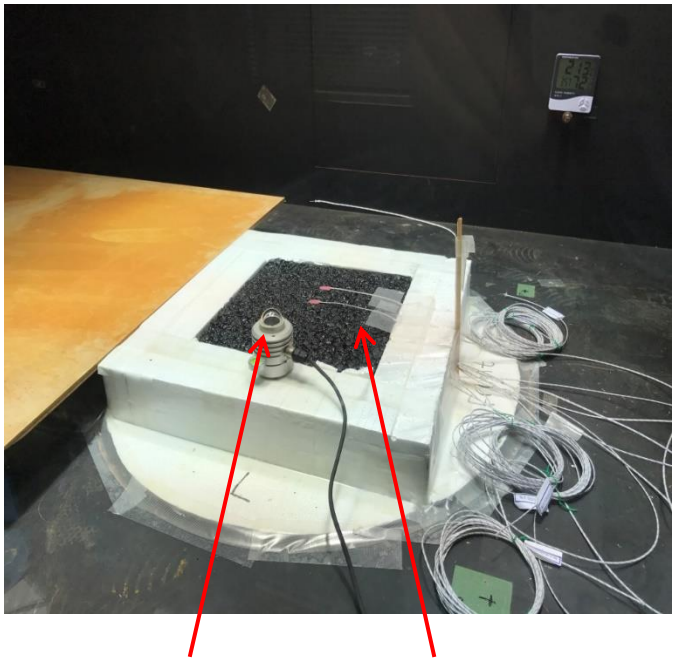

Radiation Meter Asphalt specimen

Figure 4.2 Lamp radiation system to heat AC specimens.

4.1.2 What are Porous Asphalt and Porous Asphalt with Water-Holding system?

Porous asphalt pavement can absorb water/rainwater into the pavement structure. It has high voids in the structure that cause the water to pass through the pavement structure into the stone recharge bed underneath the pavement, then transfer into the water table.

Porous Asphalt with Water-Holding system is the pavement generally uses porous asphalt mixture for the surface layer or surface/base layer. A water retentive grout which can absorb and hold water is filled to its voids and the collected water in the voids evaporates. As it evaporates, the generated heat deprives through vaporization. Thus, the pavement will have a function of suppressing a temperature increase on the road surface.

Effects of Water-Holding Porous Asphalt:

- ✓ Road surface temperature reduction effect
- ✓ Improvement of summer heat environment
- ✓ Sustained effect of water-spray by its water-holding function
- ✓ Voids at the top of the mixture functions as a drainage and noise reduction
- ✓ Light color property.

Source: "Sightline Institute"

4.1.3 Input Parameters

As input parameters, seven types of wind speed and six types of water-spray amounts were applied. The wind speeds were derived from the induced wind graph by an ordinary car passage as illustrated in Figure 4.3. According to this study, when an ordinary car passes at the velocity between 10km/h to 70km/h, it induces wind speed from 2m/s till 5.6m/s. Table 4.1 shows the values of wind speeds that were used in this experiment. Wind speeds generated by the passage of the ordinary car at more than 70 km/h were approximately derived through the graph linear-trendline and were added to the wind parameters.

Water-spray amounts chosen for the experiment vary between 0.2 L/m2 to 1 L/m2 as shown in Table 4.2. Hence, the asphalt specimen surface area is smaller than 1 m2 (0.3m x 0.3m), the water amounts for the experiment were converted into the asphalt specimen size.

Radiation amount that is generated by direct heat lamps is constant: 800 W/m^2

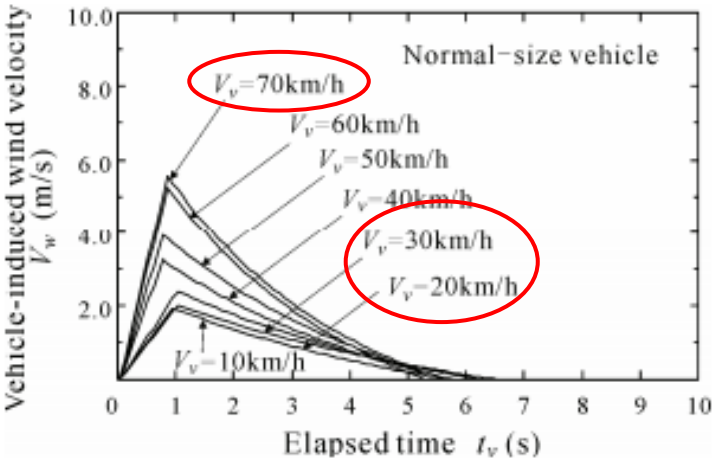

図-7 普通車通過に伴う車両誘発風の時間変化

(Source: Journal of JSCE Vol.63 No.2, 250-261, 2007,5)

Figure 4.3 Graph of induced wind velocity by the passage of ordinary car.

Table 4.1 High wind speed parameters obtained by the vehicle speed.

Vehicle speed (km/h)	0	20-30	60-70	*110*	*140*	*180-190*	*200-210*
Vehicle induced wind speed (m/s)	0	2	5.6	*8.5*	*11.1*	*14.5*	*16.3*

Table 4.2 Water amounts chosen for the water-spray experiment.

Chosen water amount L/m^2	0,2	0,26	0,4	0,55	0,6	0,8	1
Converted water amount for asphalt specimen size (ml/0.09m^2)	18	24	36	50	54	72	90

4.2 Test under High Wind Speed and Lamp-Radiation

4.2.1 Test setup

Both asphalt specimen types: ordinary type and water-holding porous asphalt were installed together in the test section area of the wind-tunnel to ensure that both specimens would have been exposed to the same environmental condition. As similar to the previous experiment, the bottom surface and side surfaces of specimens were covered with 10cm thick heat insulated material to ensure that the heat would be transferred one-dimensionally only from the upper surface. The surfaces were heated by the direct heat lamp system. The panel was installed in the up-wind side to prevent the turbulence wind flow that may be generated at the edge of insulation materials. The air temperature was measured at the 10cm high from the specimen surface to implement on numerical calculations. The temperature was recorded at every 10 seconds for totally 7200 seconds (2 hours).

Figure 4.4 Test set up.

4.2.2 Results of measured temperatures affected by the high wind speed

Figure 4.5 shows the experimental results of the transient temperature profiles of the two types of asphalt specimens that were affected by seven types of wind speed and heated at the constant heat. Here, the internal temperatures were hidden and were shown

only the surface and bottom temperatures to make the graph easy to understand.

The initial air temperatures were the same as the specimen's initial temperatures and once the heating started, the wind flow also launched. The surface temperatures started increasing quickly, after that at the specific time their increments kept the same with the internal temperature increments. However, by the increasing of the wind speed, the surface temperature increment rates are dropped faster than the internal temperature drops. Obviously, the higher the wind speed the slower increase of the temperatures.

4.2.3 Comparison of temperature distributions between the ordinary asphalt and water-holding porous asphalt

As comparing the temperature increments between the ordinary asphalt and the water-holding porous asphalt at the final time, the surface temperature reduction effect can be seen in the water-holding porous asphalt by up to 3°C as shown in Figure 4.5. This effect is equivalent at the bottom surface as well. Figure 4.6 depicts the surface temperature differences between these two asphalt specimens. As seen for from the graph, the water holding porous asphalt temperature increment is less than the ordinary one at any point of wind speed. Thus, the water-holding porous asphalt can be risen to withstand against the high-temperature environment.

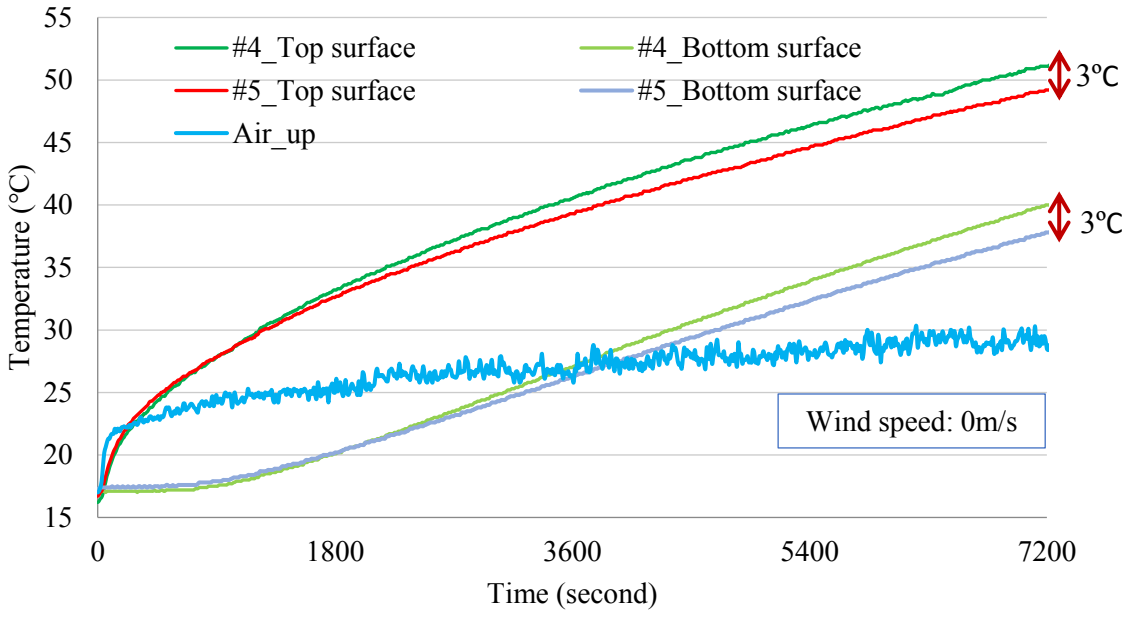

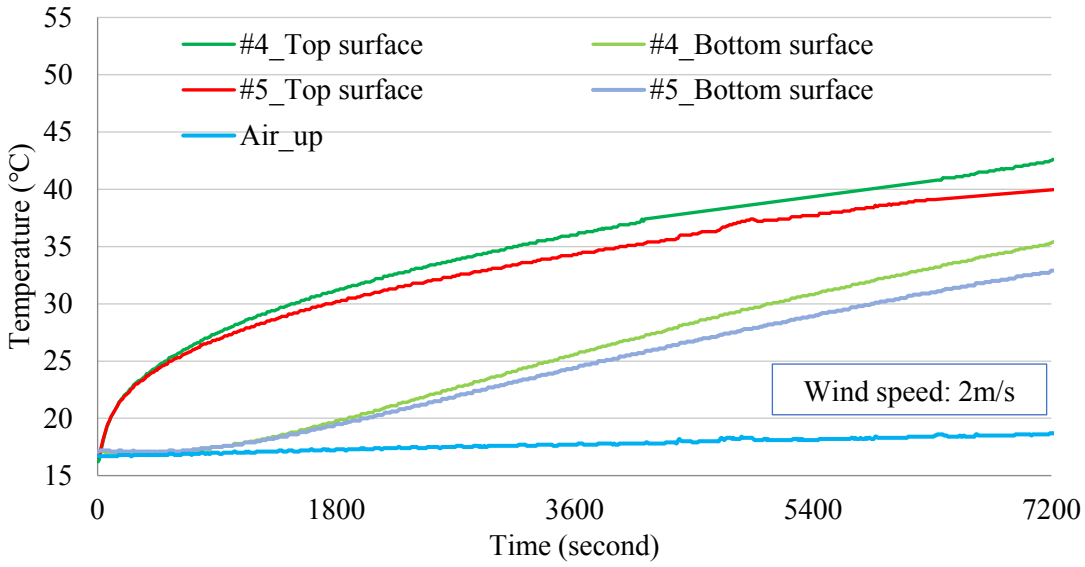
#4_Top surface
#4_Bottom surface
#5_Top surface
#5_Bottom surface
Air_up
Wind speed: 2m/s
Temperature (°C)
Time (second)
55
50
45
40
35
30
25
20
15
0
1800
3600
5400
7200

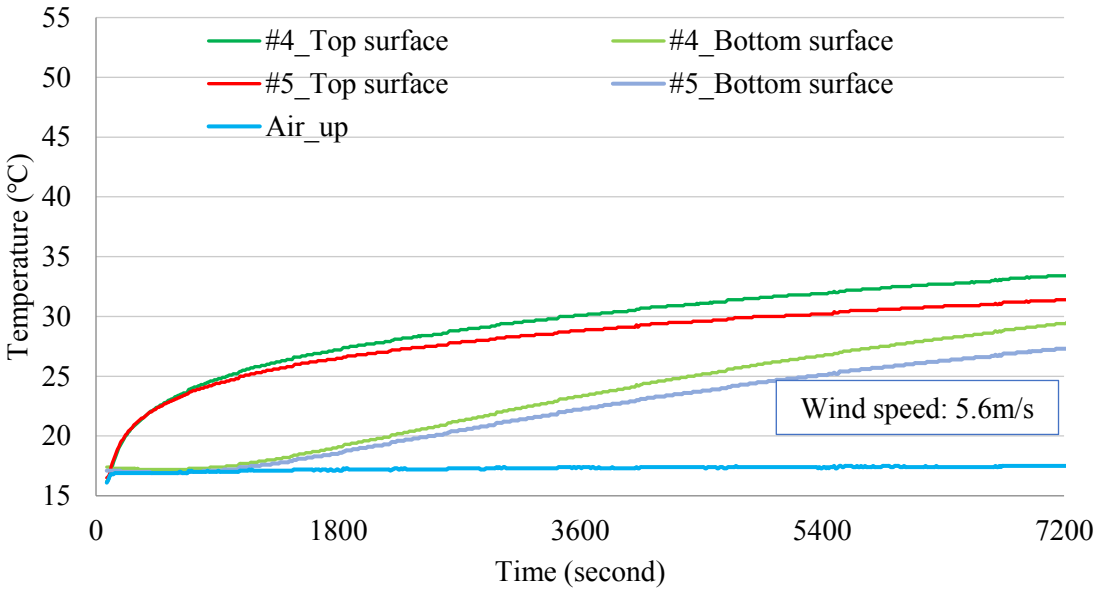
#4_Top surface
#4_Bottom surface
#5_Top surface
#5_Bottom surface
Air_up
Wind speed: 5.6m/s
Temperature (°C)
Time (second)
55
50
45
40
35
30
25
20
15
0
1800
3600
5400
7200

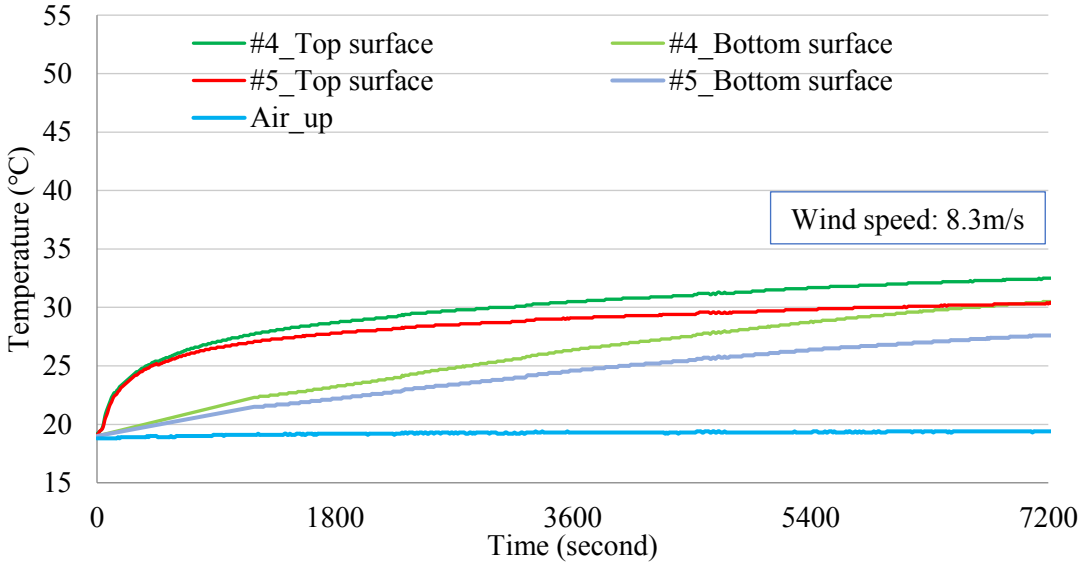
#4_Top surface
#4_Bottom surface
#5_Top surface
#5_Bottom surface
Air_up
Wind speed: 8.3m/s
Temperature (°C)
Time (second)
55
50
45
40
35
30
25
20
15
0
1800
3600
5400
7200

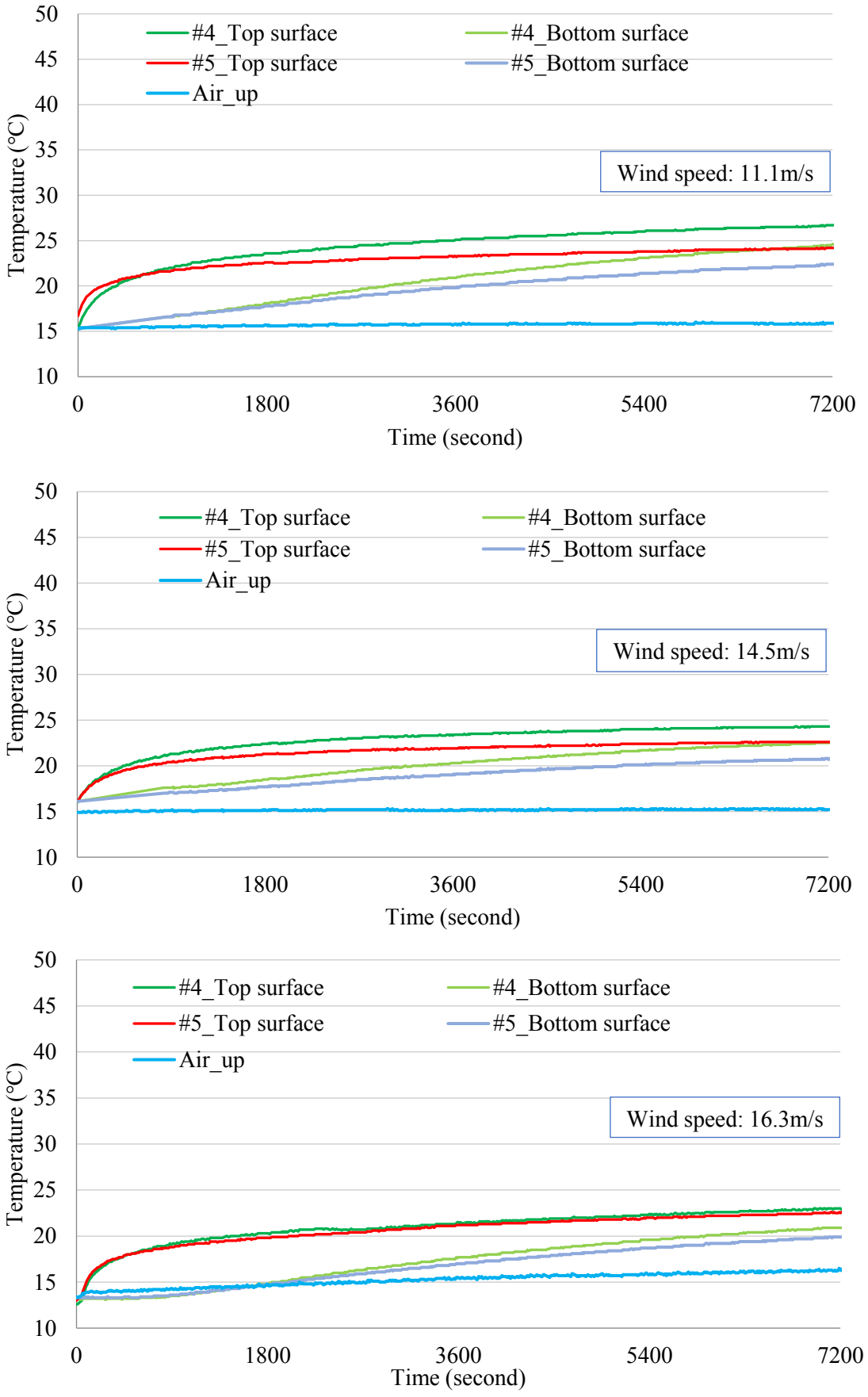

Figure 4.5 Experimentally measured results of temperature increments of AC#4 & AC#5

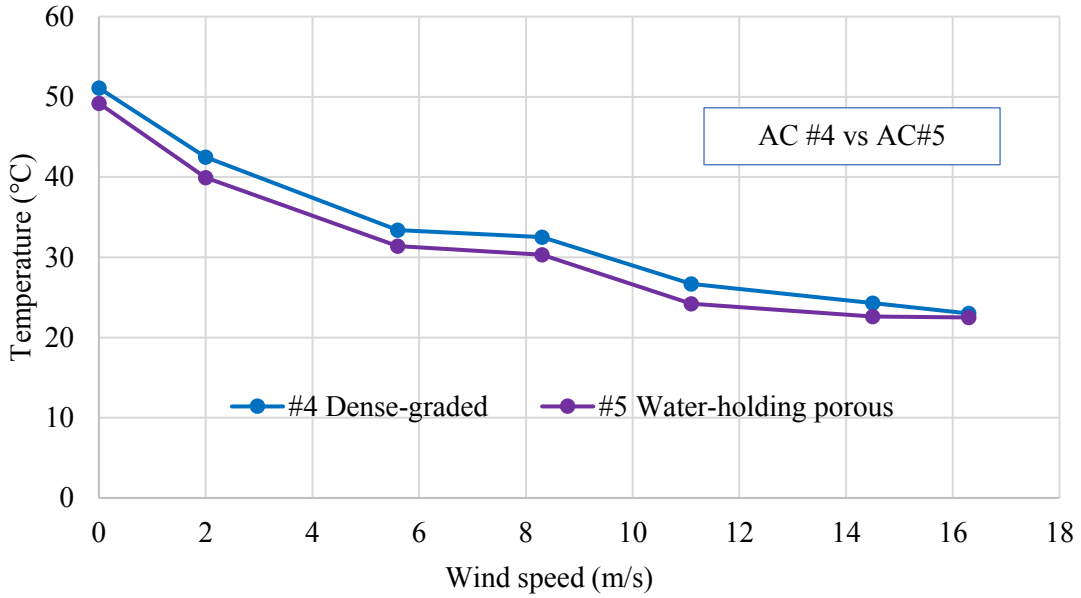

Figure 4.6 Comparison of the surface temperature differences at final time (2h)

4.3 Combined Heat transfer coefficient (CHTC)

The convective heat transfer coefficient h can be calculated by Equation 4.1 below. We obtained all the parameters through the experiment, except for the value of h. Here, h is calculated through the coding in the Matlab program. Combined heat transfer coefficient h can be defined as the rate of heat transfer between the asphalt surface and the air temperature inside the wind-tunnel combining the effects of wind and water spray. Thus, it was called as combined heat transfer coefficient (CHTC).

$$-k\frac{dT(0,t)}{dx} = h\left(T_{air,t} - T_{surf,t}\right) \tag{4.1}$$

4.4 Derivation of Combined Heat Transfer Coefficient depending on Wind

Figure 4.7 shows the derived values of CHTC with respect to wind speed. It shows the increases of CHTC values with the increase of wind speed. Besides, the water-holding porous asphalt reproduced lower value than the ordinary asphalt type which refers to the less convective heat rate between the air and the surface. Table 4.3 summarises the actual values of heat transfer coefficient with respect to wind speeds.

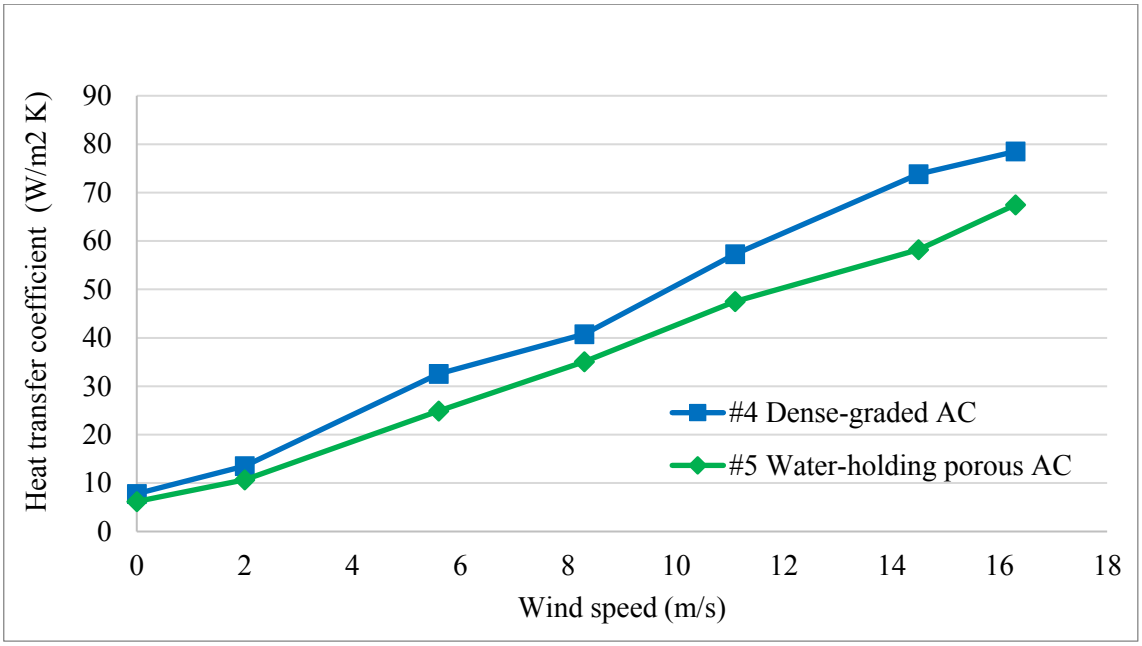

Figure 4.7 Variation of heat transfer coefficients with respect to wind

Table 4.3 Numerically obtained heat transfer coefficients with respect to wind

Wind speed (m/s)	Heat transfer coefficient (W/m^2 K)	
	#4 Dense-graded AC	#5 Water-holding porous AC
0	7.8	6.2
2	13.5	10.7
5.6	32.6	24.9
8.3	40.8	35.1
11.1	57.3	47.5
14.5	73.8	58.2
16.3	78.5	67.5

4.4.1 Example of Radiated Heat Amount

The amount of heat that taken away from the asphalt surface to surroundings by the wind speed is illustrated in Figure 4.8. The higher the wind speed increases the more amount of heat radiates to the air. Besides, the ordinary asphalt pavement radiates higher amount of heat comparing to the water-holding porous asphalt. Surprisingly, the higher wind speed reproduces the higher radiative heat amount. It means the more we flow the

surface the more effect of heat to the surrounding air. Interestingly, this phenomenon matches with the measurements by Shutoko Expressway company as illustrated in Figure 4.10. They reported that when the vehicle amount and speed is increased, the air temperature inside the Yamate Tunnel increased as well. Table 4.4 represents the values of radiated heat amounts from both asphalt surfaces to air with respect to wind.

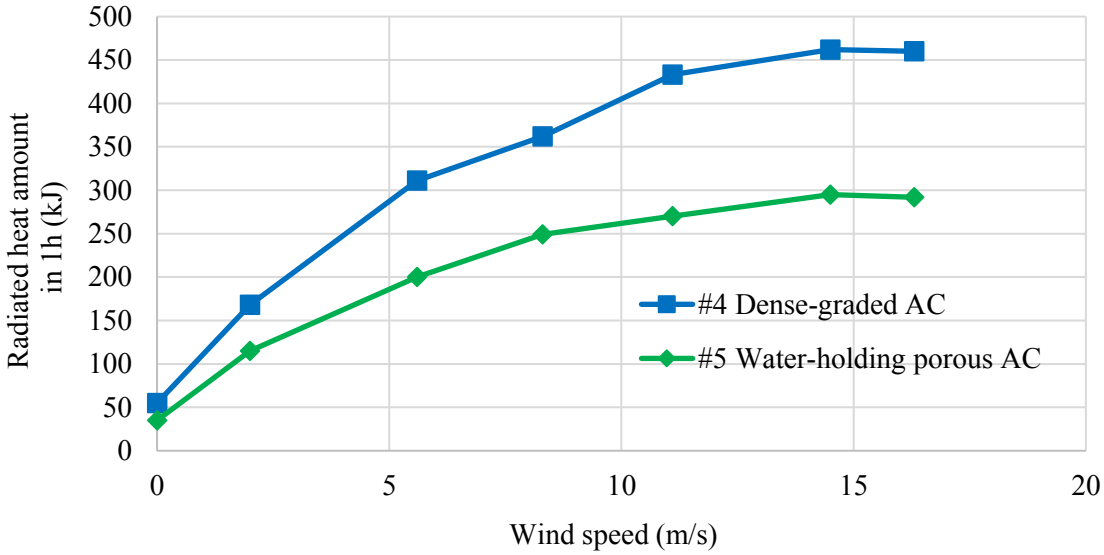

Figure 4.8 Variation of radiated heat amount with respect to wind.

Table 4.4 Values of radiated heat amounts from asphalt surface to air with respect to wind

Wind speed (m/s)	Radiated Heat Amount in 1h (kJ)	
	#4 Dense-graded AC	#5 Water-holding porous AC
0	55	35
2	168	115
5.6	311	200
8.3	362	249
11.1	433	270
14.5	462	295
16.3	460	292

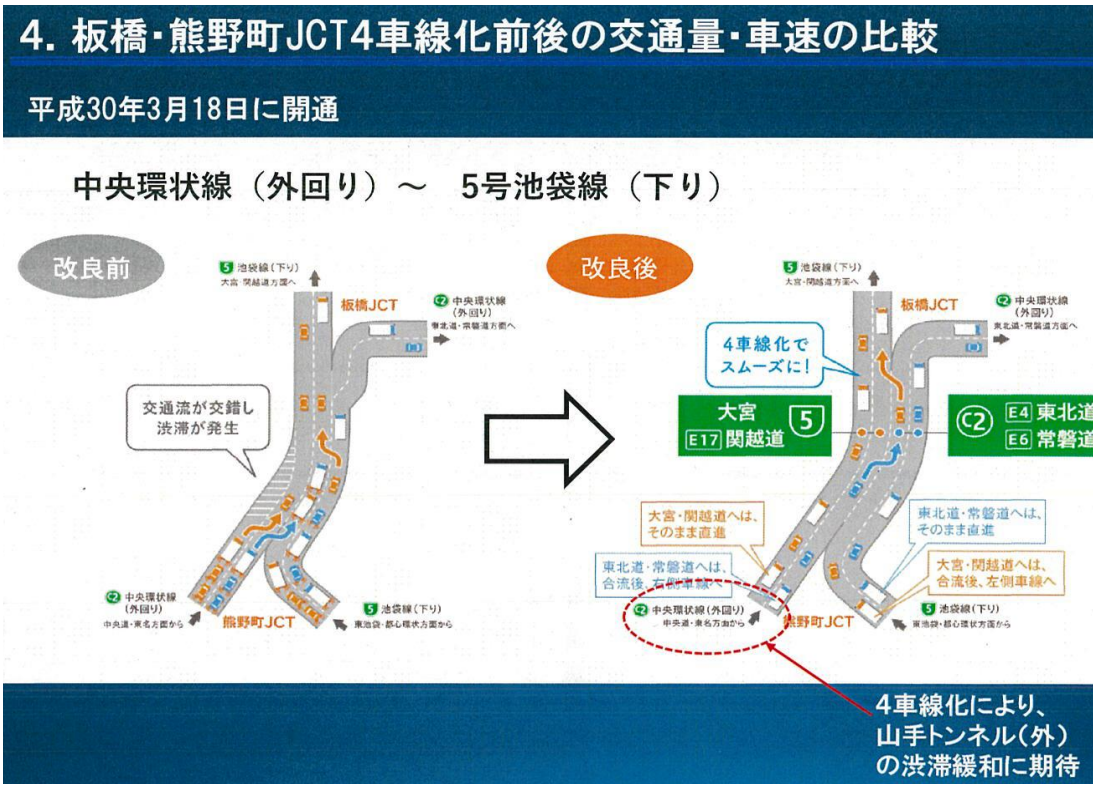

Figure 4.9 Traffic volume and vehicle speed before and after the lane increase at the Itabashi/Kumanocho junction.

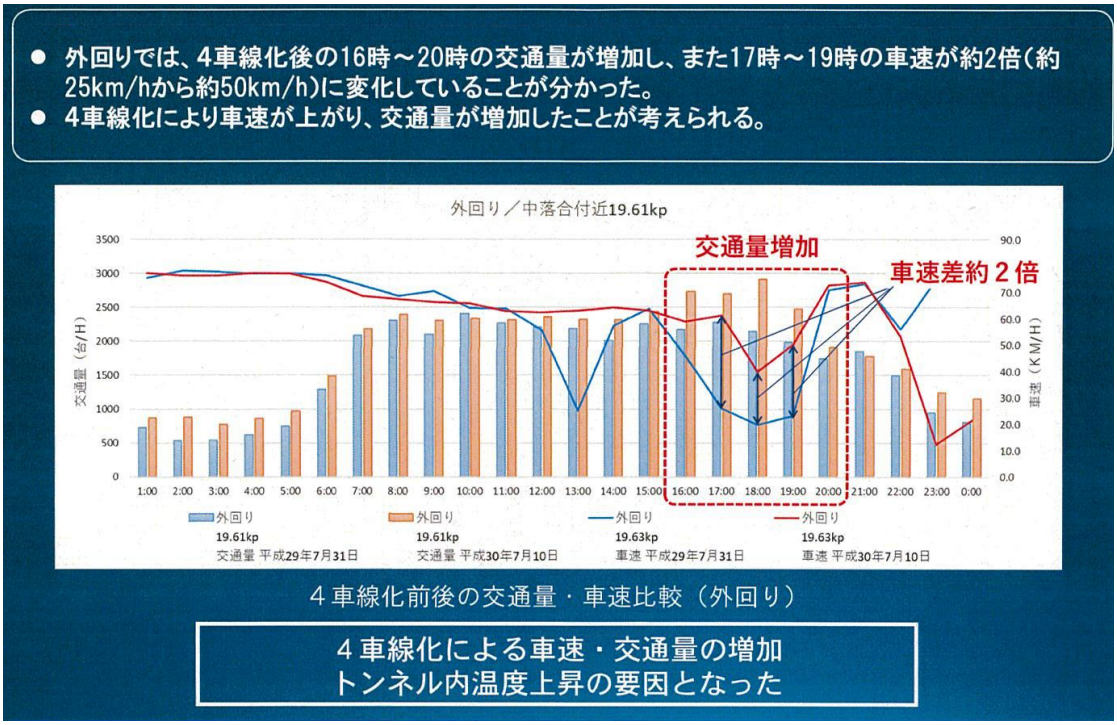

* *Source: Shutoko Expressway Company*

Figure 4.10 Temperature increase due to the increase of vehicles speeds in Yamate Tunnel.

4.4.2 Accuracy analysis

Root Mean Square Method (RMSE) analyses were conducted to check the accuracy of matching the results between the experiment and Numerical analysis. Figure 4.11 shows the variation of the values of RMSE with respect to wind speeds and Table 4.5 summarises them.

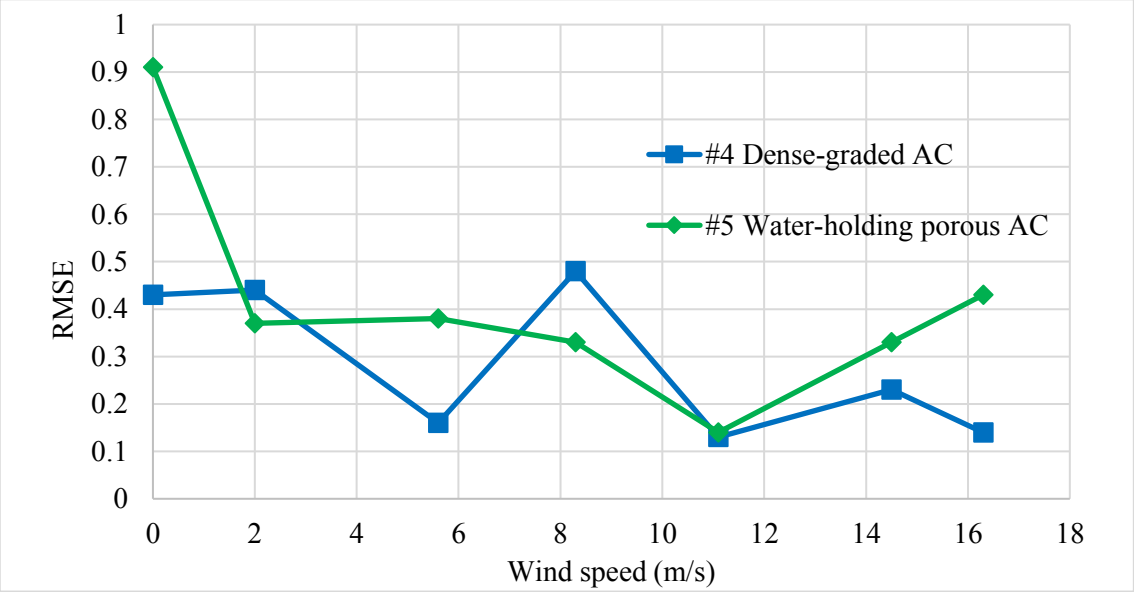

Figure 4.11 Variation of the RMSE values with respect to wind.

Table 4.5 Actual values of RMSE with respect to wind of AC#4 and AC#5.

Wind speed (m/s)	Root Mean Square Error (RMSE)	
	#4 Dense-graded AC	#5 Water-holding porous AC
0	0.43	0.91
2	0.44	0.37
5.6	0.16	0.38
8.3	0.48	0.33
11.1	0.13	0.14
14.5	0.23	0.33
16.3	0.14	0.43

4.5 Derivation of Combined Heat Transfer Coefficient depending on Water-spray

The obtained values of CHTC with respect to water-spray amount is shown in Figure 4.12. Here, the values were derived under the effect of wind speed 5.6m/s as well. The results show higher values for the ordinary asphalt (dense-graded) type until the water-spray amount 0.6l/m^2. At the water-spray amount 0.6l/m^2, both asphalt type values become close to each other and then directs at the line of convergence. This indicates both types of asphalt specimens start to show the same temperature increase when the water-spray amount is bigger than 0.6l/m^2. Table 4.6 summarises the actual values of heat transfer coefficient with respect to the water-spray effect.

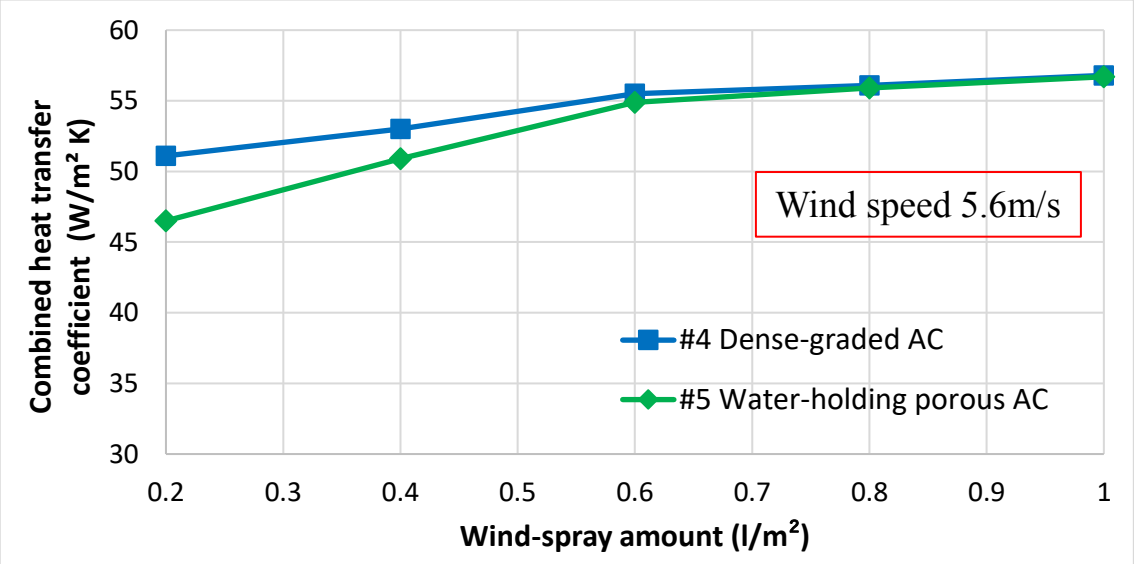

Figure 4.12 Variation of combined heat transfer coefficients with respect to water-spray.

Table 4.6 Numerically obtained CHTC with respect to water-spray amount

Water-spray amount (l/m^2)	Heat transfer coefficient (W/m^2 K)	
	#4 Dense-graded AC	#5 Water-holding porous AC
0.2	51.1	46.5
0.4	53	50.9
0.6	55.5	54.9
0.8	56.1	55.9
1	56.8	56.7

4.5.1 Example of Radiated Heat Amount

The amount of heat that taken away from the asphalt surface to surroundings by the water spray and wind speed 5.6m/s is illustrated in Figure 4.13. The higher the water-spray amount, the more amount of heat radiates to the air in case of ordinary asphalt type. However, in the case of water-holding porous asphalt, the amount of radiated heat decreases until the 0.6l/m^2 then becomes stable. Table 4.7 summarizes the actual values.

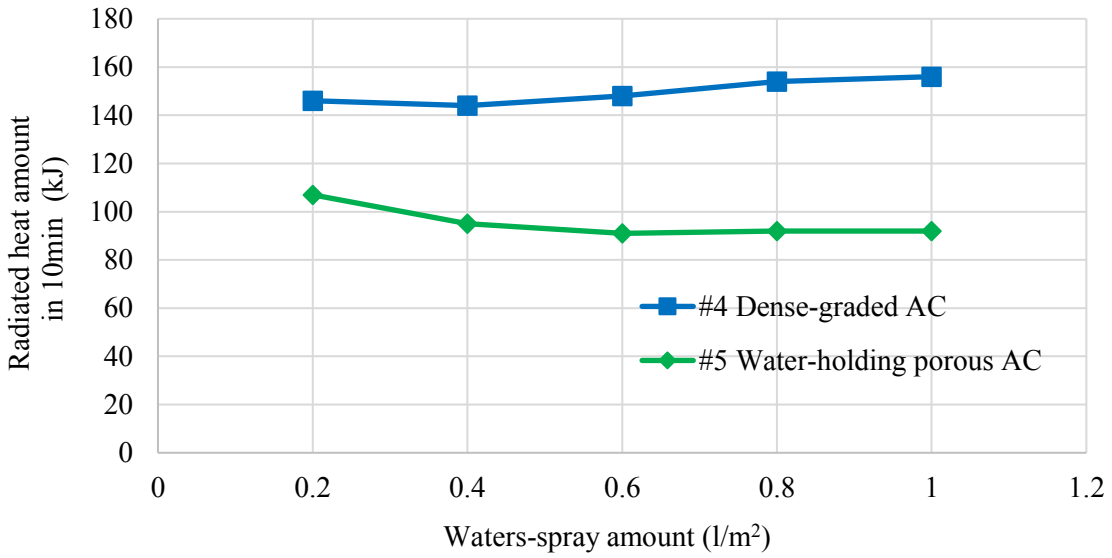

Figure 4.13 Variation of radiated heat amount with respect to water-spray.

Table 4.4 Actual values of radiated heat amounts with respect to water-spray.

Water-spray amount (l/m^2)	Radiated Heat Amount in 1h (kJ)	
	#4 Dense-graded AC	#5 Water-holding porous AC
0.2	146	107
0.4	144	95
0.6	148	91
0.8	154	92
1	156	92

4.5.2 Accuracy analysis

Root Mean Square Method (RMSE) analyses were conducted to check the accuracy

of matching the results between the Experiment and Numerical analysis as shown the results in Figure 4.13. The values of RMSE ended up with bigger numbers compared to the result of the wind effect. Thus, the results may have less accuracy and need to be reconsidered. Table 4.7 summarises the obtained RMSE values.

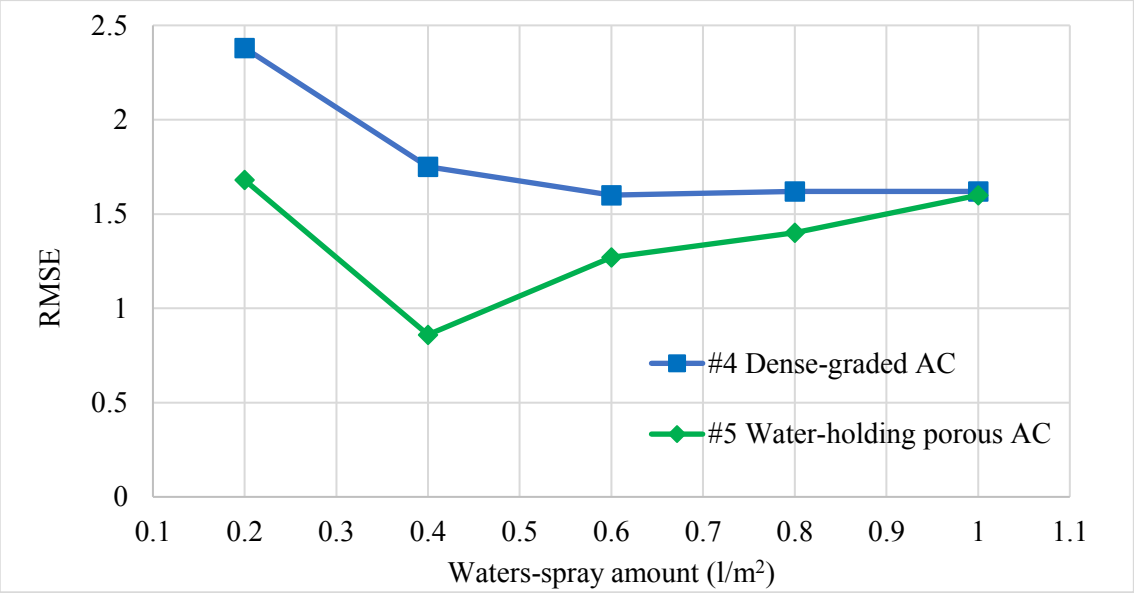

Figure 4.13 Variation of the RMSE values with respect to water-spray amount.

Table 4.5 Actual values of RMSE with respect to water-spray amount.

Wind speed (m/s)	Root Mean Square Error (RMSE)	
	#4 Dense-graded AC	#5 Water-holding porous AC
0.2	2.38	1.68
0.4	1.75	0.86
0.6	1.6	1.27
0.8	1.62	1.4
1	1.62	1.6

4.6 Test under Water-Spray Effect

4.6.1 Test input parameters

Table 4.6 Test input parameters

Asphalt type		Radiation amount	Water-spray amount
#2	Ordinary asphalt (Dense-graded AC)	800 w/m2	0.2L/m^2, 0.26 L/m^2, 0.4 L/m^2, 0.55 L/m^2, 0.6L/m^2, 0.8L/m^2, 1L/m^2
#3	Water-holding Porous AC		

4.6.2 Test for temperature cooling without water-spraying.

The surface temperatures of both specimens were heated till 50ºC and once they reached 50ºC the wind started to blow towards the specimen surfaces. Figure 4.12 represents the temperature decrease under seven types of wind speed, but no water effect. The wind flow duration was 20minutes. After that, the next higher wind speed effect was applied when the specimen reached 50ºC again. Obviously, the temperature decreases with the increase of wind speed. Here, water-holding porous asphalt shows faster cooling up to 3ºC.

4.6.3 Test for temperature cooling under water spray and wind speed effect

Figure 4.13 shows the temperature cooling under seven types of watering at the constant wind speed 2.4m/s. Once the surface temperatures reached 50ºC, the first amount of the water spray flushed quickly to them, at the same time, the wind started to flow. The watering interval was 20minutes. After 20minutes, the next higher water spray was applied when one of the specimens reached 50ºC again. The ordinary asphalt type #2 does not have a significant effect, while water-holding porous asphalt #3 shows a decrease of surface temperature. Humidity does not change with the change of wind speed. Here, water-holding porous asphalt shows better cooling rate again.

Figure 4.14 shows the temperature cooling under the same test conditions but at the wind speed 4m/s. At this wind speed, the temperature decrease was observed at both types of asphalt specimen.

For the wind speed impact at 5.3m/s Figure 4.15 was illustrated. The decrease of temperature does not differ from the previous case at the asphalt type #2, while #3 shows a higher rate of temperature cooling.

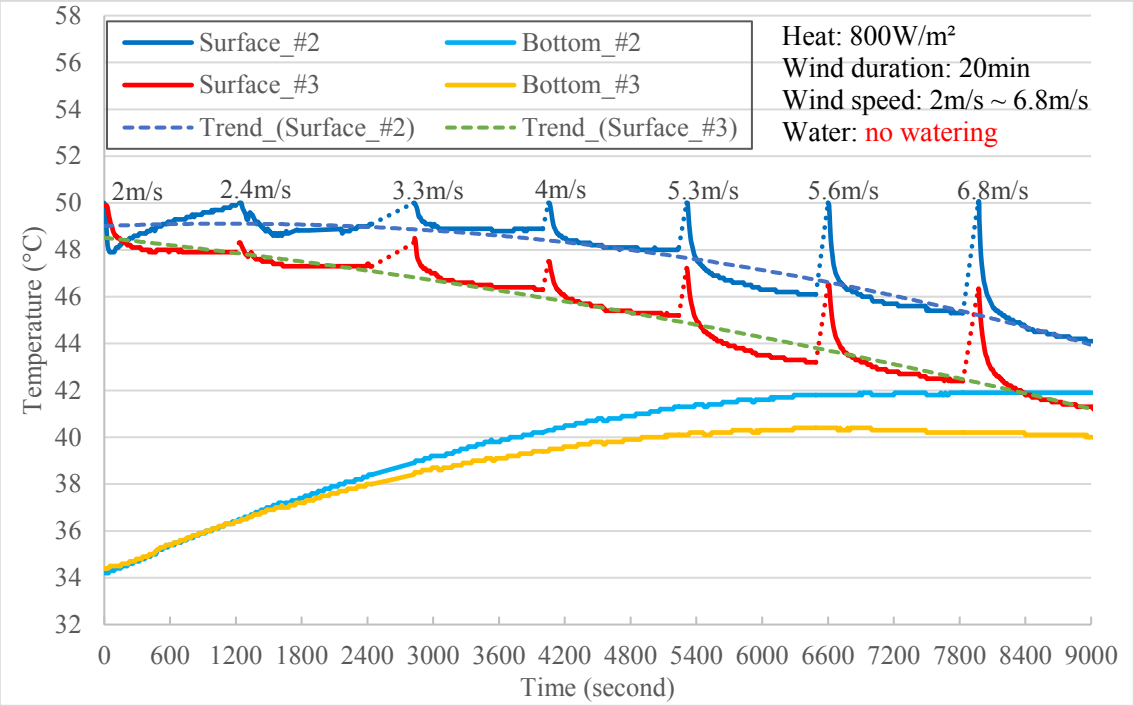

Figure 4.12 Temperature cooling under seven types of wind speed without water effect.

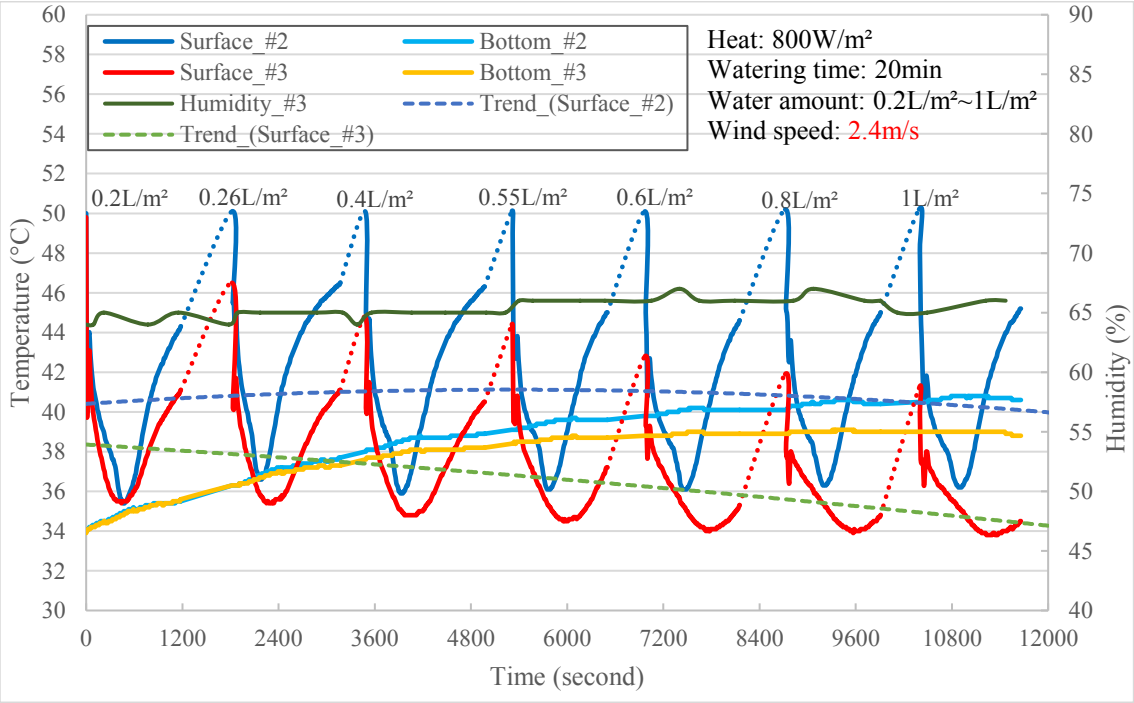

Figure 4.13 Temperature cooling under seven types of watering at the wind speed 2.4m/s.

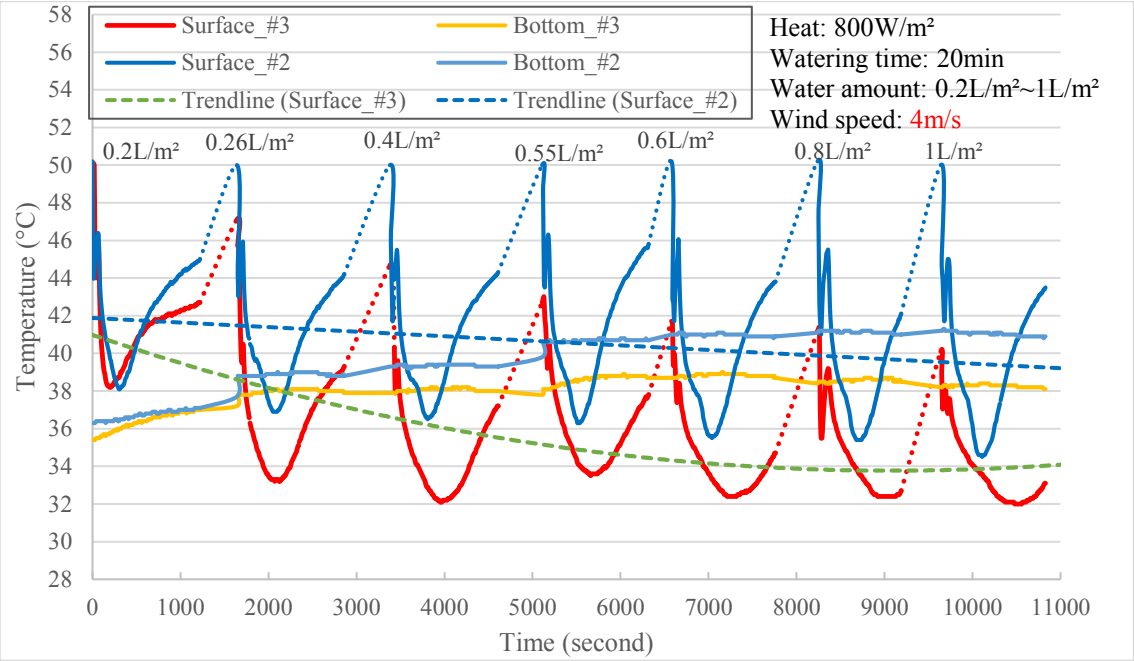

Figure 4.14 Temperature cooling under seven types of watering at the wind speed 4m/s.

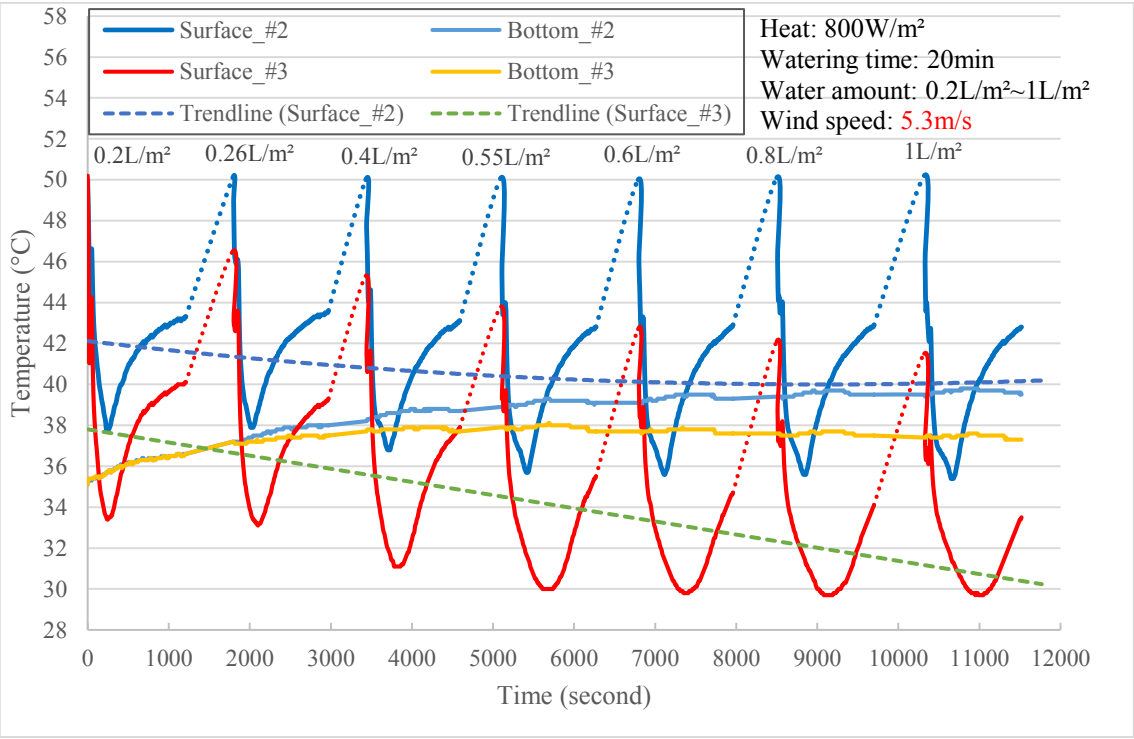

Figure 4.15 Temperature cooling under seven types of watering at the wind speed 5.3m/s.

4.7 Test under Tunnel-Environment Condition

4.7.1 Introduction of the test

The test under "Tunnel-Environment condition" was performed to check the temperature changes as well as the humidity fluctuation at the air adjacent to the asphalt specimen surfaces. The "Tunnel-Environment condition" indicates that the surfaces of specimens were covered with the materials that shape the same as the road-tunnel as shown in Figure 4.16.

4.7.2 Results

When there is no wind effect, the temperature starts to decrease after the watering amount: 0.8L/m2 at the asphalt type #2. It starts faster at the asphalt type #3. Change of humidity was not significant (Figure 4.17).

Figure 4.18 represents the effects of the watering at the wind speed 2.4m/s under the "tunnel-environment" condition. At the existence of wind, humidity remains constant. Temperature decreases faster, especially at the asphalt type #3.

Figure 4.19 shows the effects of the watering at the wind speed 5.3m/s under the "tunnel-environment" condition. The humidity starts to decrease; however, the decrease rate of surface temperature does not change significantly.

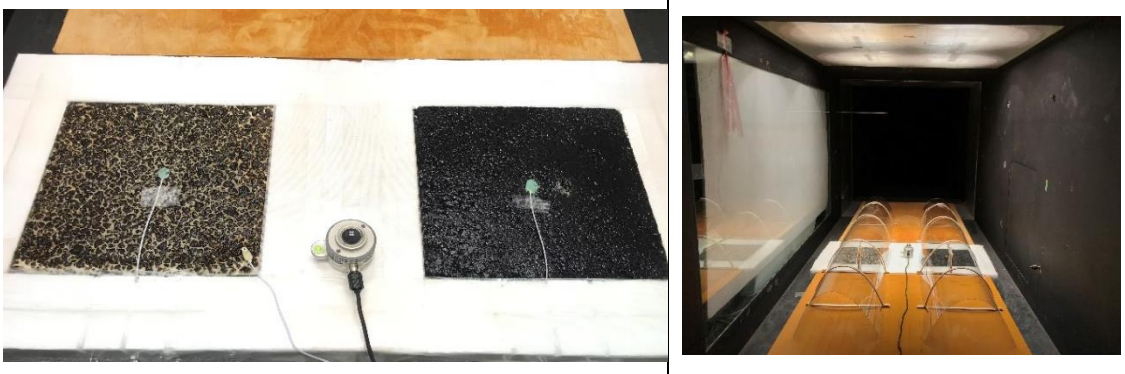

(a) (b)

Figure 4.16 (a) Water-sprayed asphalt specimen surfaces, (b) Created tunnel-environment to measure the generated humidity by water-spray.

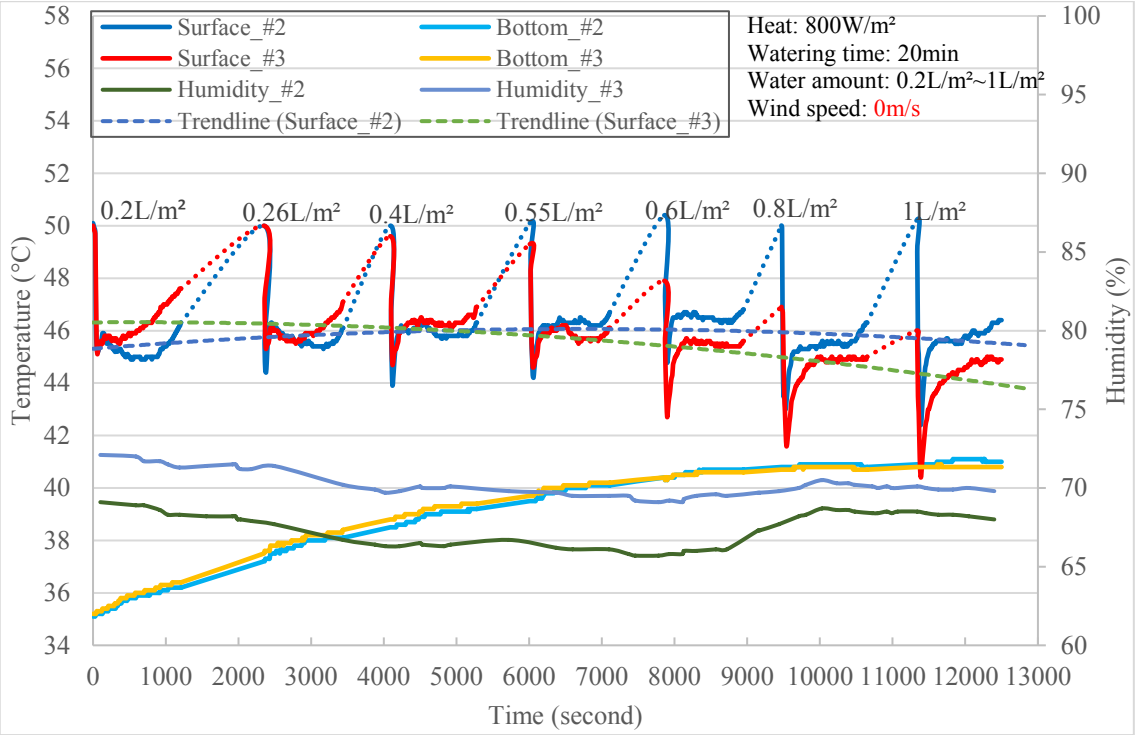

Figure 4.17 Effects of "tunnel-environment" condition without the influence of wind speed.

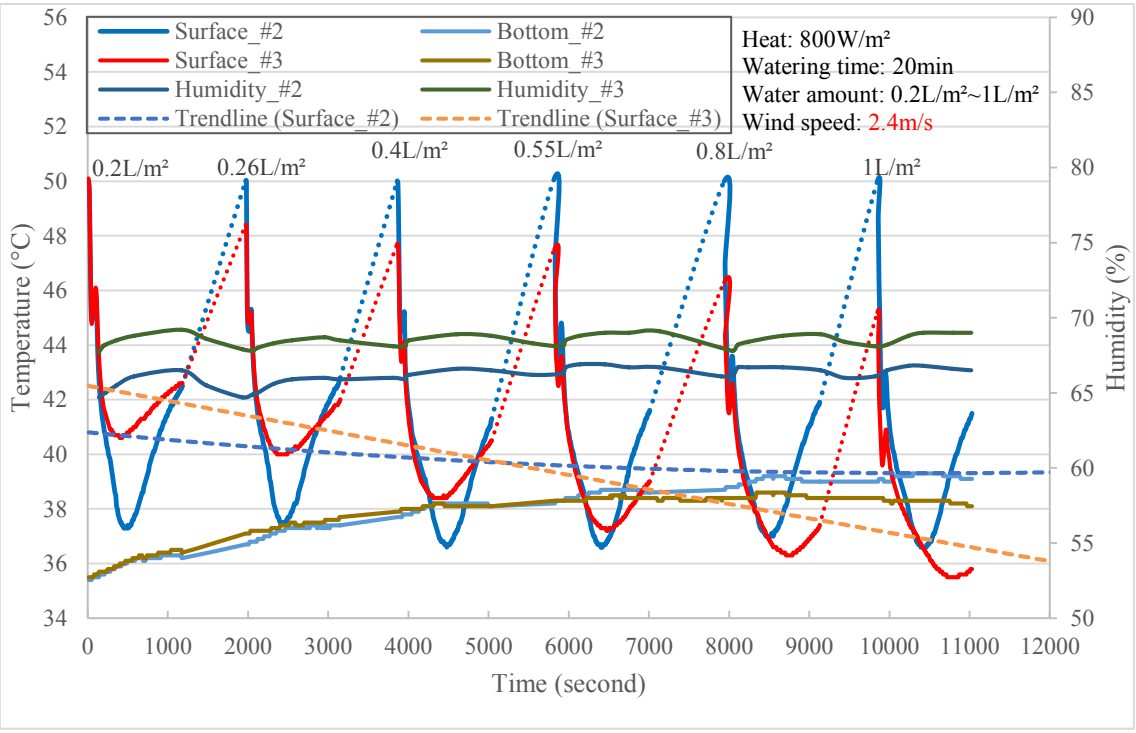

Figure 4.18 Effects of the watering at the wind speed 2.4m/s under the "tunnel-environment" condition.

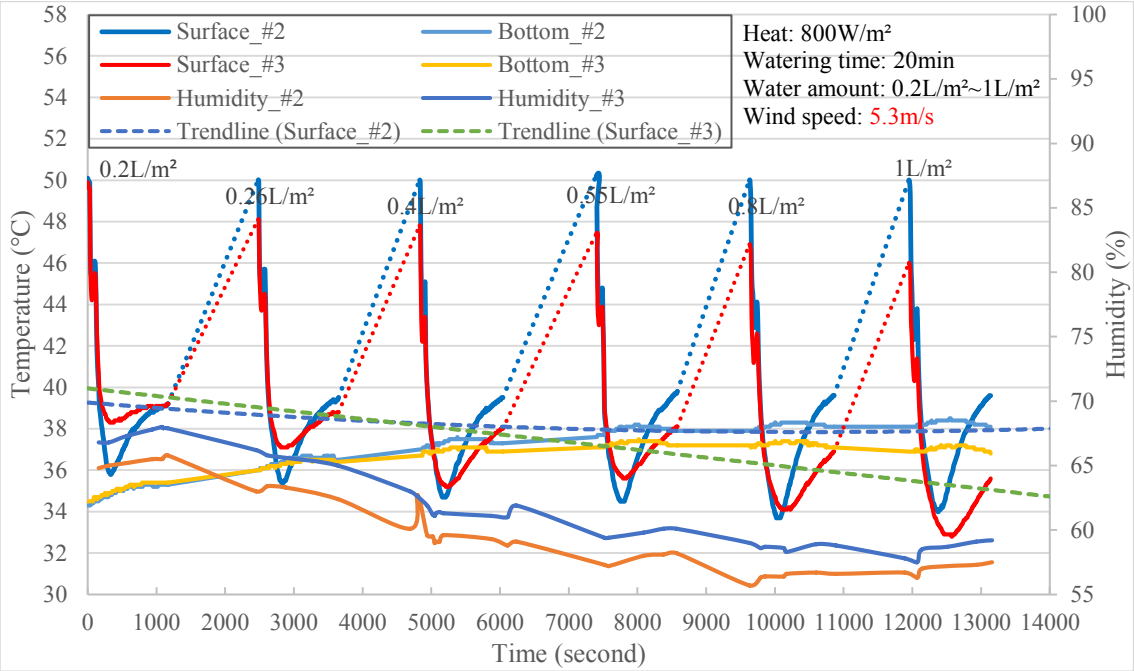

Figure 4.19 Effects of the watering at the wind speed 5.3m/s under the "tunnel-environment" condition.

4.8 Summary of Chapter 4

In this chapter, two types of AC specimens: ordinary type AC (dense-graded) and water-holding porous AC were tested in the wind-tunnel under the wind and water spray effect to analyze the efficiency of water-holding porous asphalt at the high air temperature. The specimens were heated by the direct radiative heat lamps.

Based on the obtained experimental data, the values of combined heat transfer coefficients (h) were numerically calculated. The values showed higher numbers in the case of water-spray amount effect than the effect of wind speed. The values of combined heat transfer coefficients are essential and useful in controlling the temperature rise in a road tunnel.

Finally, the test under "Tunnel-Environment condition" was performed to check the temperature changes as well as the humidity fluctuation at the air adjacent to the asphalt specimen surfaces.

Overall, the water-holding porous asphalt had a better thermal performance that can suppress the surface temperature by 3ºC compared to the ordinary asphalt specimen.

References and Suggested Readings

Sightline Institute, (2012). The Porous Road Less Traveled Retrieved from https://www.sightline.org/2012/01/03/the-porous-road-less-traveled/

Yunus A. Cengel, (Second Edition). Heat Transfer. A practical approach.

Shutoko Expressway Company (2019). Traffic volume and vehicle speed before and after the lane increase at the Itabashi/Kumanocho junction. Annual report.

R. Veerasamy, H. Rajak, and A. Jain, "Validation of QSAR Models - Strategies and Importance", International Journal of Drug Design and Discovery, 2-3, pp. 511-519, 2011/9.

JFE Steel Corporation, (2006). Experimental data of performance test of water-holding block.

Journal of JSCE Vol.63 No.2, 250-261, 2007,5.

CHAPTER V

5. APPROACHES TO IMPLEMENT COUNTERMEASURE AGAINST ASPHALT HIGH TEMPERATURE

Abstract

The effects of different basement boundary conditions and water spray on the surface temperature were investigated to find effective countermeasures to decrease the surface temperature of AC in the tunnel. Additionally, 2D model of heat transfer simulations of Yamate Tunnel considering asphalt type effects including the wind and water-spray approaches were performed to investigate the effects of water-holding porous asphalt to decrease the hot air temperature in the Tunnel.

5.1 Introduction and objectives

Extra tests were conducted in order to investigate how much the surface temperature of asphalt specimens can be decreased if their bases are replaced by different materials and the surfaces are subjected to water spray. In this study, the asphalt specimen #4 was chosen as a target.

5.2 5 Types of Countermeasure Approaches

5.2.1 Influence of Concrete Base at Thicknesses 12 cm & 30 cm

Figure 5.1 shows the scheme of the test conditions with two types of concrete base thicknesses as to measure the effect of subbase concrete against high asphalt surface temperature. In the case of (a), 12 cm of the thick concrete base was installed to examine how much the temperature of asphalt would be decreased when the bottom face has contact with concrete, and this effect was examined when the thickness of subbase concretes was increased.

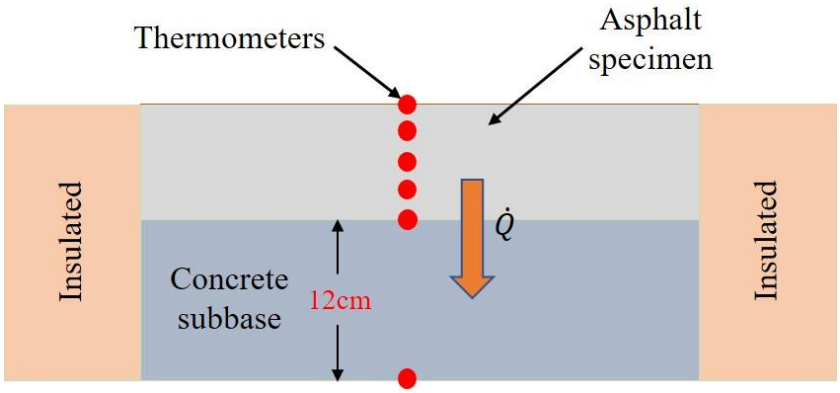

(a) Test with with 12cm of thick concrete

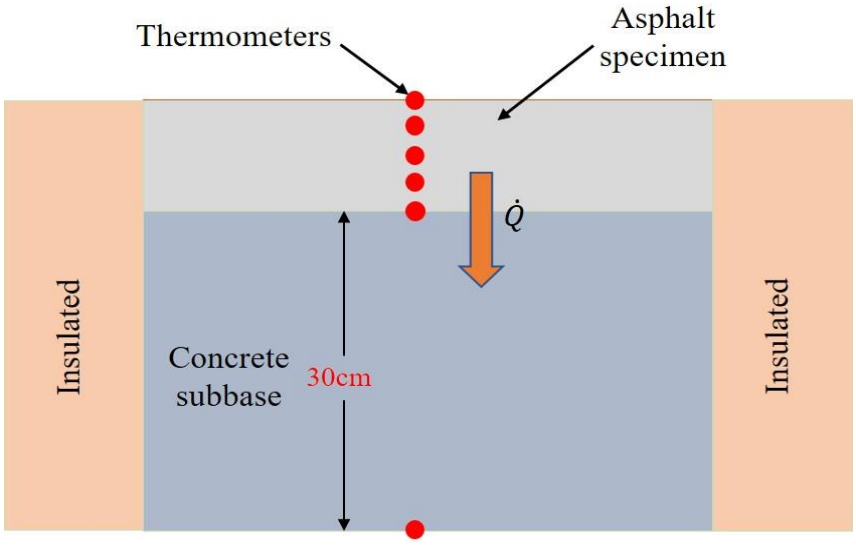

(b) Test with with 30cm of thick concrete

Figure 5.1 Scheme of the test conditions with two types of concrete base thicknesses

5.2.2 Influence of Steel Plate Base

Another approach is with a steel plate (Figure 5.2), where 1 cm thick steel plate was replaced the concrete base taking into account its higher heat conductive property. Steel plate might conduct the heat away from the asphalt much faster than concrete.

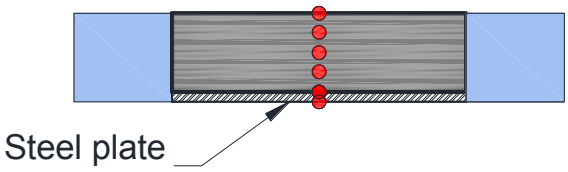

Figure 5.2 Scheme of the test condition with steel plate base

5.2.3 Influence of H-beams Together with Steel Plate Base

At the next approach (Figure 5.3), H-beams were added to the steel plate to improve the effect of steel in decreasing the temperature of the asphalt.

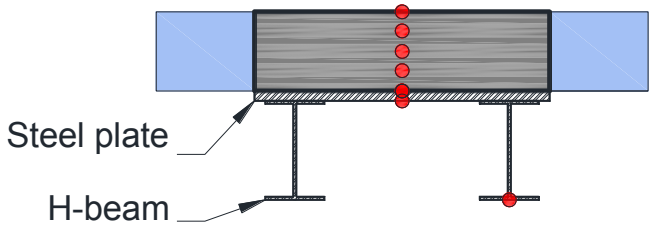

Figure 5.3 Scheme of the test condition with steel plate & H-beams base

5.2.4 Influence of Water-Spray

The last countermeasure (Figure 5.4) is a water spray which is an easy approach to implement. 0.26 l/m^2 water was sprayed to the asphalt surface at the beginning of the test.

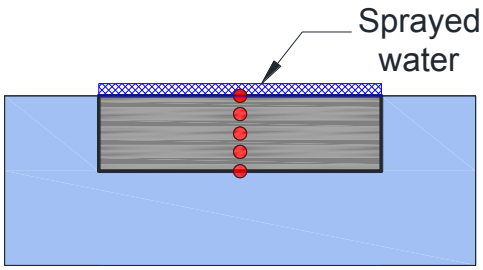

Figure 5.4 Scheme of the test condition with steel plate & H-beams base

5.3 Results and Discussions

The results of all countermeasures against high asphalt surface temperature are plotted in Figure 5.5. Here, the "only asphalt" case that is without any approaches was added as well for the comparison. The water sprayed surface revealed the biggest temperature decrease which was by 6ºC lower than the "only asphalt" case. Surprisingly, the effects of concrete and steel basement were not so big showing a similar temperature decrease that is approximately 2ºC. The water spray showed again high performance when comparing the bottom temperature decrements (see Figure 5.6). Steel basements decreased the temperature up to 3ºC while interestingly the concrete basement decreased the temperature by 5ºC performing equally as the water spray.

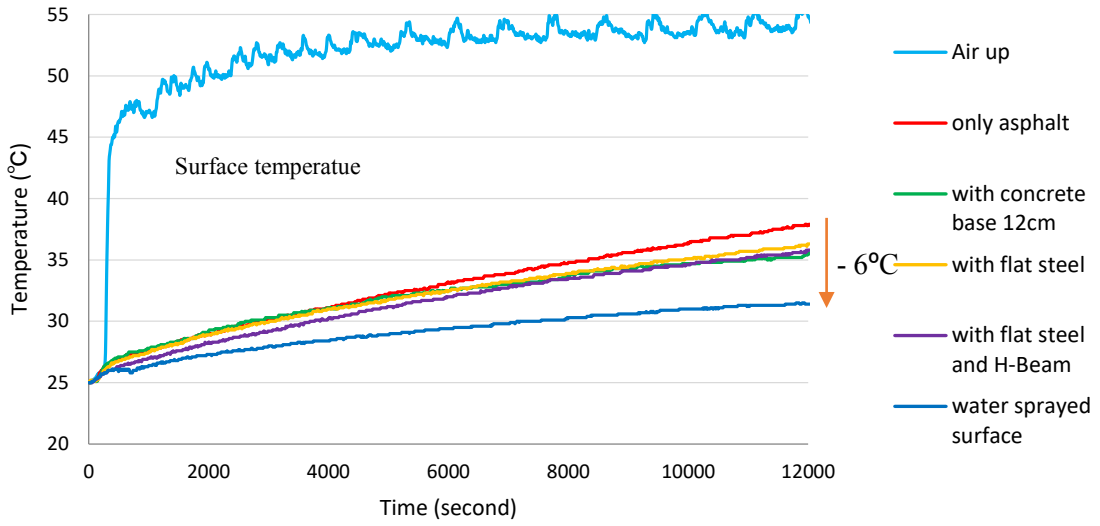

Figure 5.5 Comparison of surface temperature decrements of all "different base and water spray" test cases.

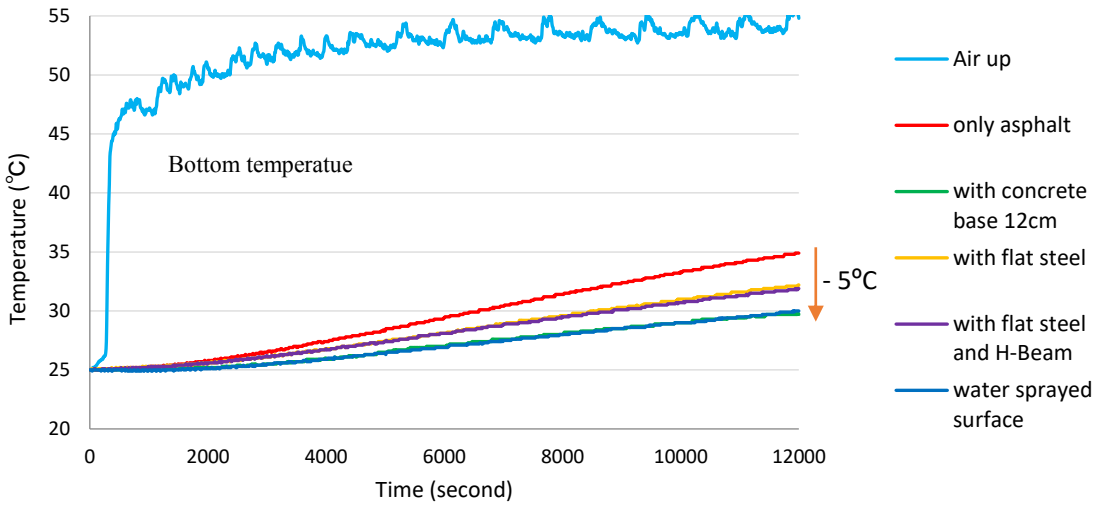

Figure 5.6 Comparison of surface temperature decrements of all "different base and water spray" test cases.

5.4 2D Simulations of Temperature Distributions in Yamate Tunnel

5.4.1 Introduction and objectives

2D Simulations were performed on the purpose of to simulate the air temperature distribution in Yamate Tunnel by using the actual traffic volume at summer season. The "water-spray approach" was demonstrated and the results were compared with the normal case. The simulation input parameters were applied from the values that were derived in this study.

5.4.2 Input parameters for simulation model

First, we chose the traffic volume of Yamate Tunnel that measured at one of the summer days, as shown in Figure 5.7. Six times were chosen, including rush hours. Then we have calculated the heat amount of vehicles each time and applied it as a heat source to the model. Also, other values as heat transfer coefficients under wind effect and water-spray effect, as well as heat conductivity and specific heat were used from our experimental results.Besides, the asphalt surface temperature and ventilation volume amount were applied as initial values from measurements. After the simulation run, we probed air temperature at two points. They are: 30cm and 150cm above from the asphalt pavement surface that is around the same level as a human body as illustrated in Figure 5.8. The input parameters are summarised in Table 5.1.

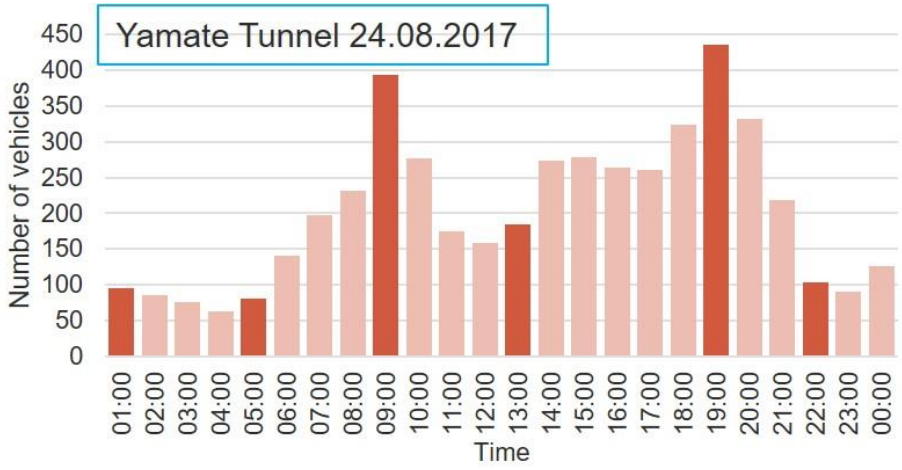

Figure 5.7 Overall traffic volume in Yamate Tunnel at summer season

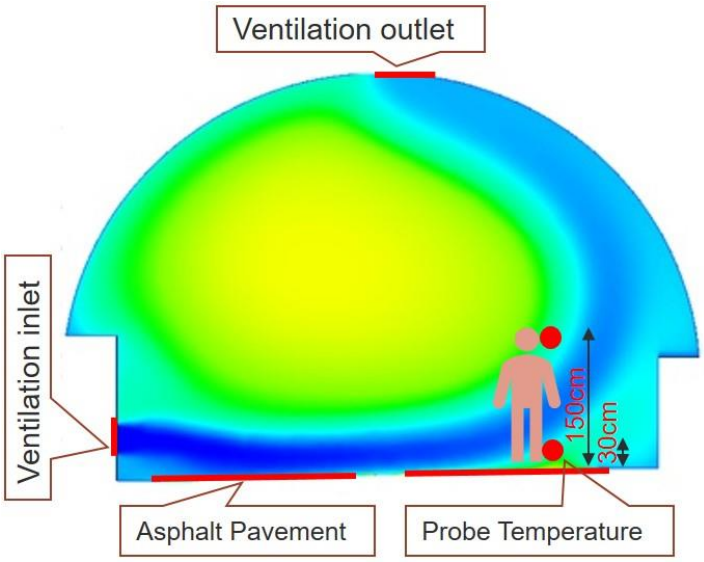

Figure 5.8 Model of Yamate Tunnel for simulation

Table 5.1 Input parameters for simulation

Vehicle heat amount W/m^3	Obtained h values from experiment W/m^2 K	Asphalt temperature ℃	Ventilation inlet m/s	Ventilation outlet m/s
3, 3.1, 10.5, 5, 12, 2.9	Wind 32.6 & 24.9 Water 56.8 & 56.7	45 & 42 40 & 37	0.5	0.5

5.4.3 Meshing quality

The mesh quality is very satisfied that the metric of Skewness Quality and Orthogonal Quality lie between "Excellent Section" (Figure 5.9). The area nearby the asphalt surface and ventilation input/output surface were meshed finely to achieve more accurate results.

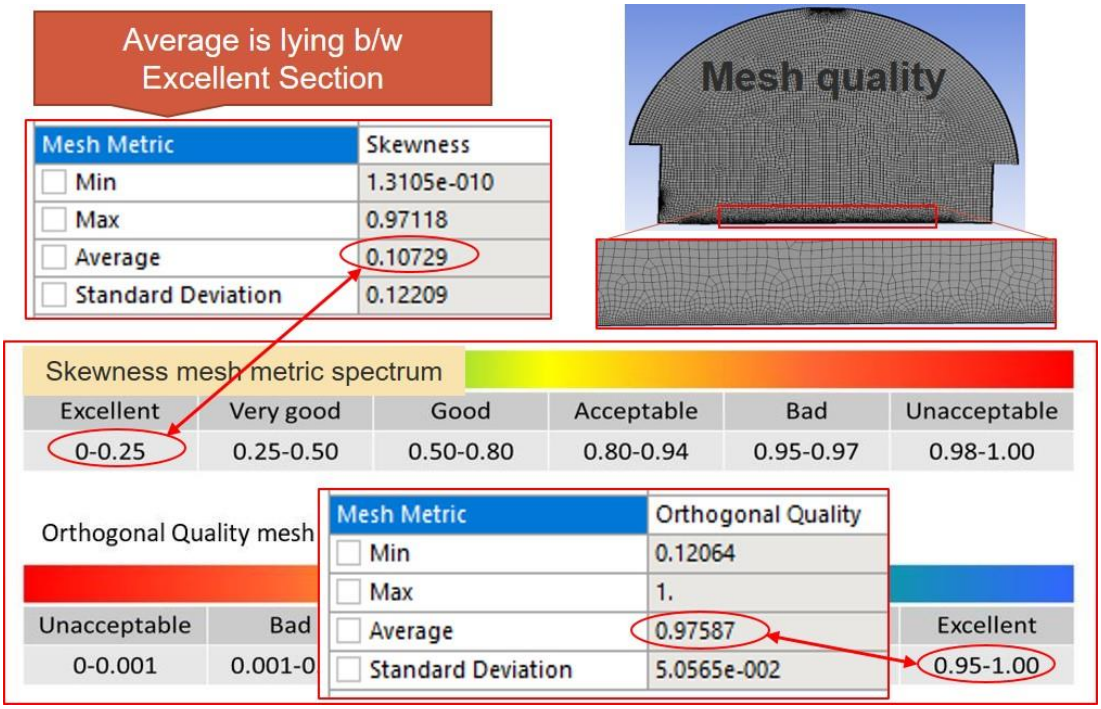

Figure 5.9 Mesh quality

5.4.4 Simulation Results

First, the simulation was performed with the asphalt type that is actually was used in Yamate Tunnel. Then it was replaced with the water-holding porous asphalt to check whether this type can reduce the air temperature or not.

The results of temperature distributions in Yamate Tunnel at each time at normal/ordinary asphalt type is presented in Figure 5.10. (a) shows the results with the wind effect, while (b) represents the results with the water-spray effect.

Figure 5.11 shows the same results but in the case when the asphalt pavement was replaced with water-holding porous asphalt.

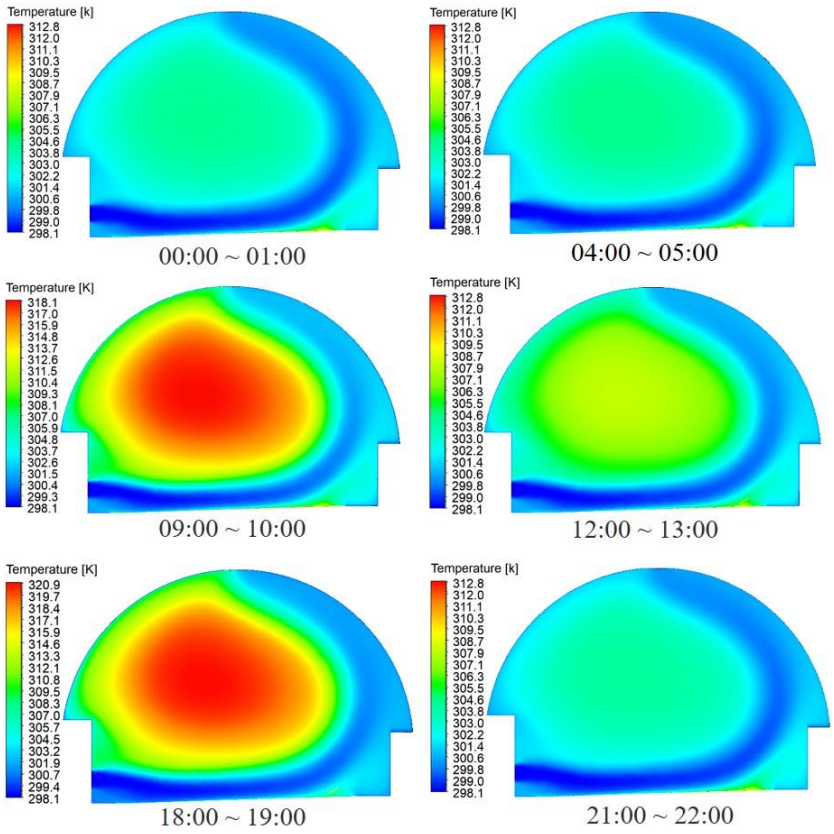

(a) With wind effect (5.6m/s)

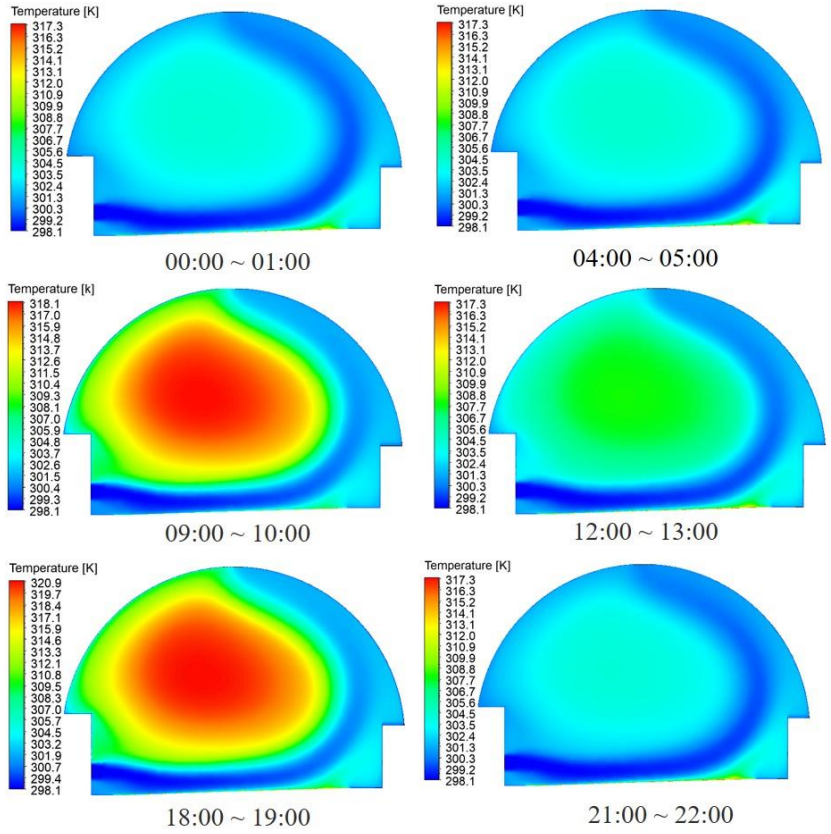

(b) With water-spray effect (1L/m^2)

Figure 5.10 Temperature distribution in Yamate Tunnel with ordinary asphalt type

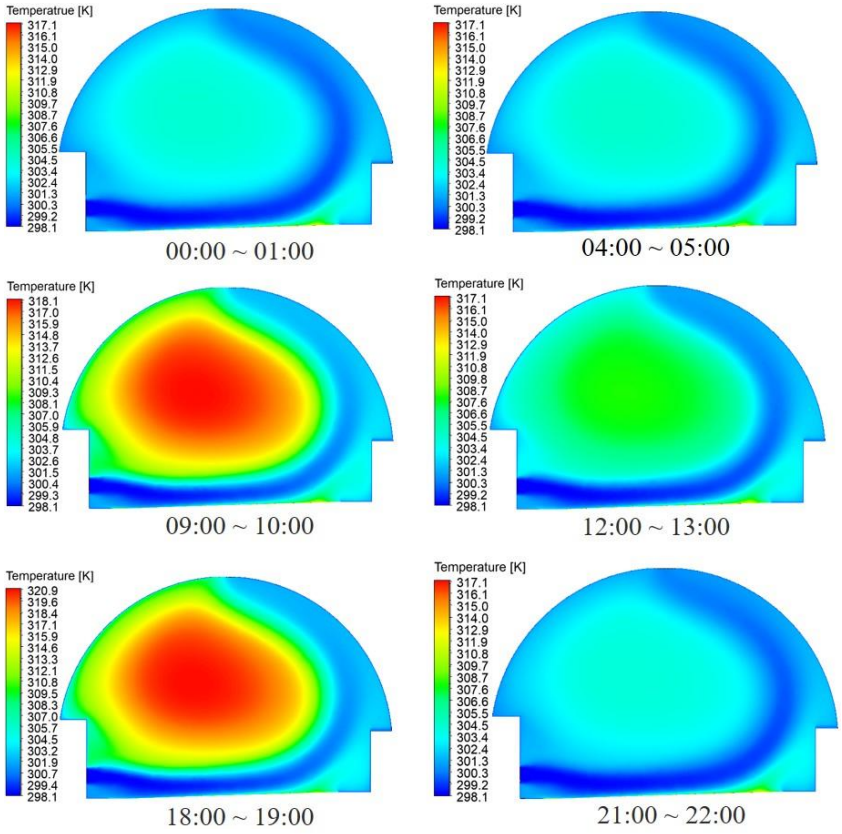

(a) With wind effect (5.6m/s)

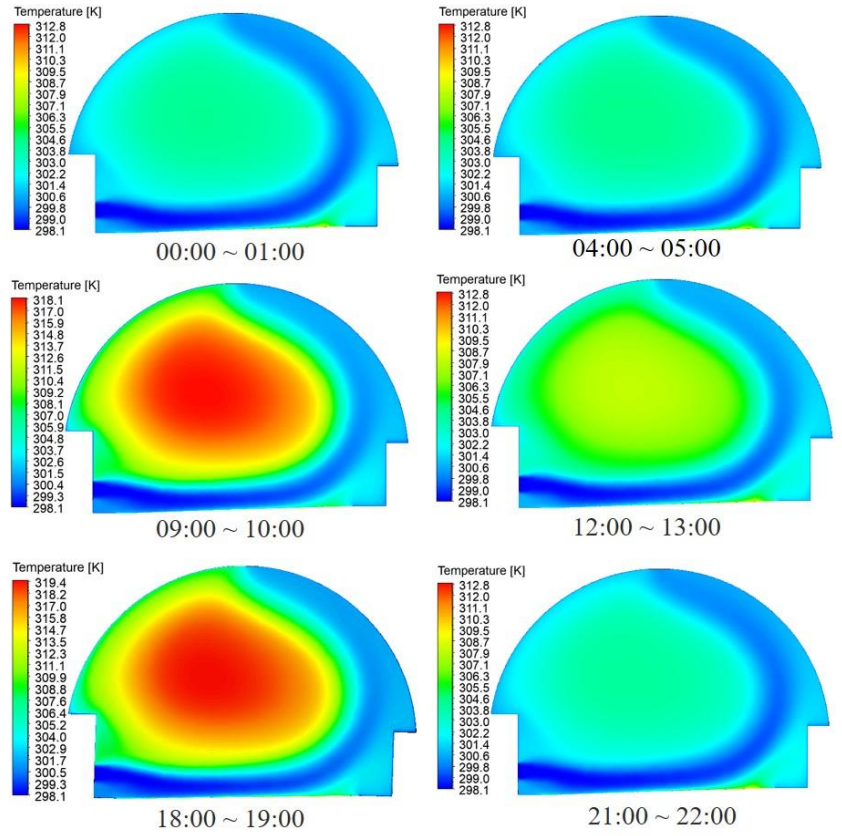

(b) With water-spray effect (1L/m^2)

Figure 5.11 Temperature distribution in Yamate Tunnel with water-holding asphalt type

5.4.5 Findings on simulation

The air temperature at two points: 30cm and 150cm above from the asphalt pavement surface was probed after the simulation run reached the steady stage. As shown in Figure 5.12, the temperature increases more than 10^0C at 150cm at rush times while the temperature at 30cm that just the upper side of the asphalt pavement does not increase much.

The effect of the water-spraying was clear and it decreased the temperature around 2 ^{0}C at 30cm. However, it did not show the effect at 150cm.

The water-holding porous asphalt gave the same scenario, except the slight effect of water-spray at the rush time: 18:00-19:00 as plotted in Figure 5.13.

Figures 5.14 and 5.15 are comparing the results between the ordinary asphalt type and the water-holding porous asphalt type at two probe points, respectively. At 150cm, only the water spray at porous asphalt effects slightly better, while no difference derived between the others. At 30cm, again the water spray approach clearly shows the effect regardless of the asphalt pavement type.

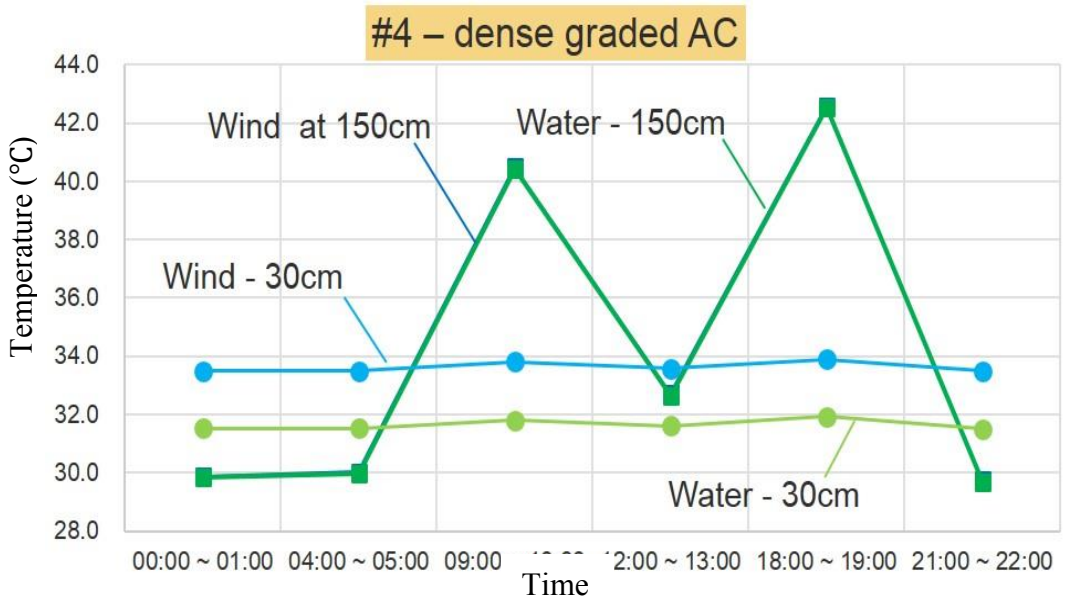

Figure 5.12 Temperature probe of two points at wind and water-spray effects, AC #4.

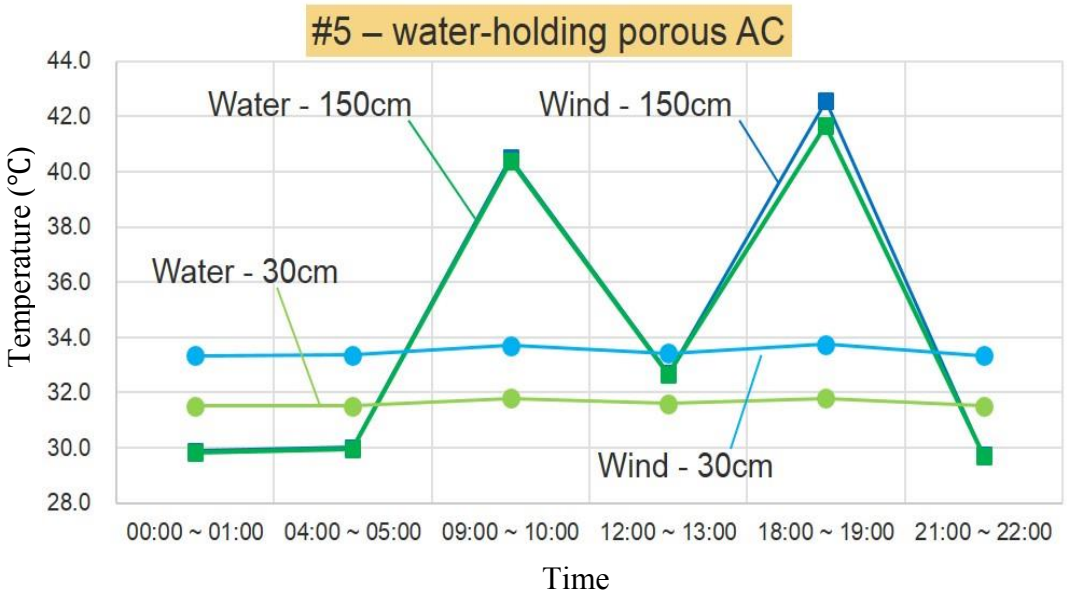

Figure 5.13 Temperature probe of two points at wind and water-spray effects, AC #5.

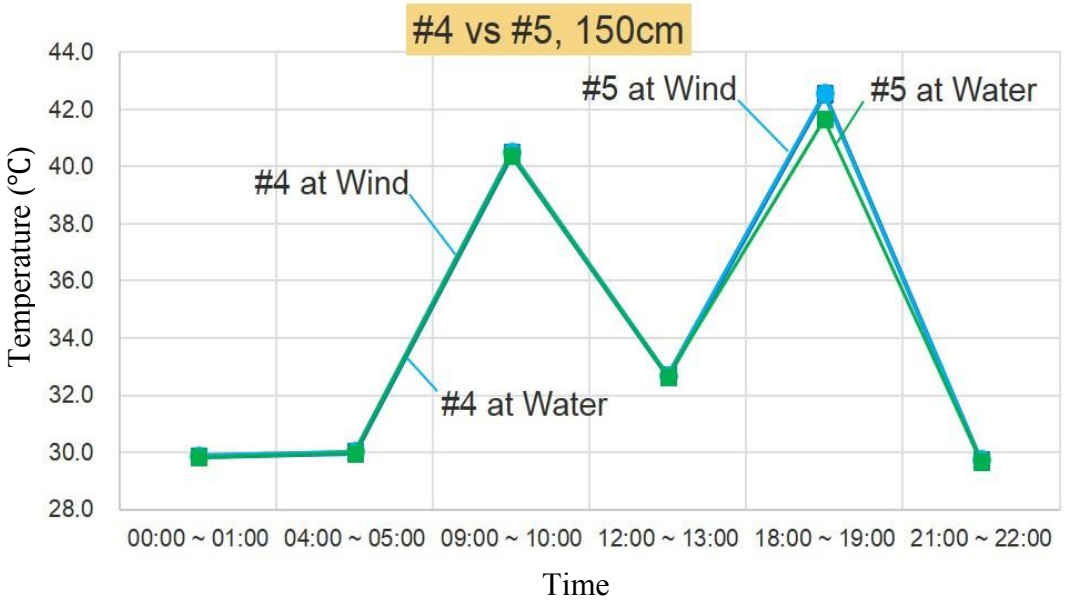

Figure 5.14 Comparison of wind and water-spray approaches between AC #4 and AC #5 at 150cm

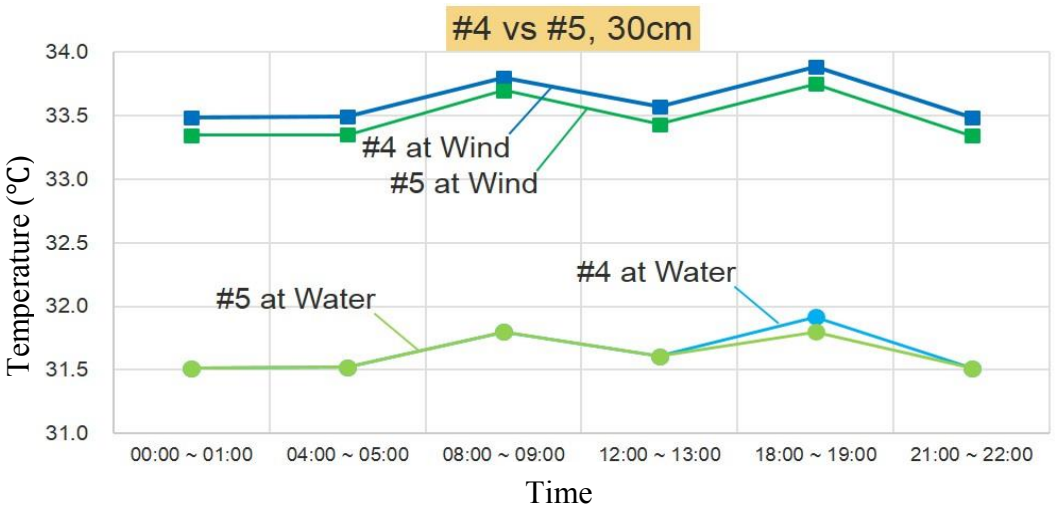

Figure 5.15 Comparison of wind and water-spray approaches between AC #4 and AC #5 at 30cm

5.5 2D Simulations of Temperature Distributions in Yamate Tunnel considering Vehicle model

5.5.1 Introduction and objectives

2D Simulations were performed on the purpose of to simulate the air temperature distribution in Yamate Tunnel by implementing the vehicle model as a heat source and by using the actual measured date of temperature and traffic volume at summer season. As a result, the percentage of the heat releasing from the asphalt and radiating to the air inside the tunnel were explained.

5.5.2 Input parameters for simulation model

The models of a vehicle bottom side (engine part) and the layer of asphalt pavement with the thickness of 8cm were constructed in the 2D model of Yamate Tunnel. The heat generated only from the vehicle model. After the simulation run, the air temperature was probed at the two points in the vertical direction at both Right and Left lanes. The points are surface of asphalt pavement and 150cm above from the asphalt pavement surface that is around the same level as a human body as illustrated in Figure 5.16. Thermal parameters of asphalt pavement were used from the experimental results. The input paramterers are summarised in Table 5.2.

The model is turbulence standard $k-\varepsilon$ model and Steady-state simulation.

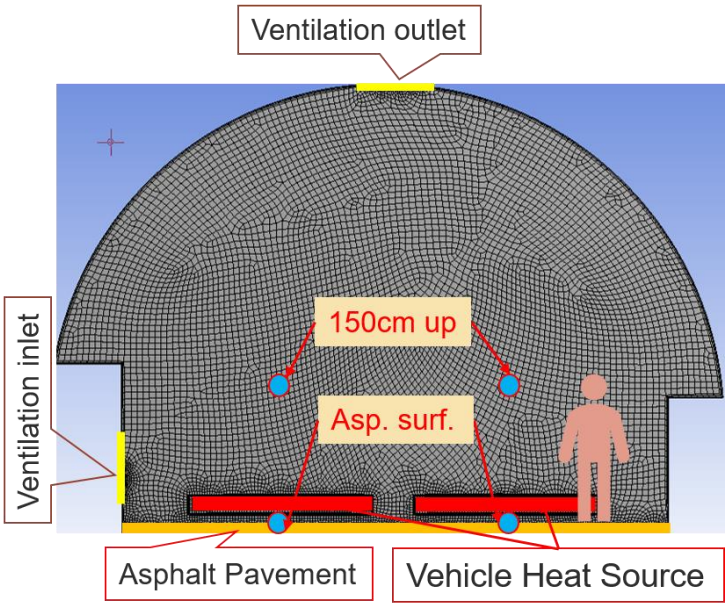

Figure 5.16 Model of Yamate Tunnel with Vehicle heat source

Table 5.2 Input parameters for simulation

Vehicle heat amount W/m^3	Obtained h values from experiment W/m^2 K	Asphalt temperature °C	Ventilation inlet m/s	Ventilation outlet m/s
700 & 310	Wind 32.6 & 24.9 Water 56.8 & 56.7	27	0.5	0.5

5.5.3 Meshing quality

The mesh is unstructured mesh. Its quality is very satisfied that the metric of Skewness Quality and Orthogonal Quality in a perfect range as shown in Figure 5.9. The area nearby the asphalt surface, vehicle model and ventilation input/output surface were meshed finely to achieve more accurate results.Total nodes number are 510000.

Mesh Information			
Name	Nodes number	Quality	
Unstructured	510000	Skewness 0.10729	Orthogonality 0.97587

Figure 5.17 Mesh information

5.5.4 Simulation Results

Figure 5.18 shows the results of temperature distribution in Yamate Tunnel at two types of the heat source amount: 700W/m^2 & 310W/m^2. The amounts were chosen based on the traffic volume at night and at noon, respectively. Figure 5.18 also shows the air velocity in both cases: in case of with ventilation and without ventilation. We see how the fluid direction changes when there is ventilation and thus it causes a high-temperature accumulation in a specific area in the tunnel.

Figure 5.19 shows the same results but in the case when the asphalt pavement was replaced with water-holding porous asphalt. We can see, the changing of the asphalt type not really decreases the temperature of the air in the tunnel.

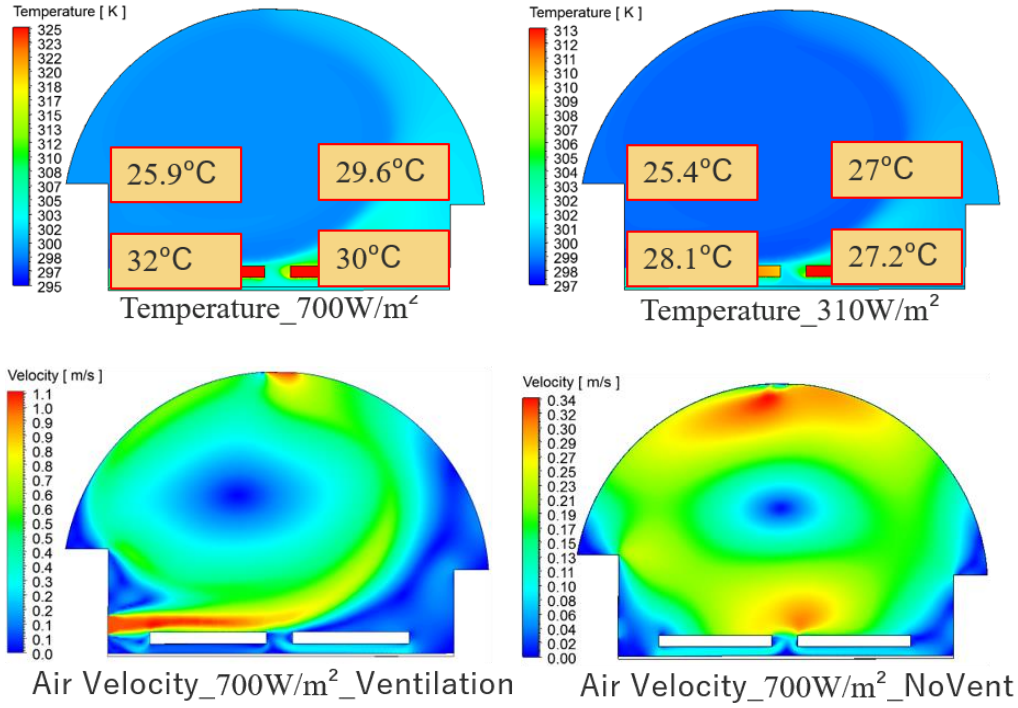

Figure 5.18 Temperature and Air Velocity plot. Ordinary asphalt type - #4

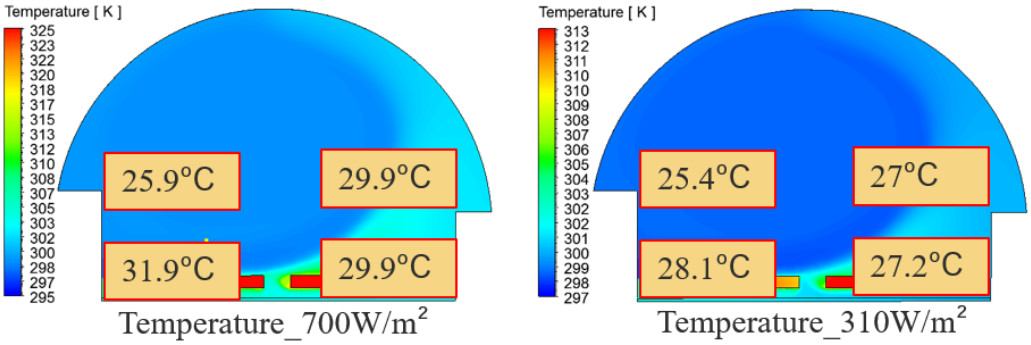

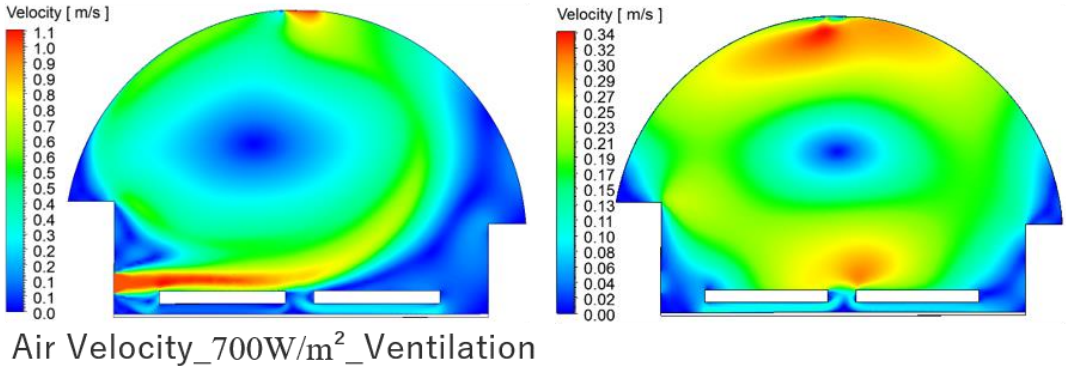

Figure 5.19 Temperature and Air Velocity plot. Water-holding porous asphalt type - #5

5.6 Analyses of heat distribution percentage in "Yamate" Tunnel

5.6.1 Introduction and model specifications

Analyses were performed to analyze the heat distribution percentage in Yamate Tunnel. Based on the Nakamura Model (2018) the air temperature inside the tunnel and the heat distribution percentages of tunnel components were calculated as shown in Figure 5.20. In the Nakamura Model, the heat from the asphalt pavement was neglected and the "error" between the measured and predicted model was considered because of this neglection. In our research, we took into account also the effect of the asphalt pavement heat. By using the actual measured temperature and the thermal parameters of asphalt concrete obtained from our experimental works, we have calculated the percentage of the heat distributed in Yamate Tunnel. Used actual data is the half-day date of 1st June of 2017.

Heat flux by the asphalt pavement was calculated based on the following equation:

$\dot{q} = k\dfrac{(T_{surf} - T_{bott})}{x}$ where k is the asphalt heat conductivity, x is the thickness and T_{surf} and T_{bott} are the measured temperatures of the asphalt surface and bottom, respectively.

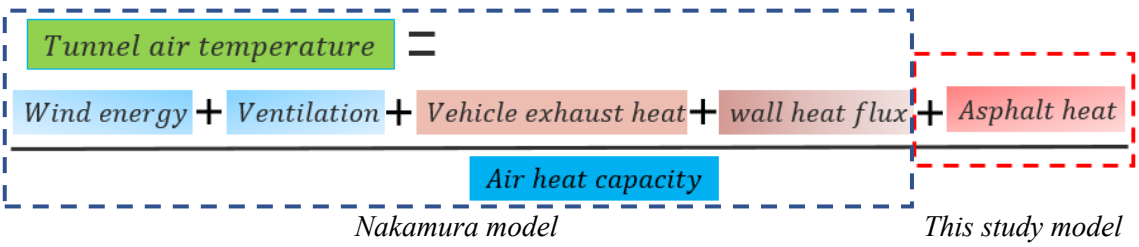

Figure 5.20 Prediction model of the temperature in "Yamate Tunnel".

5.6.2 Simulation Results

Taking into account the asphalt pavement heat and implementing to the "Prediction model of the temperature in "Yamate" Tunnel" by Nakamura 2018, the error decreased by 3% and 2% at Ordinary asphalt and Porous asphalt, respectively (Figure 5.20). It means, not all the errors are related to the asphalt heat. Figure 5.21 illustrates the heat flux distribution at the inner track of the tunnel. At the noontime, the asphalt pavement tends to release heat to the air rather than absorbing it. Here, the porous asphalt releases 50% less heat compared to the ordinary type. Figure 5.22 shows the heat distribution percentage. Overall, the ordinary asphalt type caused 9% of air temperature increase, while the porous asphalt type increased just 5%. Figure 5.23 shows the same results of heat flux distribution and heat distribution percentage of the ordinary asphalt type in the case of the outer track. There was no data of water-holding porous asphalt type.

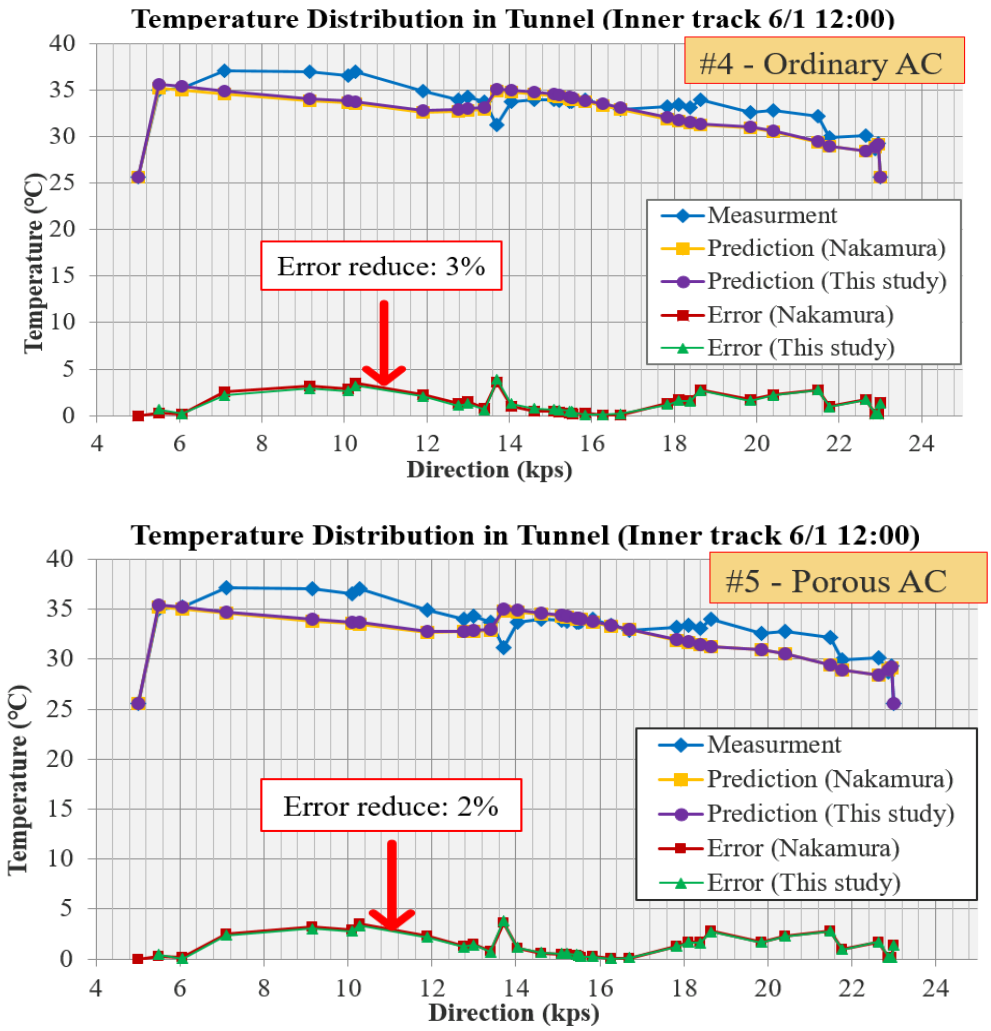

Figure 5.20 Temperature distribution in Yamate Tunnel (Inner Track, 6/1 12:00)

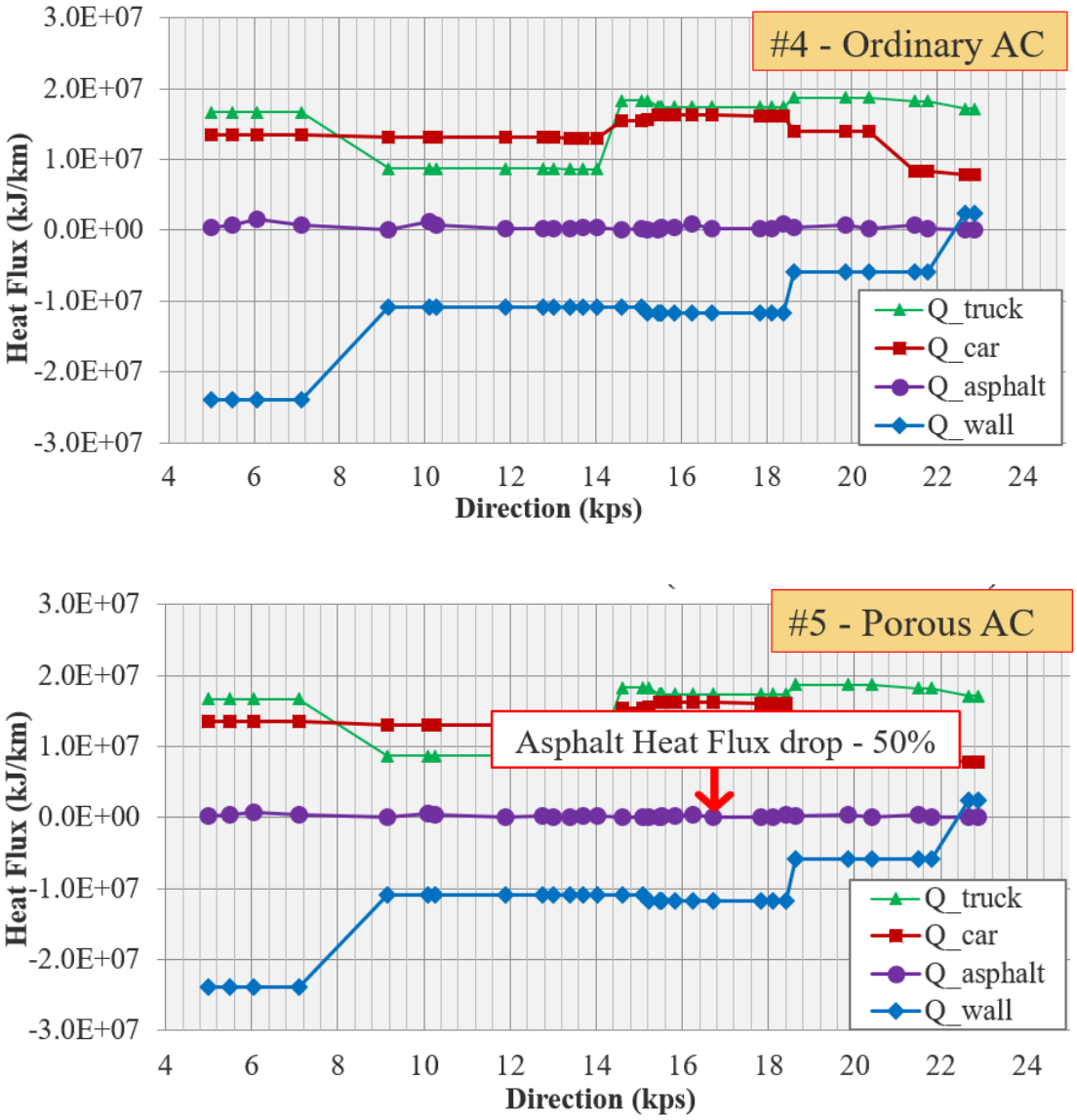

Figure 5.21 Heat flux distribution in Yamate Tunnel (Inner Track, 6/1 12:00)

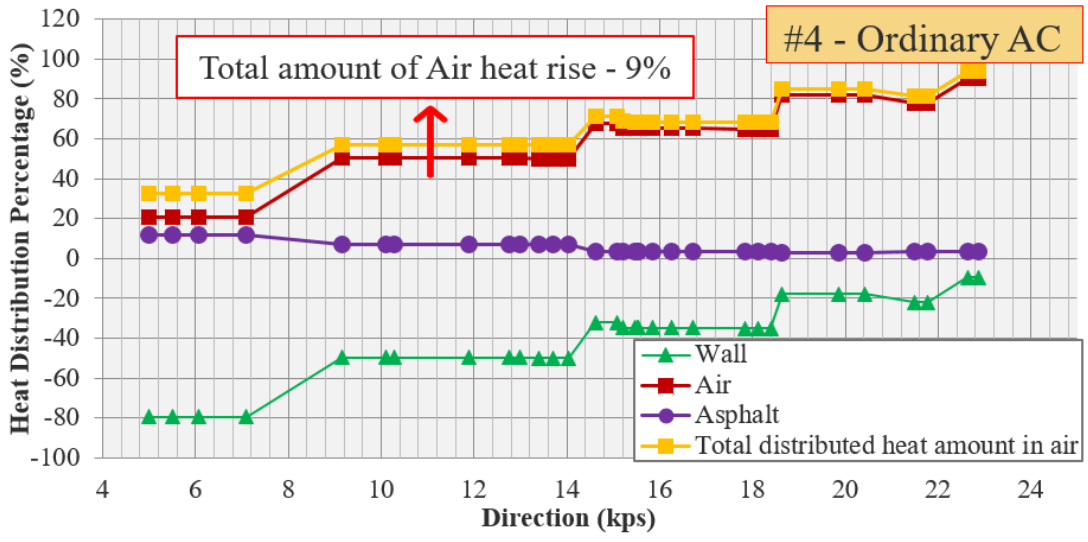

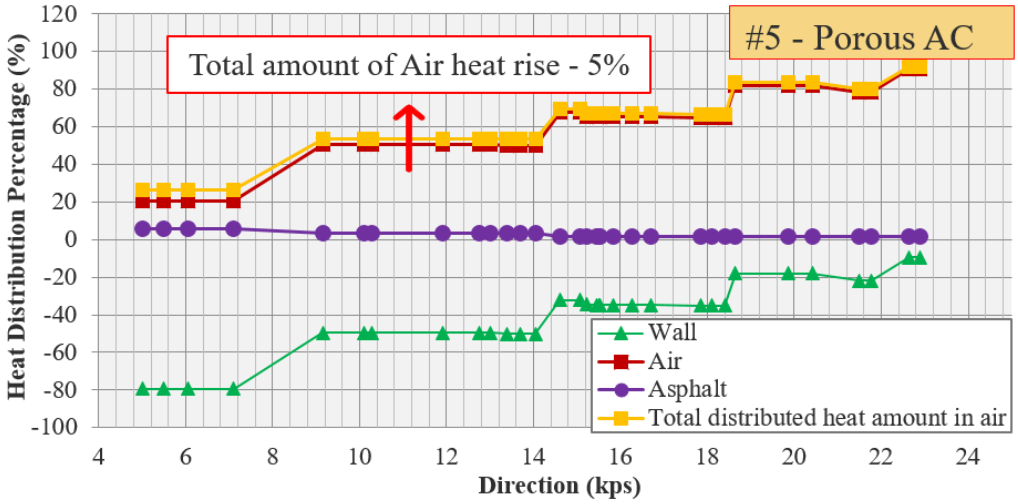

Figure 5.22 Heat distribution percentage in Yamate Tunnel (Inner Track, 6/1 12:00)

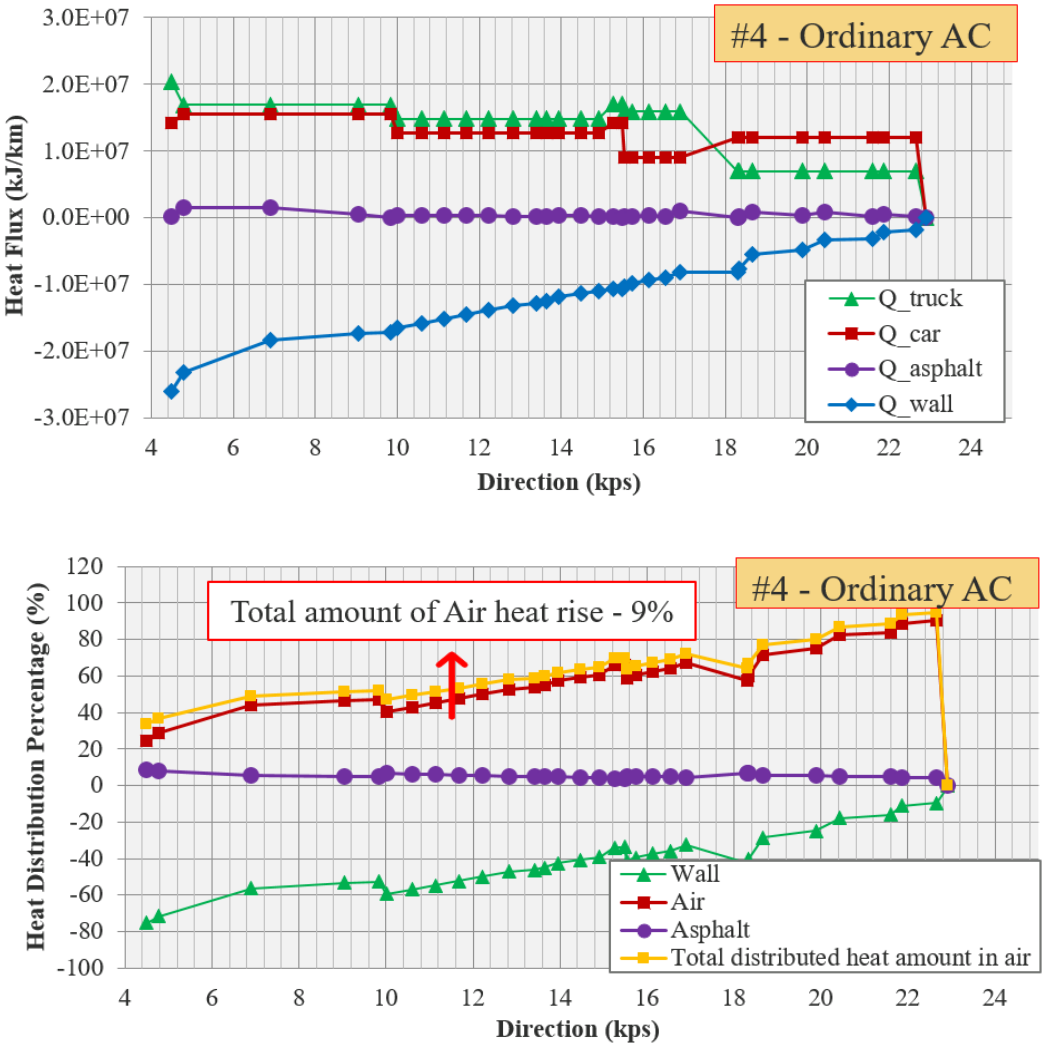

Figure 5.23 Heat flux distribution and heat distribution percentage in Yamate Tunnel (Outer Track, 6/1 12:00)

5.7 Summary of Chapter 5

5.7.1 Summary of experimental results

Effects of different basement boundary conditions and water spray on the surface temperature were investigated to find an effective approach to decrease the surface temperature. The findings are can be summarized as below:

- The water-spray approach showed the dominance and it suppressed the top and bottom surface temperature increments by up to 6^0C and 5^0C respectively.
- The concrete basements decreased the bottom temperature by 5^0C performing equally as the water-spray, however, only 2^0C decrement was observed at the top surface.
- At the cases of steel plate basement and steel plate with H-beams showed fewer effects i.e. 2^0C decrement on the top surface and 3^0C decrement on bottom temperature, respectively.
- The higher the water-spray amount, the higher the suppression of temperature increase. The water-holding porous AC revealed great performance showing the temperature suppression up to 10^0C.

5.7.2 Summary of 2D simulation results

2D Simulations were performed on the purpose of to simulate the air temperature distribution in Yamate Tunnel by using the actual traffic volume at summer season. The "water-spray approach" was demonstrated and the results were compared with the normal case. The simulation input parameters were applied from the values that were derived in this study. Additional 2D Simulations were performed considering a heat source from the vehicle models. The summaries of the findings are:

- The high temperature tends to be accumulated upside area of ventilation inlet and does not get affected much by the approach of water-spray on the asphalt pavement surface.
- The water-spray approach reduces the air temperature by 2 ^{0}C until the distance 30cm high from the asphalt pavement surface. However, at a higher distance at around 150cm, the water-spray approach is weak.

- The replacement of AC with a water-holding porous asphalt type does not influence significantly the temperature inside Yamate Tunnel at both cases of heat source: heat applied to the air and heat from the vehicle motel.
- Higher asphalt surface temperature was obtained nearby the inlet area. It can be considered due to the higher heat transfer coefficient because of the higher wind speed.

5.7.3 Summary of analyses

Analyses were performed to analyze the heat distribution percentage in Yamate Tunnel including the effect of the asphalt pavement portion. By using the actual measured temperature and the thermal parameters of asphalt concrete obtained from the experimental works, the percentage of the heat distributed in Yamate Tunnel was calculated. The conclusions are summarized below:

- Taking into account the asphalt pavement heat to the "Prediction model of the temperature in "Yamate" Tunnel", the error decreased by 3% and 2% at Ordinary asphalt and Porous asphalt, respectively.
- In a long tunnel with high traffic volume, the asphalt pavement mostly functions as a heat radiator rather than heat absorber. In terms of asphalt type, the Porous asphalt radiates about 50% less heat compare to Ordinary asphalt.
- Overall, the Ordinary asphalt type causes 9% of air temperature increase, while Porous asphalt type increases just 5%.

CHAPTER VI

6. CONCLUSIONS AND RECOMMENDATIONS

6.1 Conclusions

Six types of AC specimens were tested in a wind-tunnel where a hot temperate air inside was generated by a forced circulation boiler system. Based on the obtained experimental data, numerical simulations were performed to derive thermal parameters of each asphalt type. Additionally, the effects of different basement boundary conditions and water spray on the surface temperature were investigated to find effective countermeasures to decrease the surface temperature of AC in the tunnel. The following conclusions can be drawn from the present research:

1. One layered coarse-graded and dense-graded asphalt specimens revealed 1~2℃ higher top surface temperature increments than the specimens with two layers (#3, #4) when the contents of the materials were the same. The water-holding porous asphalt and the dense-graded asphalt with heat insulation unit had a similar surface temperature trend showing 1℃ lower than the one layered specimens.
2. The internal and bottom temperature increments at a different type of asphalt specimens: coarse-graded, dense-graded, water-holding porous and dense-graded with heat insulation unit asphalt did not differ from each other significantly.
3. The thermal properties as specific heat capacity, heat conductivity and heat transfer coefficient of six types of asphalt concrete were derived through the wind-tunnel experiments and Numerical calculations. Among the types, the water-holding asphalt gave a good thermal performance i.e. lower heat conductivity and lower heat transfer coefficient. It conducts less heat transfer from the asphalt surface to a subsequent base layer and prevents a big amount

of heat transfer between the surface and surrounding air.

4. Tests on the effect of the boundary conditions on the purpose against high surface temperature showed the dominance of the water spray. It suppressed the top and bottom surface temperature increments by up to 6^0C and 5^0C respectively. The concrete basement decreased the bottom temperature by 5^0C performing equally as the water spray, however only 2^0C decrement for the top surface. Other cases i.e. steel plate basement and steel plate with H-beams showed less effect i.e. 2^0C decrement on the top surface and 3^0C decrement on bottom temperature, respectively.
5. The high temperature tends to be accumulated upside area of ventilation inlet and does not get affected much by the approach of water-spray on the asphalt pavement surface. It only gets affected by the fluctuation of the heat source amount.
6. The water-spray approach reduces the air temperature by 2 ^{0}C until the distance 30cm high from the asphalt pavement surface. However, at a higher distance at around 150cm, the water-spray approach tends to behave weakly.
7. The replacement of the ordinary asphalt type with a water-holding porous asphalt type does not influence significantly the air temperature inside Yamate Tunnel.
8. Overall, the Ordinary asphalt type causes 9% of air temperature increase, while Porous asphalt type increases just 5% in Yamate Tunnel.

6.2 Final Remarks

- Asphalt pavement thermal parameters were derived under tunnel environmental condition. There is no research that considered this condition.
- The values of Heat transfer coefficient (h) depend on wind speed and water spray. Until now, no researches have estimated these values, since, it is difficult to create a tunnel environment where wind flows constantly. We found these values under both wind speed and water-spray.
- Presented asphalt thermal values of *h* can help engineers to control and calculate a temperature flow in Tunnel Roads.

- In a long tunnel with high traffic volume, the asphalt pavement mostly functions as a heat radiator rather than heat absorber. In terms of asphalt type, the Porous asphalt radiates about 50% less heat compare to Ordinary asphalt.
- Through this research, we understand that effect of spraying water on a pavement surface or replacing pavement with the water-holding porous asphalt is not really helpful. It decreases the temperature only at around pavement surface area. Thus, it requires to focus on how to decrease the accumulated high temperature at the upper area rather than focusing on the asphalt itself.

6.3 Prospects for future researches

6.3.1 Yamate Tunnel model with vehicle heat source

On the purpose of enhancement of the simulation model, the transverse 2D model has to be changed to the longitudinal direction. 2D model of longitudinal cross-section works if we neglect the side ventilation and consider only the wind flow induced by vehicles and heat source. However, the 3D model would be perfect as long as we deal with the longer calculation procedures. Then, investigate the effects on both, the asphalt pavement surface temperature and the air temperature when changing the type of asphalt pavement and apply countermeasures as wind and water spray.

6.3.2 Water-pipe inside Yamate Tunnel

An approach to eliminate the accumulated high temperature requires. This might work through installing a water-pipe along the wall near the high-temperature area. Because a water-pipe has a significant absorptivity of high air temperature. For this, a new 3D model is recommended to be performed.

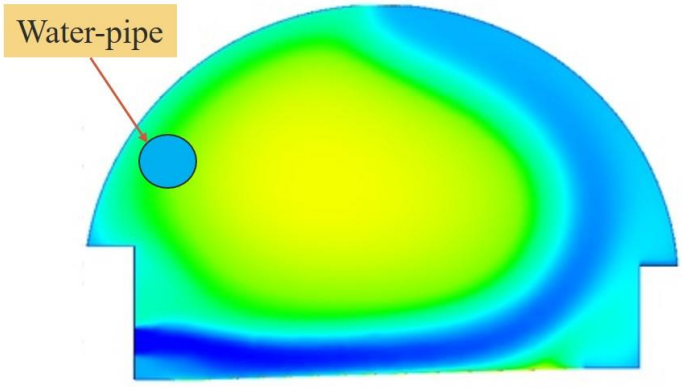

Figure 6.1 Model of Yamate Tunnel with water-pipe approach

6.3.3 Suppression of Yamate Tunnel air temperature with Liquid Nitrogen

Liquid Nitrogen was proposed to forcibly freeze the asphalt pavement in "Yamate" Tunnel to suppress the hot air temperature inside the tunnel. Although it is not a good idea in a point of the pavement strength and the safety factors for drivers, yet it can be studied to evaluate how much the high air temperature of "Yamate Tunnel" can be decreased due to the extremely low temperature of the asphalt pavement.

As for how to apply Liquid Nitrogen, Figure 6.2 briefly explains this. The Figure illustrates the asphalt side faces and bottom face are immersed in a Liquid Nitrogen. The liquid should be appropriately insulated from the ambient temperature. This methodology should be applied after the experimental test verification.

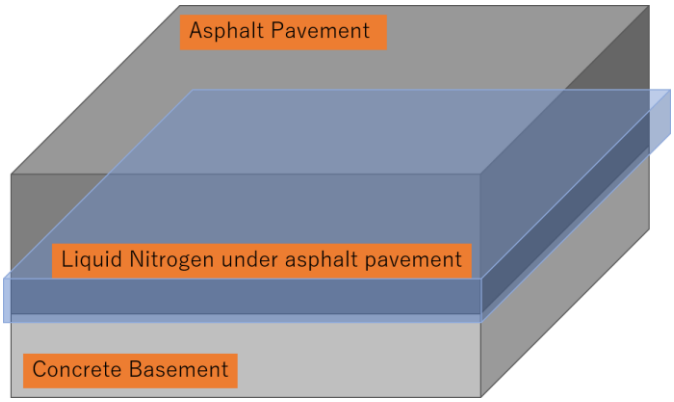

Figure 6.2 Application of Liquid Nitrogen to extremely suppress the asphalt pavement temperature in order to decrease the hot air temperature inside a tunnel.

REFERENCES and SUGGESTED READINGS

Aoki, D., Yoshinaka, T., & Fujinami, K. (2005/12). A study of thermal parameter estimation for pavement. *J-STAGE, 10*, 225-231 (in Japanese).

A. S. A. Alghamdi. (2010) Inverse Estimation of Boundary Heat Flux for Heat Conduction Model. *JKAU: Eng. Sci., Vol. 21* No.1 pp: 73-95.

Byong, C. B., Dae-Wook, P., Hai, V. V., Samer, D., & Ji, S. I. (2015). Thermal Properties of Asphalt Mixtures Modified with Conductive Fillers. *Journal of Nanomaterials, Vol. 2015,* Article ID 926809.

Data-Logger TDS-530-30H. Retrieved from https://www.techno.co.jp/pc_rental/cmp/search/detail_2203TQ0045.html

Engineering ToolBox, (2003). Thermal Conductivity of common Materials and Gases. Retrieved from https://www.engineeringtoolbox.com/thermal-conductivity-d_429.html

Fujimoto, A., Saida, A., Fukuhara, T., & Futagami, T. Heat transfer analysis on road surface temperature near a traffic light. ResearchGate, Pub. No 268351732, n.d.

Goto, S., & Matsubayashi, O. (2009). Relations between the thermal properties and porosity of sediments in the eastern flank of the Juan de Fuca Ridge. Earth Planets Space. *61,* 863–870.

Himeno, K., Watanabe, T., & Suguro, F. (1986). Estimation of the temperature distribution in the asphalt pavement. *J-STAGE, 4,* No 366, 123-132 (in Japanese).

Kawana, F., Kawamura, N., & Matsui, K. (2012). Evaluation of pavement thermal properties using heat flux sensor. *J-STAGE, Vol. 68,* No 3, I_5- I_12 (in Japanese).

Kosaku, K., & Hiroshima, M. (2005). *Measurement of Specific Heat, Thermal Conductivity, and Diffusible Humidity for Water-absorptive Pavement*, (Report No. ISSN 0387-2416, 233-238). The Institute of Civil Engineering of the Tokyo Metropolitan Government (in Japanese).

K-Type thermometer specs. Retrieved from https://jp.rs-online.com/web/p/thermocouple-extension-wire/0151209/

Marcus A. Lobbia. (2014/1). *1-D Heat Transfer in Multilayer Materials Using a Finite Volume Approach.* AEROSPACE REPORT NO. TR-2014-01128.

Mohammad H. Alawi & Medhat M. Helal. (2014). A mathematical model for the distribution of heat through pavement layers in Makkah roads. *Journal of King Saud University − Engineering Sciences*, 26, 41−48.

Nakayama, T., & Fujita, T. (2010). Cooling effect of water-holding pavements made of new materials on water and heat budgets in urban areas. *Landscape and Urban Planning, Vol 96,* 57-67.

Necati Özişik, M. (1994). Finite Difference Methods in Heat Transfer. Boca Raton, Florida: CRC Press, inc.

Nishioka, M., Nabeshima M., Wakama, S., & Ueda, J. (2006). Effects of Surface Temperature Reduction and Thermal Environment on High Albedo Coating Asphalt Pavement. *Journal of Heat Island Institute International, Vol.1,* 46-52.

Raheb, M., Pär, J., & Sotirios A.G. (2018/01). Thermal properties of asphalt concrete: A numerical and experimental study. *Construction and Building Materials, Vol. 158,* 15, 774-785.

Shutoko driver's website (2015). Countermeasures against high temperature in Yamate Tunnel. Retrieved from ttps://www.mathworks.com/help/matlab/ref/interp1.html

Siti, H., Syarifah, I., Salmia, B., & et al. (2017). Heat Lump in Different Pavement Layer Using Ethylene Glycol as A Solar Heat Collector. *MATEC Web of Conferences 87, 01015.*

Toktorbai uulu, A., Katsuchi, H., Yamada, H., & Kim, H. (2019). Study on thermal parameters of asphalt concrete for countermeasures against high surface temperature of pavement in tunnel. Journal of Road Materials and Pavement Design (under review).

Veerasamy, R., Rajak, H., Jain, A., Sivadasan1. S., Varghese, C., & Agrawal, R. (2011/9). Validation of QSAR Models - Strategies and Importance. International Journal of Drug Design and Discovery, 2, 511-519.

Yoshida, N., Nishimura T., & Hino, Y. (2000). Experimental Study on Association of Surface Characteristics of Road Pavement with Surface Temperature. *J-STAGE, 29,* No 7, 66-74 (in Japanese).

Yunus A. Cengel, (Second Edition). Heat Transfer. A practical approach.